DOCTORAL THESIS

Surfactant-Polyelectrolyte Complexes: Structure and Interactions

---

Author:

MEERA THOMAS

Supervisor:

PROF. V. A. RAGHUNATHAN

Thesis submitted to the

Jawaharlal Nehru University for the award of the degree of

Doctor of Philosophy

Raman Research Institute

Bangalore 560080

April 1, 2019

DECLARATION

I hereby declare that this thesis is composed independently by me at Raman Research Institute, Bangalore under the supervision of Prof.V.A.Raghunathan. The subject matter presented in this thesis has not previously formed the basis of the award of any degree, diploma, associateship, fellowship or any other similar title. I also declare that I have run it through the Turnitin plagiarism software.

Meera Thomas
Raman Research Institute
Bangalore 560080

V. A. Raghunathan
Raman Research Institute
Bangalore 560080

CERTIFICATE

This is to certify that the thesis entitled **Surfactant-Polyelectrolyte Complexes : Structure and Interactions** submitted by Meera Thomas for the award of the degree of DOCTOR OF PHILOSOPHY of Jawaharlal Nehru University is her original work. This has not been published or submitted to any other University for any other degree or diploma.

Prof. R. Subrahmanyan
Director
Raman Research Institute
Bangalore 560080

V. A. Raghunathan
Thesis Supervisor

ACKNOWLEDGEMENTS

It has been my extreme privilege to work with Prof. V. A. Raghunathan. He has been the best teacher and mentor. I am extremely grateful to him for his constant guidance, encouraging discussions, inspiration and support. I cannot emphasize enough how fortunate I am to have worked with him all these years. I am overwhelmed by his patience and humility. I am proud to say that I still have a lot to learn from you. Thank you, Raghu.

I am thankful to Prof. Yashodhan Hatwalne and Prof. Ranjini Bandyopadhyay for being part of my thesis advisory committee. I would like to thank Prof. N. V. Madhusudana, Prof. V. Lakshminarayanan, Dr. Pramod Pullarkat, Prof. R. Pratibha and Dr. Arun Roy, Dr. Sayantan Majumdar, Prof. Sandeep Kumar, Dr. Gautam V Soni for all the discussions, suggestions and help. I would like to thank all the RRI faculties for all the support and encouragement. I would like to thank Prof. Ravi Subrahmanyan for all the support and help.

I am thankful to Radhakrishna for all his help. I am thankful to Mani, Dhason, Yatheendran, Serene and Durai for all technical support for my experimental work. I am extremely thankful to Vasudha for all her help with my experiments and also for being a family away from home. I would like to thank Srinivasa and Gowda (deceased) for their help in the chemistry lab. I am thankful to Raja and Murali for all their help.

I thank all the library staff for their help, especially Meera, M. Manjunath, Nagaraj, Geetha, Vrinda, Vani, Elumalai, and Manjunath K. I would like

to thank everyone at the computer section for their help especially Jacob, Sridhar, and Krishnamurthy. I thank everyone in the administrative department especially Krishnamaraju, C.S.R. Murthy, Naresh, Marisa, Radha, Vidya, Shailaja, and Ram. I would like to thank the Purchase section and Accounts section for all their help. I thank Raveendran and Srinivasmurthy for all their help. I would like to thank GB, Sasidharan, Haridas, Sridhar, Munishwar, and others from civil and electrical department. I am thankful to everyone in the Mechanical Engineering department and workshop.

I am very fortunate to get the best colleagues in lab. Madhukar and Santosh are the best seniors one could ask for. Thanks for all the guidance, inspiration, good times, fun and discussions. Sreeja, I don't have words to express my gratitude to you. Thanks for being my best friend, sister and colleague. Thanks for all your help, support, encouragement, and awesome dishes. You are the best. Anindya, thanks for being the cool junior in the lab. You make lab lively. Thank you for all the help, and for being a good friend. I would like to thank Surya, Ayush, and Shabeeb for their friendship, help and support. I thank Amit for all the discussions and help.

I am thankful to Umaji, Padmaji and Sharadaji for cooking with so much love all these years and for all the help and support.

I am glad to say that I had the best batch-mates. I am lucky to have a friend like Karamveer. I would like to thank you for all the awesome times we have spent, support, motivation, and help. Special thanks to Sushil and Raj for the get togethers keeping our friendship alive. I would also like to thank Priyanka, Nafisa, Raviranjan, Debsankar, Niranjan, Abhijith, Anirudh, Abir, Kartick, Deepak, Sivam, Ashish, and Shabbir.

My hostel time wouldn't have been enjoyable without my dearest juniors. Thank you Adwaith, Arsalan, Silpa, Bhagya, Hemanth, and Arun. You are

amazing. I would like to thank Sanjay, Santanu, Swamy, Mari, JK, Jaggu, Irla, Chandan, Asha, Amit, Debadrita, Rituparna, and Swapna. I would also like to thank Saichand, Nishanth, Sayooj, Nancy, Anand, Vardan, Anju, Shovan, and Sreyas. I am thankful to Giri, Habiba, Jyothi, Samim, Shafi, Femida, Prasad, Arnab, Ishita, Amrita, Debasish, Chaithra, Rajib, Anjan, Anagha, Nazma, Nipanjana, and other seniors for the wonderful days we spent in hostel.

I thank Usha, Divya, Maya, and Swati for all the interesting discussions and awesome dinners.

I am thankful to my dearest friends Carina and Sharannia for their endless support and friendship.

I am thankful to my parents and grandparents for their unconditional love, support, encouragement, blessings and prayers. I am thankful to Teena, who has been amazing. I am overwhelmed by her love and belief she has for me. Thank you dear. My heartfelt thanks to Suvodip and his family for their unfailing love, support and encouragement at all times. I also thank all my other family members and friends for their support and encouragement.

I am thankful to God for all his blessings.

"The answers are all out there, we just need to ask the right questions."

Oscar Wilde

To my family

SYNOPSIS

This thesis describes studies on the self assembly, phase behaviour, structure and stability of ionic surfactant-water systems in the presence of oppositely charged linear polyelectrolytes and deoxyribonucleic acid (DNA). Using a variety of experimental techniques, such as small angle x-ray scattering (SAXS), polarizing optical microscopy (POM) and cryogenic scanning electron microscopy (Cryo-SEM), we probe diverse phases formed by these systems and the underlying interactions. Research work presented in this thesis can be broadly divided into two parts: (i) Interaction of a linear anionic polyelectrolyte with the lamellar phase of a cationic surfactant, and (ii)Interaction of cationic surfactants with DNA

Interaction of a linear anionic polyelectrolyte with the lamellar phase of a cationic surfactant

Polyelectrolytes are polymers which acquire a charge when dispersed in an aqueous solution. They form complexes with oppositely charged macroions, by releasing the condensed counterions[1,2]. In this work, we have studied the interaction of the linear anionic polyelectrolyte, polyacrylic acid (sodium salt) (PAANa), with the lamellar phase formed by the cationic surfactant, didodecyldimethyl ammonium chloride (DDAC). The phase behaviour of the system was studied, by varying various parameters, such

as the water content, molecular weight of the polyelectrolyte, concentration of the polyelectrolyte and the ionic strength of the solution.

Cryo-SEM and POM images of complexes of DDAC and PAANa (fig.1 (a)) indicate that these complexes have a lamellar structure. SAXS data collected from these samples (fig. 1(b)) show a collapsed (L_α^{c1}) $\rightarrow$ swollen (L_α^{s}) $\rightarrow$ collapsed (L_α^{c2}) transition of the lamellar complex with decreasing water content. The lamellar periodicity of the L_α^{c1} phase is $\sim$ 3.5 nm, whereas that of the L_α^{s} phase $\sim$ 36 nm. The L_α^{c2} phase has a slightly lower periodicity of $\sim$ 2.8 nm, compared to that of the L_α^{c1} phase (fig. 2(a)).

Since decreasing the water content at fixed PAANa/DDAC weight ratio is equivalent to increasing the concentration of Na^+ and Cl^- ions in the solution, the observed swelling transition must be driven by the increasing ionic strength of the solution. To confirm this, the effect of salt on the structure of the complex was studied (fig. 2(b)). As expected, it is found that the transitions occur on increasing salt concentration. A similar behaviour is observed for polyelectrolyte molecular weight M_w=5100 (fig. 3(a)). However, the swelling transition is not observed when the molecular weight is increased to 8000 (fig. 3(b)).

We have also studied the effect of salt on the lamellar phase of the DDAC-water system. Figure 4(a) shows the variation of the lamellar periodicity of a 20 wt% solution of DDAC in water as a function of NaCl concentration. The lamellar periodicity of this system is around 12 nm and does not vary significantly as the salt concentration is increased up to around 350 mM. However, the diffraction patterns show significant changes over this range of salt concentration. At very low salt concentrations the diffraction patterns show a set of sharp peaks, as expected from a lamellar phase stabilized by electrostatic repulsion[3]. At higher salt concentrations only one or two broad peaks

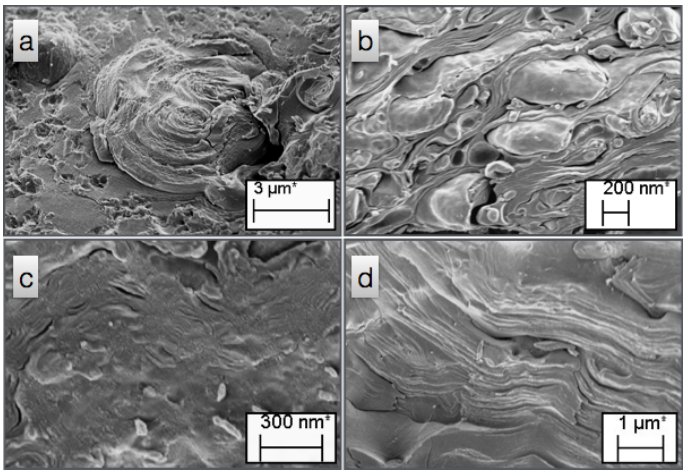

(a)

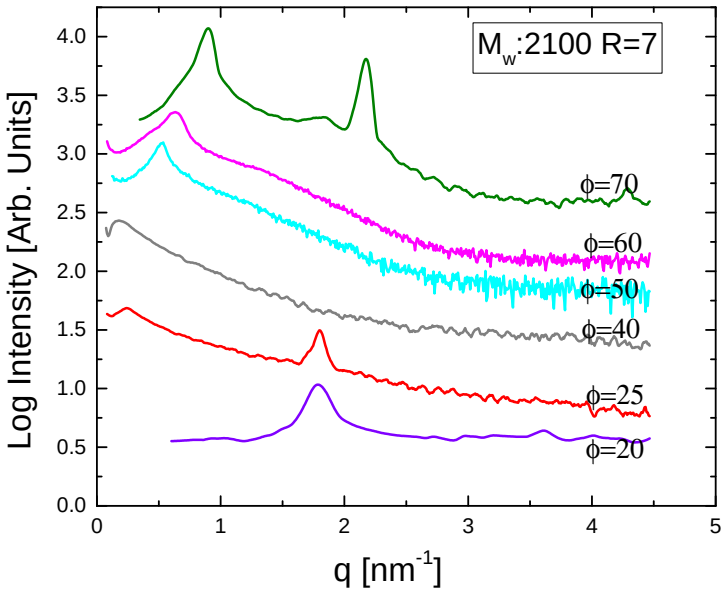

(b)

FIGURE 1: (a) Cryo-SEM images of the DDAC-PAANa system at ϕ=30, 40, 50, 60 and R=7, showing multilamellar vesicles and layered morphology, typical of a lamellar phase. (b) SAXS profiles of the DDAC-PAANa system at concentrations varying from ϕ=20 to 70 at R=7 and T=25°C. ϕ is the total weight percentage of DDAC & PAANa and R is the polyelectrolyte to surfactant weight ratio. The molecular weight of PAANa used was 2100.

are observed in the diffraction pattern, indicating that this phase is stabilized by steric repulsion arising from thermal undulations of the bilayers[3]. The large periodicity of this phase is consistent with a value of K of the order of a few kT. We have analyzed the diffraction data[4] and the Caillé parameter η is found to increase from 0.06 to 0.51 as the salt concentration is varied from 0 to 200 mM, confirming that the electrostatically stabilized lamellar phase in the absence of salt gets transformed into an undulation stabilized phase at high salt concentration. At very high NaCl concentrations a collapsed lamellar phase with a periodicity of 3.1 nm is observed, indicating the dominance of van der Waals attraction between the bilayers when the electrostatic repulsion is strongly screened out. The swelling transition is not observed when DDAC is replaced with the cationic lipid 1,2-dioleoyl-3-trimethylammonium-propane (chloride salt) (DOTAP), which has a much higher value of the bilayer bending rigidity, K.

Based on our observations, we propose the following mechanism for the swelling transitions of the DDAC-PAANa complexes demonstrated in fig. 4(b). At low salt concentrations, the adsorbed polyelectrolyte forms a laterally heterogeneous layer on the bilayer surface due to interchain electrostatic repulsion. This leads to a patch-charge attraction between the bilayers[5], resulting in the collapsed lamellar phase L_α^{c1}. Bridging interaction is yet another possibility for the formation of this collapsed phase. Increasing the salt concentration leads to the screening of the inter-chain repulsion and an increased adsorption of the polyelectrolyte[6]. The patch-charge attraction is absent in this situation and the L_α^s is formed due to steric repulsion between the polymer adsorbed-bilayers due to thermal undulations if the bilayer bending rigidity is sufficiently small. At still higher salt concentrations the polyelectrolyte desorbs from the bilayer surface. Since electrostatic repulsion is heavily screened, the van der Waals attraction is dominant[7] at

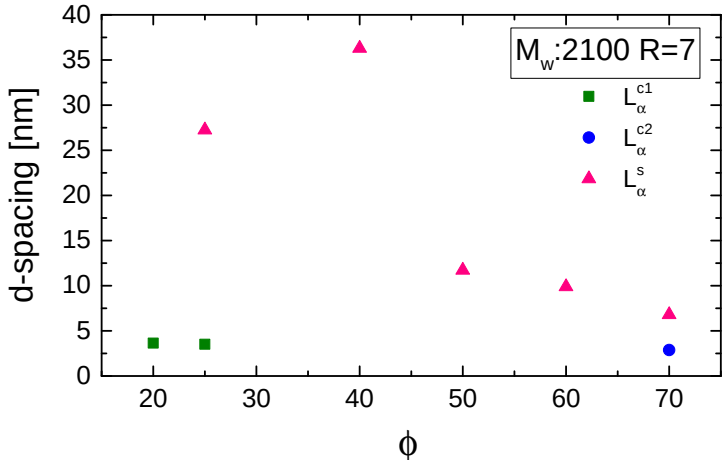

(a)

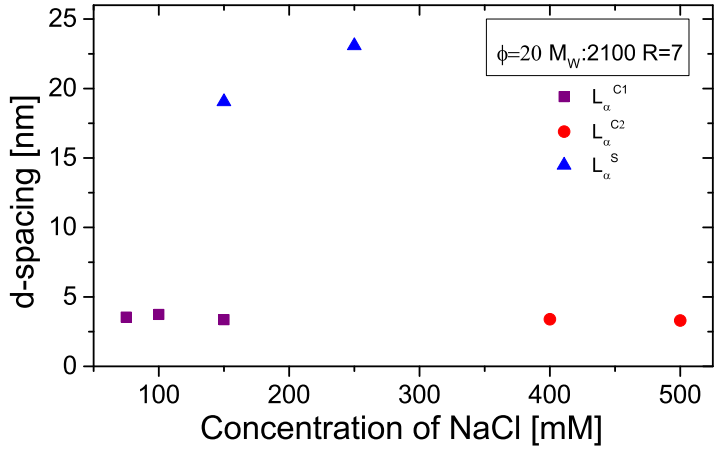

(b)

FIGURE 2: Lamellar periodicity (d) of the DDAC-PAANa2100 system at R=7 in (a) water and in (b) NaCl solution. Both the figures show the sudden transition from an initial collapsed lamellar phase (L_α^{c1}) to a swollen lamellar phase (L_α^{s}) with very large d-spacing. At very high values of ϕ or salt concentration, a second collapsed lamellar phase (L_α^{c2}) is observed at T=25°C.

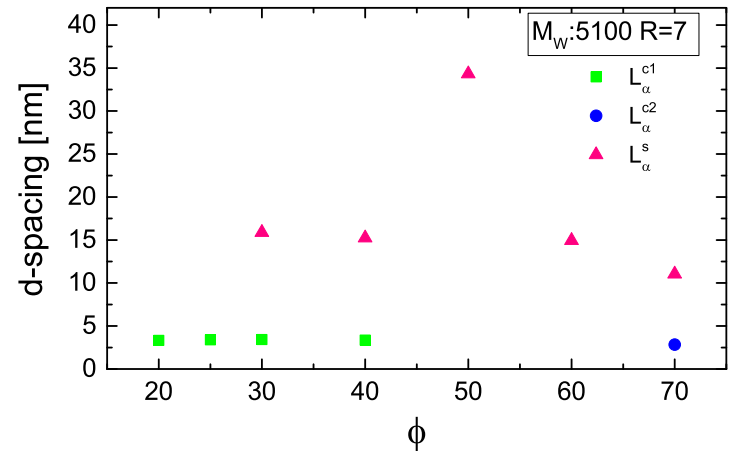

(a)

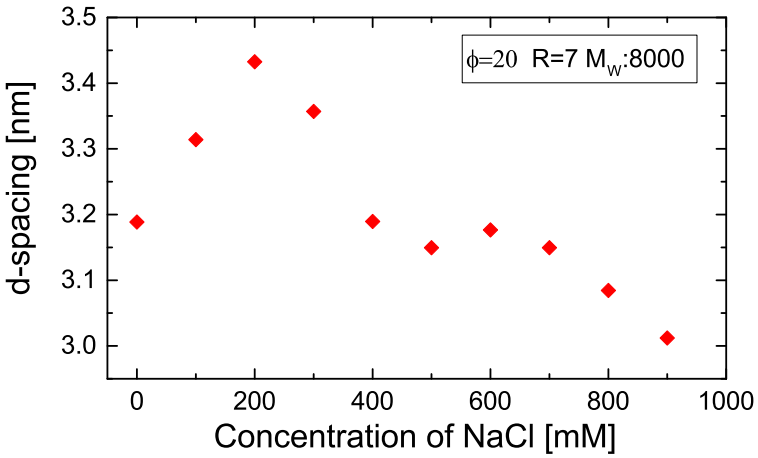

(b)

FIGURE 3: Lamellar periodicity (d) of the (a) DDAC-PAANa system with M_w=5100 as a function of ϕ at R = 7, showing a similar swelling transition as that of the M_w=2100 system and (b) DDAC-PAANa system with M_w=8000 as a function of NaCl concentration at R = 7. No swelling is observed in the case of M_w=8000. T=25°C.

these salt concentrations and the collapsed L_{α}^{c2} phase is formed. The absence of any adsorbed polyelectrolyte results in the lower periodicity of this phase compared to that of the L_{α}^{c1} phase observed at low salt concentrations. The absence of the swelling transition in the case of M_w=8000 can be explained in terms of an increase in the strength of the patch-charge attraction with the molecular weight of the polyelectrolyte or bridging interaction.

Interaction of cationic surfactants with DNA

In the second part of the thesis we present studies on the structural polymorphism of surfactant micelle-DNA complexes. DNA, the carrier of hereditary information in living organisms, is an anionic polyelectrolyte. Double stranded DNA is much more rigid than PAANa and in the presence of oppositely charged surfactant micelles, self-assemble into 2-dimensional crystalline structures in water, which mimic 2-dimensional ionic crystals. This self-assembly is driven mainly by the release of counterions that are initially condensed on the two types of macro-ions, namely, DNA and the surfactant micelle. These complexes exhibit various structures and their stability has been studied in the past by varying several factors, such as the relative DNA concentration, salt concentration, and type of surfactant counterion. It has been shown that complexes of DNA with the cationic surfactant, cetyltrimethyl ammonium bromide (CTAB), exhibits only an intercalated hexagonal structure[8]. On the other hand, replacing the bromine counterion with the strongly binding tosylate counterion leads to the formation of three different structures, depending on the relative surfactant/DNA concentration and salt concentration[9]. In the present work we have studied the influence of the micellar size and salt concentration on the structure of the

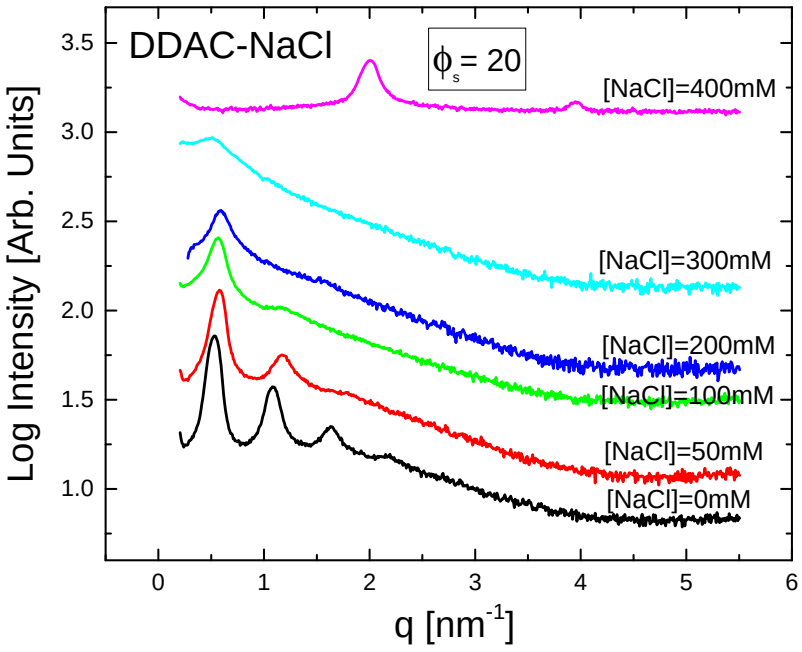

(a)

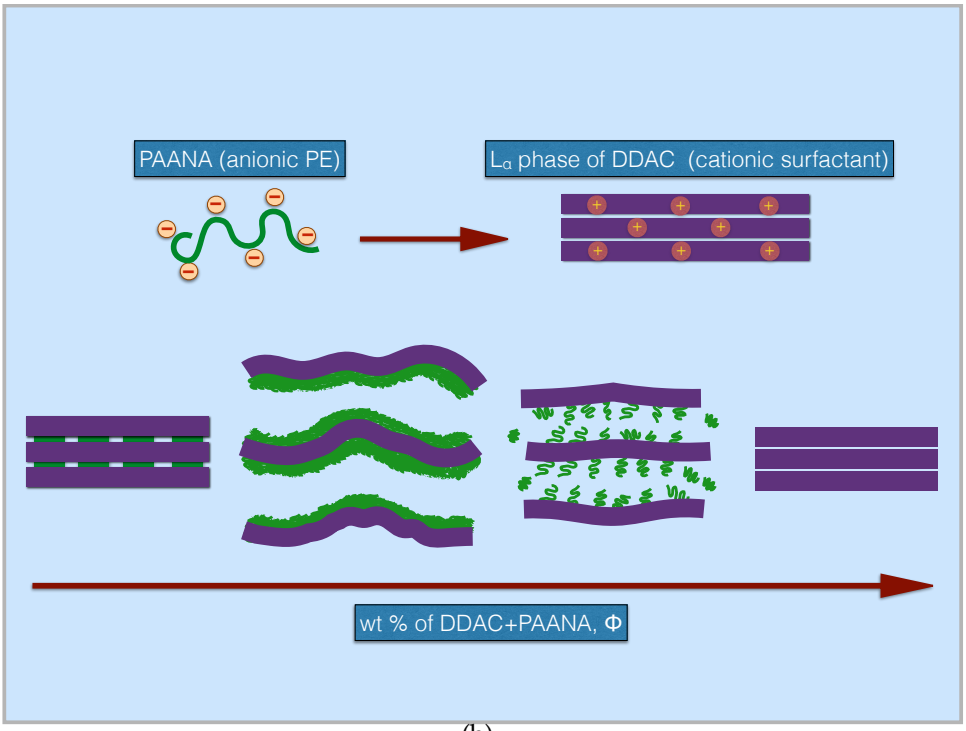

(b)

FIGURE 4: (a) The SAXS data obtained for DDAC-NaCl system at ϕ_{DDAC}=20, showing the transition from an electrostatically stabilised lamellar phase at low ionic strength to an undulation stabilised phase at higher ionic strength. (b) Schematic representation of proposed mechanisms involved in the swelling transitions of the DDAC-PAANa system.

complexes. The surfactants used were myristyltrimethyl ammonium bromide (MTAB) and dodecyltrimethyl ammonium bromide (DTAB) and their mixtures. Complexes were probed using SAXS and cryo-SEM techniques. Their structures were deduced from electron density maps calculated from the SAXS data. Elemental analysis of the complexes were carried out to obtain additional structural information.

MTAB-DNA complexes are found to exhibit only a hexagonal phase, irrespective of the relative MTAB/DNA concentration as shown in Fig. 5. Thus reducing the chain length from CTAB to MTAB does not change the structure of their complexes with DNA. The addition of NaCl is found to swell the complex gradually, with the crystalline complex melting into an isotropic phase at higher salt concentration. On the other hand, the addition of sodium tosylate is found to transform the hexagonal phase into a square phase, as depicted in Fig. 6(a).

In the case of DTAB-DNA complexes, the SAXS patterns exhibit only a broad peak. However, the addition of salt results in patterns with sharp peaks. Two different structures are observed in this system; a square phase at high DTAB/DNA concentration and a super hexagonal phase at low DTAB/DNA concentration. The lattice parameters of these two structures are around 4.06 nm and 8.24 nm, respectively. In order to understand the formation of different structures in MTAB-DNA and DTAB-DNA complexes, micelles were prepared with binary mixtures of DTAB and MTAB, with the amount of DTAB ranging from 10% to 98% by weight, and their complexes with DNA were studied. SAXS data for low and high values surfactant/DNA molar ratio are given in Fig. 7(a) and Fig. 7 (b), respectively. These samples were prepared at [NaCl] = 300 mM, in order to obtain sharp SAXS patterns. At low surfactant/DNA ratio, the hexagonal phase is found at low DTAB concentrations. At [DTAB]=33%, the lattice parameter has a

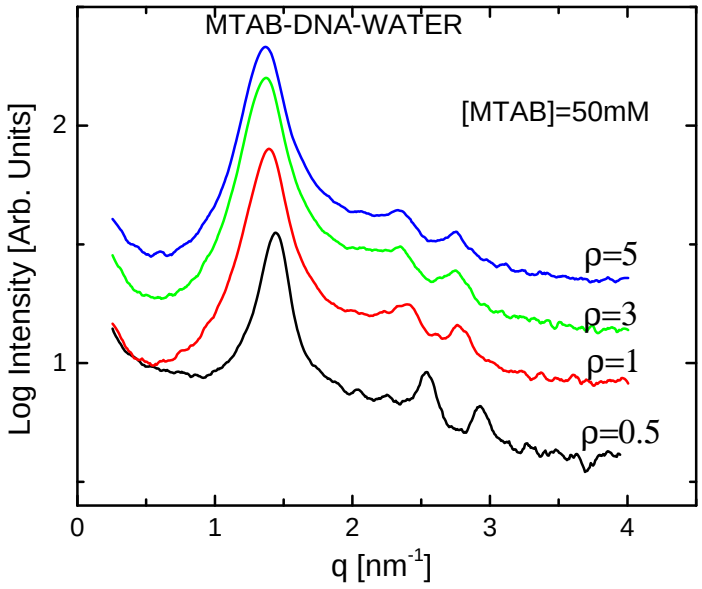

(a)

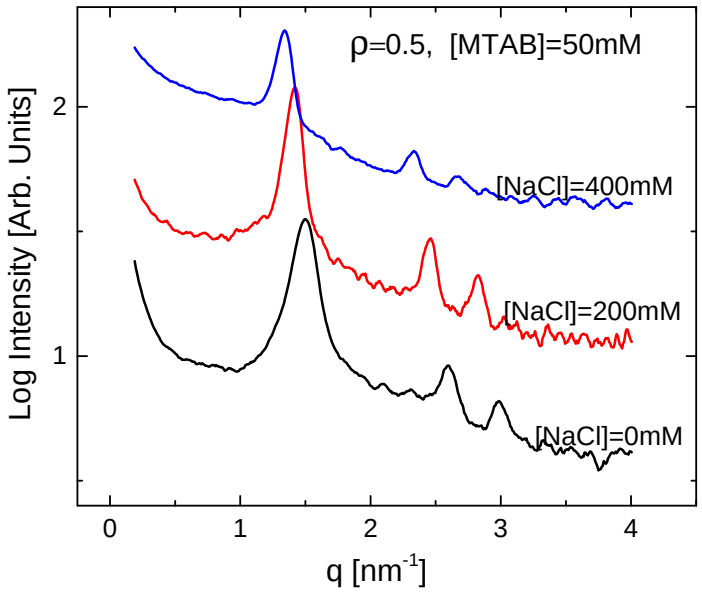

(b)

FIGURE 5: SAXS data obtained from MTAB-DNA complexes for different MTAB/DNA molar ratios (ρ) in (a) water and (b) NaCl solutions with different ionic strengths. MTAB concentration in the solution was 50 mM.

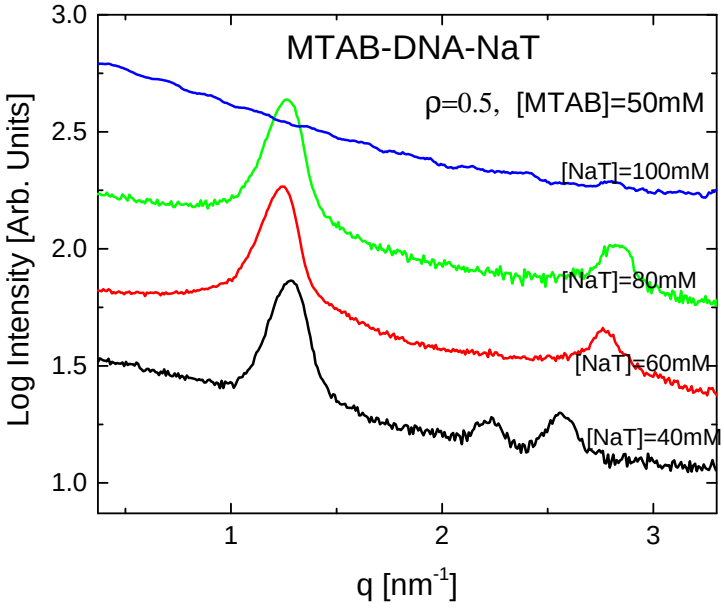

(a)

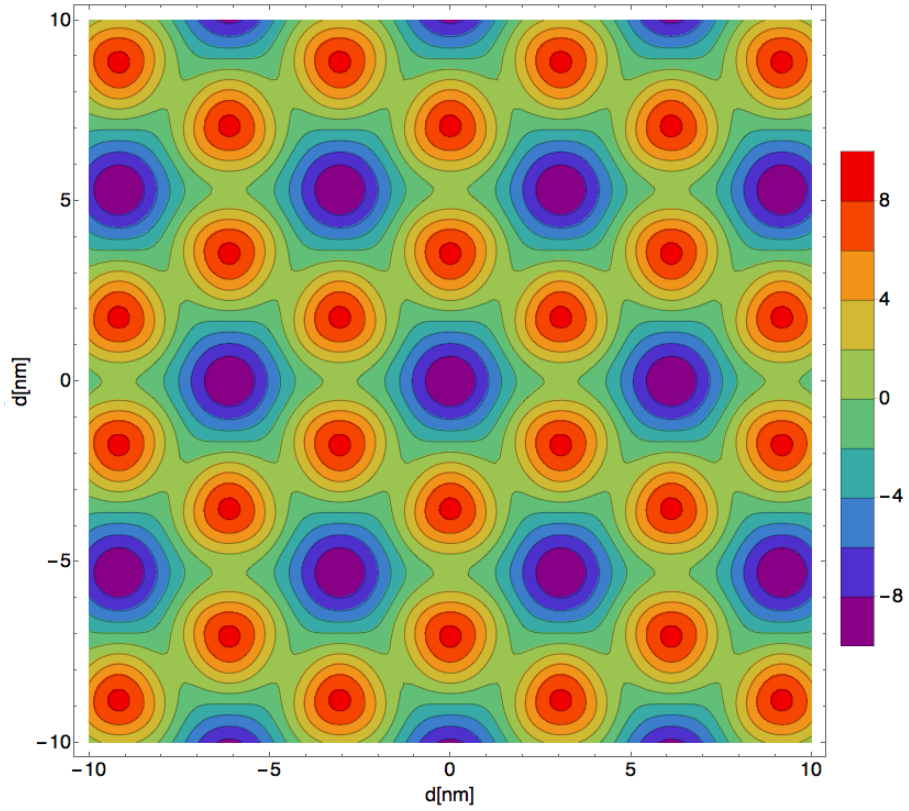

(b)

FIGURE 6: (a) SAXS data obtained from MTAB-DNA complexes ρ=0.5 in the presence of sodium tosylate (NaT). An hexagon to square transition is observed at [NaT] 60 mM. An isotropic phase is observed at [NaT] 100 mM. (b) Electron density map of the hexagonal phase of MTAB-DNA complexes determined from the SAXS data.

value of 5.43 nm. As the DTAB concentration is increased beyond 75% the hexagonal phase transforms into the super hexagonal phase with a much higher value (9.02 nm) of the lattice parameter (Fig. 7(a)).

At high surfactant/DNA concentrations, the hexagonal phase is again observed at low DTAB concentrations. At [DTAB]=10%, the system has a lattice parameter of 5.27 nm. On increasing the concentration of DTAB, transition from a hexagonal to a square phase is observed. The square phase at [DTAB]= 60% has a lattice parameter of 4.26 nm (Fig. 7(b)).

The changes in the SAXS patterns of DTAB-DNA complexes with NaCl concentration can be understood in terms of salt-induced growth of DTAB micelles. At low salt the DTAB micelles are known to have an ellipsoidal shape[10]. These micelles cross-link the DNA strands forming the complex. Since the DNA-DNA separation would depend on the orientation of the micelles, we can expect these complexes to have only short-range orientational order, resulting in broad SAXS peaks. The addition of NaCl would result in the growth of these micelles into rod-like objects, which can pack better between the DNA strands, resulting in long-range translational order of these complexes. MTAB can form rod like micelles and can therefore pack better than DTAB and arrange themselves in a hexagonal lattice. Therefore the SAXS data show sharp peaks in the case of MTAB-DNA complexes. In the presence of a strongly binding counterion, transition from a hexagonal to a square phase is observed. This can be understood from the fact that, for forming the square phase the amount of counterion needed to be released is only half as compared to the case of hexagonal phase. Therefore the tosylate counterion being strongly bound to the surfactant micelle favours square phase.

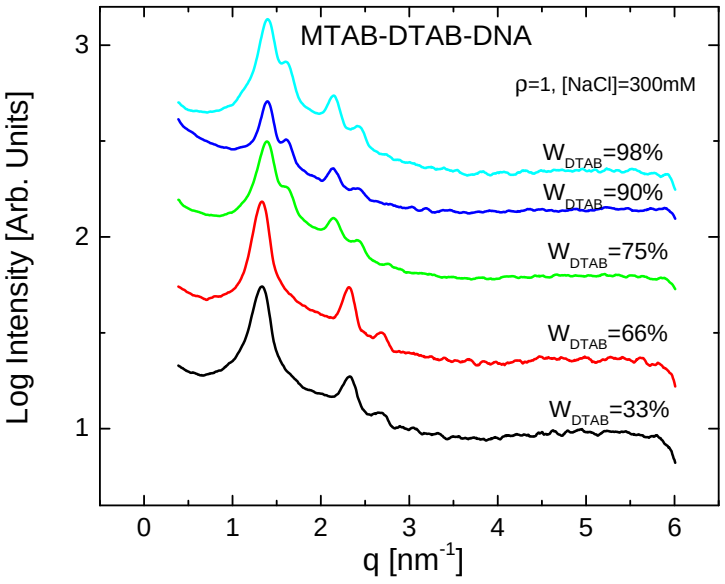

(a)

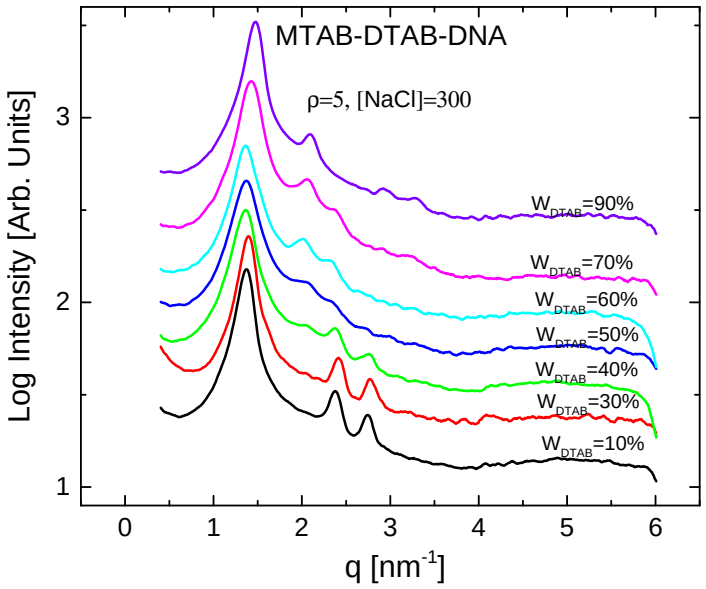

(b)

FIGURE 7: SAXS data obtained from MTAB-DTAB-DNA complexes at [NaCl]=300 mM with increasing DTAB concentration at (a) ρ=1 and (b) ρ=5. At ρ=1, a transition from an hexagonal phase to a super-hexagonal phase is observed, and at ρ=5, an hexagonal phase to a square phase transition is observed on increasing DTAB concentration.

However, in the case of MTAB-DTAB complexes, as the relative concentration of DTAB is slowly increased, the diameter of the micelle reduces. This is due to the smaller chain length of DTAB compared to MTAB. As can be seen from the electron density map of the hexagonal phase (Fig. 6(b)), each micelle in this structure is surrounded by 6 DNA strands. Decreasing the micellar diameter, decreases the DNA-DNA separation, thereby increasing the mutual repulsion between the DNA strands. On the other hand in the square phase, there are only 4 DNA strands surrounding each micelle[9]. Hence for the same micellar size, DNA-DNA repulsion can be expected to be much higher in the hexagonal phase compared to the square phase, resulting in a hexagon to square transition. At low surfactant/DNA molar ratios, hexagonal phase transforms into a super hexagonal phase with a much higher value of the lattice parameter. The super hexagonal phase is the $\sqrt{3} \times \sqrt{3}$ super lattice of the hexagonal phase.

The main results of the thesis are summarised in the last chapter, which also discusses a few directions for further studies.

Bibliography

[1] Overbeek, J. T. G. and Voorn M. J. Phase separation in polyelectrolyte solutions. Theory of complex coacervation. *J. Cell.Comp. Physiol.* **1957**, *49*(S1), 7-26.

[2] Wang, M. and Wang, Y. Development of amphiphile coacervation in aqueous solution. *Soft Matter* **2014**, *10*, 7909-7919.

[3] Roux, D. and Safinya, C. R. A synchrotron x-ray study of competing undulation and electrostatic interlayer interactions in fluid multimembrane lyotropic phases. *J. Phys.* **1988**, *49*, 307-318.

[4] Pabst, G.; Rappolt, M; Amenitsch, H and Laggner, P. Structural information from multilamellar liposomes at full hydration: Full q-range fitting with high quality x-ray data *Phys. Rev. E.* **2000**, *62*(3), 4000-4009.

[5] Perkin, S.; Kampf, N. and Klein, J. Long-range attraction between charge-mosaic surfaces across water. *Phys. Rev. Lett.* **2006**, *96*, 038301.

[6] Szilagyi, I.; Trefalt, G.; Tiraferri, A.; Maroni, P. and Borkovec, M. Polyelectrolyte adsorption, interparticle forces, and colloidal aggregation *Soft Matter* **2014**, *10*, 2479-2502.

[7] Israelachvili, Jacob N. *Intermolecular and surface forces* Third edition, Elsevier, **2011**.

[8] Krishnaswamy, R.; Pabst, G.; Rappolt, M.; Raghunathan, V. A. and Sood, A. K. Structure of DNA-CTAB-hexanol complexes *Phys. Rev. E.* **2006**, *73*,

031904.

[9] Radhakrishnan, A. V.; Ghosh, S. K.; Pabst, G.; Raghunathan, V. A. and Sood, A. K. Tuning DNA-amphiphile condensate architecture with strongly binding counterions *Proceedings of the National Academy of Sciences* **2012**, *109*(17), 6394-6398.

[10] Bergström M. and Pedersen J. S. Structure of pure SDS and DTAB micelles in brine determined by small-angle neutron scattering (SANS) *Phys. Chem. Chem. Phys.* **1999**, *1*, 4437-4446.

List of Publications

- **Meera Thomas**, K. Swamynathan, and V. A. Raghunathan, *Salt-induced swelling transitions of a lamellar amphiphile-polyelectrolyte complex* J. Chem. Phys. 150, 094903 (2019).
- Lachit Saikia, Tanmoy Sarkar, **Meera Thomas**, V. A. Raghunathan, Anirban Sain, and Prerna Sharma, *Curvature instability of chiral colloidal membranes on crystallization* Nature Communications 8, 1160 (2017).

Contents

List of Figures

List of Tables

Chapter 1

Introduction

This thesis describes studies on the structure and interactions in surfactant - polyelectrolyte complexes. In water, surfactant molecules spontaneously self assemble to form different kinds of aggregates. The phase behaviour of such self assembled structures in the presence of a macromolecule, a strongly biding counterion etc. has a lot of interest in various fields. In this chapter, we give an introduction to surfactants, polyelectrolytes and an overview of self assembly of soft matter systems. Then we will discuss the associative interaction of oppositely charged macroions, leading to the formation of complexes, which is the theme of this thesis. The underlying interactions driving these processes, experimental techniques for identification of the structure and phase behaviour and SAXS data analysis are also discussed.

1.1 Surfactants

Amphiphilic molecules are those which contain both, a hydrophilic part and a hydrophobic part. Surfactant molecules are amphiphilic molecules, which possess the property of reducing the surface tension of water. They contain hydrophobic hydrocarbon chain(s) and a hydrophilic head group which can

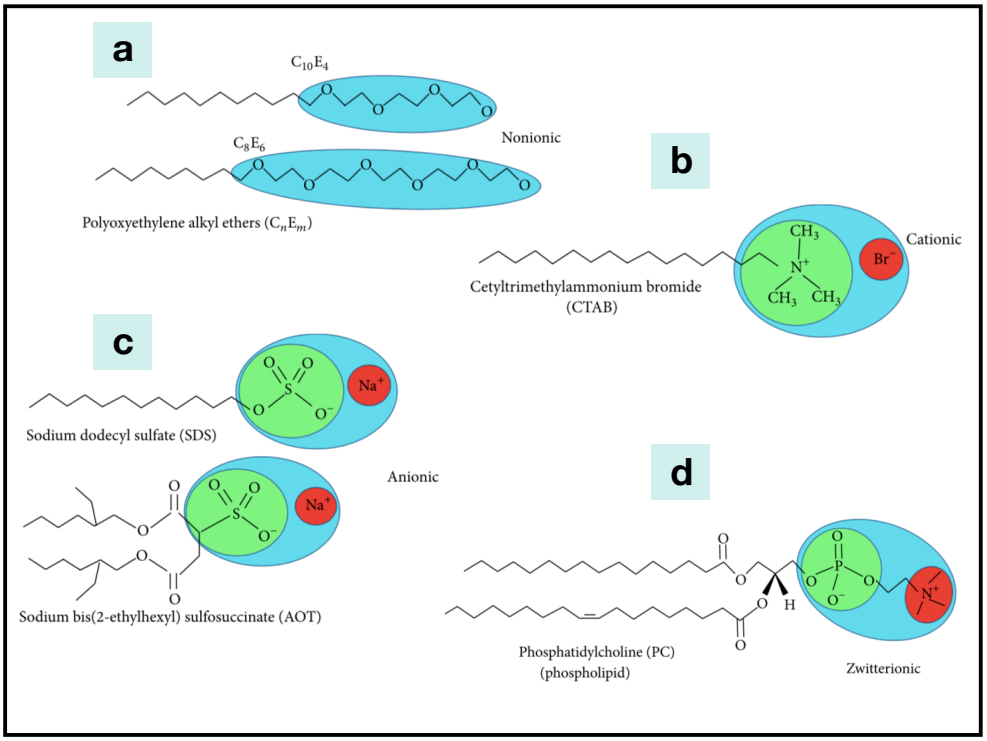

FIGURE 1.1: Chemical structures of (a)non-ionic, (b)cationic, (c)anionic and (d)zwitterionic amphiphilic molecules[3].

be non-ionic, cationic or anionic. In water, these molecules can self-assemble to form aggregates, with the hydrophobic part oriented away from water and the head group close to water[1–3].

Polyoxyethylene alkyl ethers (C_nE_m), are a common example of nonionic surfactants which contain 'm' number of hydrophilic oxyethylene units and 'n' methyl groups in the hydrophobic part[3]. Surfactants which acquire a positive charge in aqueous solution are cationic (eg. cetyltrimethylammonium bromide (CTAB)) and which acquire a negative charge are anionic (eg. Sodiumdodecyl sulfate (SDS), Sodium bis(2-ethylhexyl) sulfosuccinate (AOT))[3]. Phospholipids are zwitterionic molecules containing both cationic and anionic centres attached to the same molecule (eg. phosphatidylcholine (PC))[3]. As the concentration of monomer in the solution is increased above the critical micellar concentration (CMC), they self assemble to form micelles. This phenomenon is further discussed in the upcoming sections.

1.1.1 Hydrophobic Effect

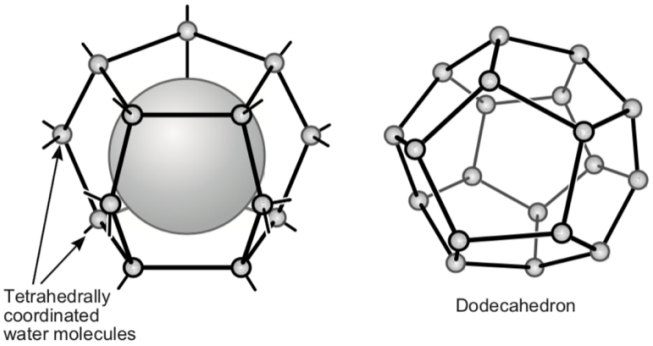

FIGURE 1.2: Water molecules form Clathrate cages and gas hydrates around small nonpolar (hydrophobic) solute molecules, leading to a reduction in entropy[1].

Water is a polar molecule which has the ability to form inter-molecular hydrogen bonds. In water, non-polar solute is unable to create any hydrogen bond with water molecules. In the presence of such a non-polar solute, the water molecules can pack around by re-ordering themselves, without breaking any of its hydrogen bonds. This solution is energetically less costly. In the liquid state, water molecules on an average can participate in 3 to 3.5 hydrogen bonds. However, in the presence of the solute, they have a coordination number of around 4, which results in a reduction in entropy. Since the entropy loss is more that the energy gain, this configuration is unfavourable. Therefore non-polar solutes are sparingly soluble in water. This phenomenon is referred to as the hydrophobic effect[1–3]. Thus the hydrophobic effect plays an important role in self-aggregation of non-polar (hydrophobic) molecules in many soft matter systems.

1.1.2 Self Assembly

One of the most important properties of soft matter systems is their ability to self assemble. Let us consider a dilute solution of self-assembled micelles,

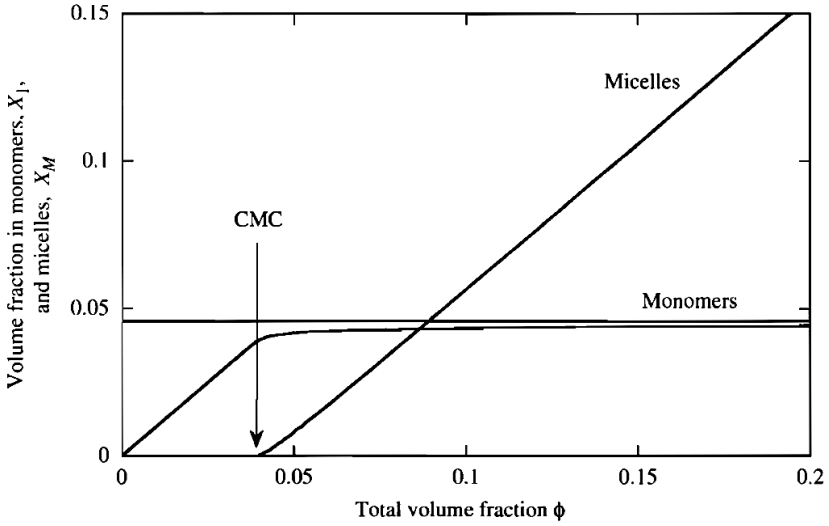

FIGURE 1.3: The amphiphile volume fraction in monomers X_1 and micelles X_M as a function of total volume fraction of amphiphiles, when all the micelles have an aggregation number $\sim M$ taken from 2.

with aggregation number varying from 1 to N. From the equilibrium considerations, the chemical potential of a monomer in each aggregate should be the same. This can be represented by the equation[1,2]

$$\mu_0^N + (1/N)kTlog(X_N/N) = \mu_0^1 + kTlogX_1 \tag{1.1}$$

where N=1, 2, 3,...., μ_0^N is the mean interaction free energy per molecule. The total concentration of surfactant in the solution, C is given by $C = \sum_N X_N$ The concentration of aggregate of size N is given by

$$X_N = N[X_1 e^{(\mu_0^1 - \mu_0^N)/kT}]^N \tag{1.2}$$

$$X_N = N[X_1 e^{\alpha}]^N \tag{1.3}$$

where $\alpha = (\mu_0^1 - \mu_0^N)/kT$ is a positive constant[1].

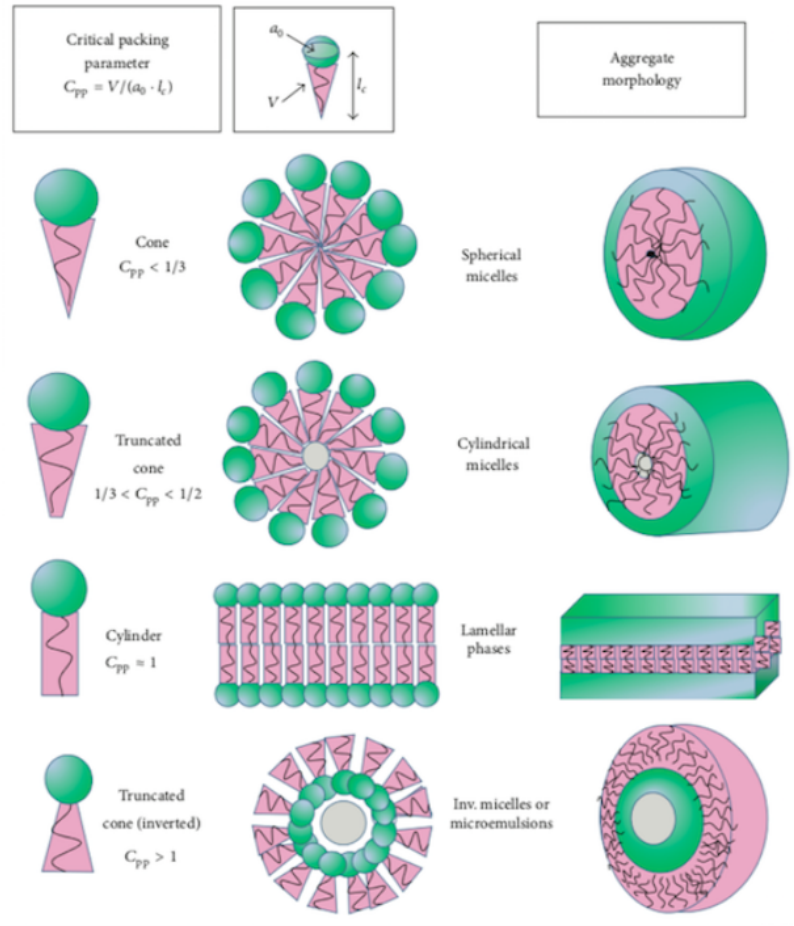

FIGURE 1.4: Critical packing papameter C_{pp} of amphiphile molecules and the corresponding possible aggregate structures that can be predicted.[31].

When the concentration of monomers in the solution X_1 is small, then X_N is also small, $C \sim X_1$. As the value of X_1 approaches $(X_1)_{crit} = e^{-\alpha}$, X_N increases, resulting in the formation of aggregates. This critical concentration of monomers $(X_1)_{crit}$, above which aggregation occurs is defined as critical micellar concentration (CMC). Therefore above CMC, monomer concentration remain more or less unchanged and further addition of solute molecules results in the formation of more aggregates[1]. Fig. 1.3 shows that below CMC, the amphiphilic molecules exist as monomers and above CMC, they exist as micelles with the monomer concentration increasing very slowly.

In aqueous solution these amphiphilic molecules can self-assemble to form several kinds of aggregates like spherical micelles, cylindrical micelles, bilayers etc[1–3]. The shape of the aggregates can be classified depending on the geometry of the molecule. Based on the geometry, one can define a parameter called the critical packing parameter ($C_{pp} = v/a_0 l_c$), where v is the volume of the hydrocarbon chain, a_0 is the optimal head group area and l_c is the hydrocarbon chain length[1]. The optimum head group area is determined by various interactions present in the system.

In case of a spherical micelle, the packing parameter of the amphiphile can be found to be $C_{pp} \leq 1/3$[1]. For cylindrical micelles, $1/3 \leq C_{pp} \leq 1/2$[1]. For $C_{pp} \sim 1$, the favoured configuration is a bilayer[1]. In the last case a typical example is a phospholipid molecule containing two hydrocarbon chains. Fig. 1.4, shows different kinds of aggregates that can be formed by the surfactant or lipid molecules. Surfactants with smaller head group areas or large C_{pp} can form inverted micellar phases.

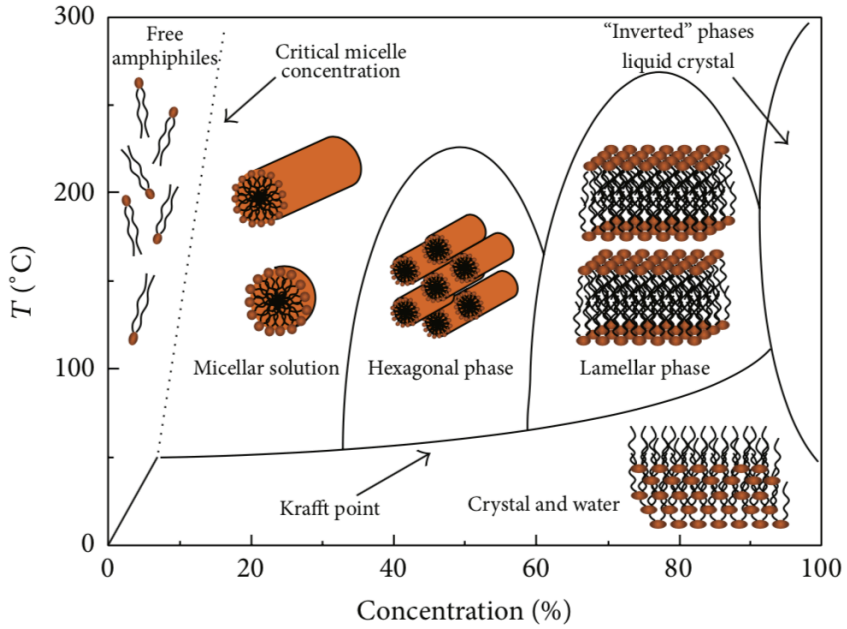

FIGURE 1.5: Typical phase diagram of surfactant - water system[3].

1.1.3 Phase behaviour of the self assembled aggregates

A typical phase diagram of a surfactant solution is depicted in Fig. 1.5. Below CMC, the surfactant molecules exists as free monomers. Krafft point, shown in the figure is the temperature below which the surfactant molecules are insoluble in water. As the concentration increases above CMC, micelles start forming. Initially at low surfactant concentrations above CMC, an isotropic dispersion of micelles form. As the concentration is gradually increased, a hexagonal phase made up of cylindrical micelles arranged in a hexagonal lattice is observed. At yet higher surfactant concentrations, lamellar phase made up of stacks of bilayers is observed. At very high concentrations of surfactant, inverted phases with negative curvature is observed. It is also possible to observe several complex phases like bicontinuous cubic in a narrow range of concentrations.

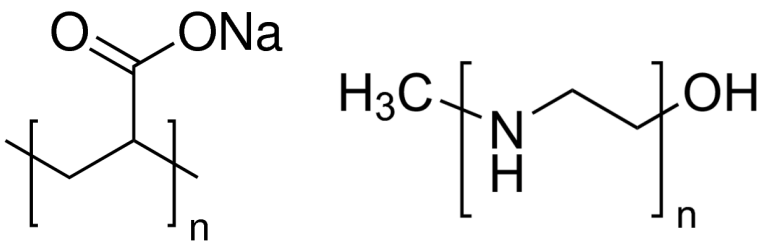

(a) (b)

FIGURE 1.6: Examples of (a) anionic polyelectrolyte Polyacrylic acid (sodium salt) and (b) cationic polyelectrolyte Polyethylene imine (linear).

1.2 Polyelectrolytes

Polyelectrolytes (PE) are polymers having charged groups, which ionise in water by releasing ions (counterions). Broadly, polyelectrolyte can be classified into strong or weak, based on its ionisation properties. A strong polyelectrolyte dissociates completely in solution where as, the dissociation of a weak polyelectrolyte depends on the solution pH, counter-ion concentration etc. Many biomolecules like DNA, RNA, polysaccharides etc. are polyelectrolytes. Due to the charges present on them, long range repulsive electrostatic interactions exists between polymer chains. Oppositely charged polyelectrolytes can associate to form complex.

When the charge density on a polyelectrolyte is high, the electrostatic interactions become stronger and as a result the counterions stay near the vicinity of the polyelectrolyte. This phenomenon, which arises from the competition between entropy and energy is called counterion condensation. The effective separation between two adjacent charges in such a polyelectrolyte is given by Bjerrum length ($l_b = e^2/\epsilon_0 K_B T$). Bjerrum length is the length for which the thermal energy is equal to the Coulombic energy between two

unit charges. At room temperature this distance is around 0.70 nm in water[7]. The correlations of tangent vectors along a polymer chain decay exponentially, and the characteristic length of this decay is called the persistence length, l_p[9]. It is a measure of the flexibility of a polymer.

Salt is yet another factor playing an important role in these systems. At very low ionic strengths the screening length is much larger than the chain dimensions, so the polyion can be regarded as unscreened. As long as the screening length remains large compared to the chain size, increasing the salt concentration does not affect the intramolecular interactions and the chain extension is constant, corresponding to its maximum value depending on the charge on the chain. When the screening length becomes comparable to the chain dimensions, the interactions within the chain start to be screened and the flexibility increases[10]. The extent of screening in these cases is given by the Debye length κ^{-1}, which will be discussed later in this chapter.

In the presence of oppositely charged self assembled surfactant molecules, polyelectrolytes can form complexes releasing their condensed counterions. As already mentioned, DNA is an anionic polyelectrolyte. The persistence length of DNA is around 30 - 50 nm, even at very high salt concentrations[10].

1.3 Interaction forces

Most of the interaction forces, present in soft matter systems have an electrostatic origin, though their manifestations are very diverse. In this section we discuss these interaction forces briefly.

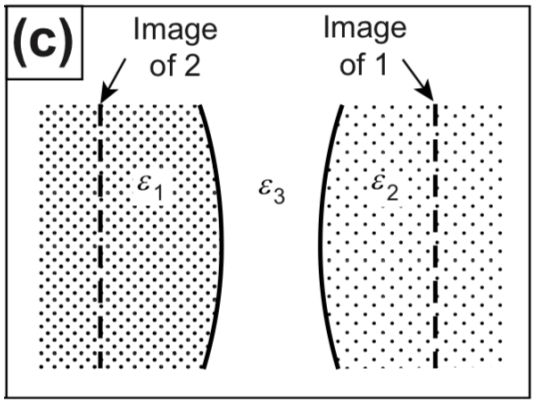

FIGURE 1.7: Two media of dielectric constants $\epsilon_1$and ϵ_2 separated by a medium of dielectric constant ϵ_3[1].

1.3.1 Van der Waals Interaction

Van der Waals force is an attractive force which exists between any pair of atoms or molecules. This force exists even in the absence of any charge or dipole moment. It arises from the interaction between fluctuating dipoles of each atom[1,10]. The interaction between two objects can be understood as the sum of all interactions between pairs of atoms. For a pair of atoms the Van der Waals potential can be written in the form $W(r) = -C/r^6$. In the case of two infinite planar surfaces, separated by a distance D, the Van der Waals interaction energy per unit area can be written as

$$W(D) = -A/12\pi D^2 \tag{1.4}$$

where A is the Hamaker constant. An expression for Hamaker constant, A in terms of dielectric constants is given by Lifshitz theory as follows[1]

$$A = \frac{3kT}{4}\frac{(\epsilon_1-\epsilon_3)(\epsilon_2-\epsilon_3)}{(\epsilon_1+\epsilon_3)(\epsilon_2+\epsilon_3)} + \frac{3h}{4\pi}\int_{\nu 1}^{\infty}\frac{(\epsilon_1(i\nu)-\epsilon_3(i\nu))(\epsilon_2(i\nu)-\epsilon_3(i\nu))}{(\epsilon_1(i\nu)+\epsilon_3(i\nu))(\epsilon_2(i\nu)+\epsilon_3(i\nu))} \tag{1.5}$$

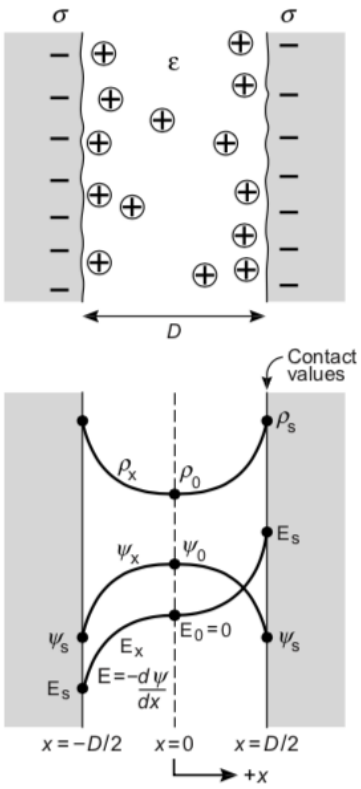

FIGURE 1.8: Two negatively charged surfaces separated by a distance D in water[1].

where ϵ_1, ϵ_2 and ϵ_3 are the static dielectric constants of media 1, 2 and 3 respectively (Fig. 1.7), $\epsilon(i\nu)$ are the values of ϵ at imaginary frequencies. This is the interaction energy per unit area of one of the surfaces, interacting with the infinite area of the opposite surface. Even though the interaction energy between a pair of atoms is very weak, due to the additive property, this energy increases, as the macroscopic size of the body increases[1,10].

1.3.2 Electrostatic Double Layer Interaction

Ionic surfactants have ionisable groups which can release ions (counterions) into the aqueous solution thereby acquiring a charge. In the case of a cationic surfactant like didodecyldimethyl ammonium bromide (DDAB), the molecule ionises to give negatively charged Br^- (*counterion*), and the

DDA^+ forms the positively charged bilayer. In these systems and also in other charged soft matter systems, electrostatic interaction play an important role. The system on the whole is electrically neutral, due to the presence of equal number of oppositely charged ions. These counterions screen the electrostatic interaction in these systems. Some of them may bind to the charged surface strongly, giving rise to a *Stern* layer and the rest form a *diffuse electric double layer*[1,10]. An expression for this concentration profile is calculated below.

In the absence of added electrolyte:

Consider two charged surfaces separated by a distance D, where ψ is the electrostatic potential and ρ is the number density of ions of valency z at any point x between two surfaces (Fig. 1.8). The chemical potential of an ion can be written as[1]

$$\mu = ze\psi + kTlog\rho \tag{1.6}$$

Using the condition that at equilibrium the chemical potential is the same everywhere in the solution, we obtain the Boltzmann distribution of counterions at any point x, from Eqn. 1.6[1]

$$\rho = \rho_0 \, exp(\frac{-ze\psi}{kT}), \tag{1.7}$$

where ρ_0 is the number density of ions at zero potential. Then the Poisson's equation can be written as[1]

$$\frac{d^2\psi}{dx^2} = \frac{-ze\rho}{\epsilon_0\epsilon} \tag{1.8}$$

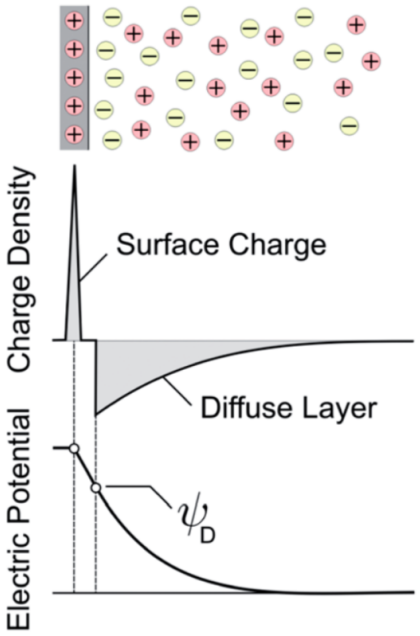

FIGURE 1.9: A charged surface with its electric double layer and its corresponding charge density and electric potential[8].

where ϵ_0 and ϵ are the permittivity of free space and relative permittivity of the medium respectively. Combining the above equations, we obtain the Poisson-Boltzman equation, which can be written as[1]

$$\frac{d^2\psi}{dx^2} = \frac{-ze\rho_0}{\epsilon_0\epsilon} exp(\frac{-ze\psi}{kT}) \tag{1.9}$$

In the presence of added electrolyte:

In practice, we deal with cases where a surface is in contact with an electrolyte solution (Fig.1.9). In such cases both positive and negative ions are present. Let us consider a charged surface, in an electrolyte solution. Let us denote the ionic species present as i, with corresponding valencies z_i. The fundamental equations we derived above are true for the ionic species present in the solution. In this case, we can rewrite the equation 1.9 as[1]

$$\sum_i \rho_{xi} = \sum_i \rho_{\infty i} + \frac{\epsilon_0\epsilon}{kT}(\frac{d^2\psi}{dx^2}) \tag{1.10}$$

where $\rho_{\infty i}$ is the ionic concentration of ions i in the bulk. For 1:1 electrolyte, the potential at a distance x can be written as[1],

$$\psi(x) = \frac{4kT/e}{\gamma} e^{-\kappa x} \tag{1.11}$$

where,

$$\gamma = Tanh \frac{e\psi_0}{4kT} \tag{1.12}$$

At high potentials $\gamma \sim 1$. At potentials less than 25mV, the exponential in Eqn. 1.11 can be expanded, keeping only the leading terms. Then $\psi(x)$ reduces to the Debye-Huckel approximation, given by Eqn. 1.13[1],

$$\psi(x) = \psi_0 e^{-\kappa x}, \tag{1.13}$$

where κ^{-1}, is the Debye screening length, where κ is given by[1,10]

$$\kappa = \sqrt{\frac{2e^2\rho_0 z^2}{\epsilon\epsilon_0 kT}} \tag{1.14}$$

The counterion concentration decay exponentially from the charged surface. This characteristic decay length is called the Debye length κ^{-1}. The magnitude of κ^{-1} solely depends on the property of the solution and not on the property of the charged surface[1,10]. For monovalent salts, the Debye length in terms of the molar concentration of salt, C is given by

$$\kappa^{-1} = \frac{0.304}{\sqrt{C}} \quad nm \tag{1.15}$$

Between two planar surfaces of constant potential, the electric double layer interaction free energy per unit area $W(D)$ is given by

$$W(D)_{ed} = \frac{64\pi\epsilon_0\epsilon(kT/e)^2}{2\pi} Tanh^2(\frac{e\psi_0}{4kT})\kappa e^{-\kappa D} \tag{1.16}$$

From the equation 1.16, it is clear that the electrostatic interaction decay exponentially, with characteristic decay length, Debye length κ^{-1}[1].

1.3.3 Undulation Repulsion Interaction

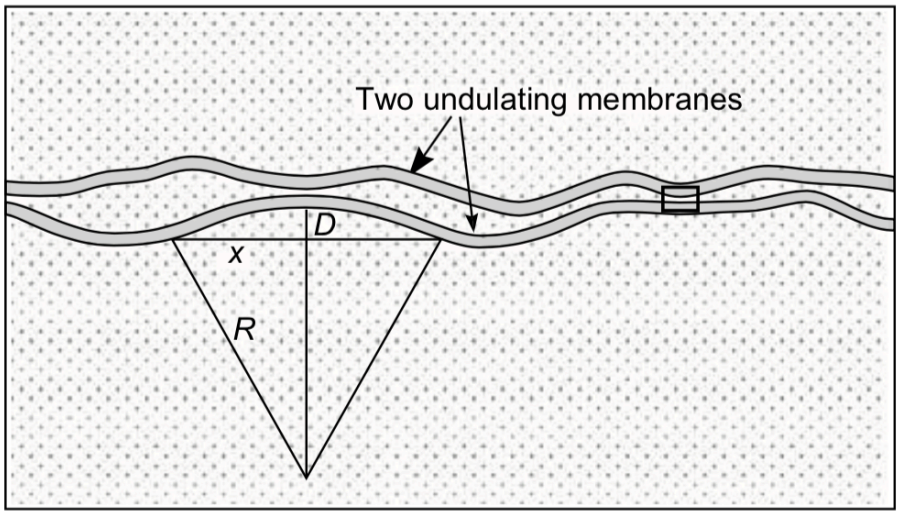

FIGURE 1.10: The thermal undulations of elastic bilayer membranes[1].

Helfrich said in his paper "A special feature of planar fluid layers is their freedom to escape into the third dimension, e.g. by thermal undulations"[11]. For example, bilayer membranes can be compared to elastic sheets, prone to thermal fluctuations or undulations (Fig. 1.10)[11]. When these membrane fluctuations are confined by another membrane or a boundary the thermal undulations of the membrane try to push the neighbouring membrane[1]. So they feel repulsive pressure[1]. This long range repulsive interaction is called the Helfrich undulation repulsion interaction[1,11]. This repulsive interaction

is very sensitive to the membrane's bending rigidity. The interaction energy of two undulating membranes of bending modulus K, separated by a distance D, at a temperature T is given by the expression[1]

$$W(D)_{und} = \frac{3\pi^2(kT)^2}{128KD^2} \tag{1.17}$$

Bending rigidity of charged bilayers also has a significant contribution from electrostatic interactions. Therefore in water (absence of electrolyte screening), charged membranes remain flat and rigid, because they have large elastic constants. Addition of electrolyte, screen charges on the membrane thereby reducing the bending modulus[9].

1.4 Experimental Techniques

1.4.1 X-Ray diffraction

X-rays are electromagnetic radiation whose wavelength ranges from 0.01 nm to 10 nm. When x-rays fall on a material, they are scattered by the electrons present in it. As a result the amount of scattering encountered by the x-rays depends on the electron density distribution of the irradiated material. The scattered radiation from the material interferes to form the observed diffraction pattern.

The theory of x-ray diffraction[12,13] is briefly discussed in this section. Fig. 1.11 shows a plane wave of amplitude ϕ_o and wave vector $\vec{\kappa}_o$ incident on a point scatterer. Then the incident wave can be written as

$$\phi_{in} = \phi_o e^{i\vec{\kappa}_o.\vec{r}} \tag{1.18}$$

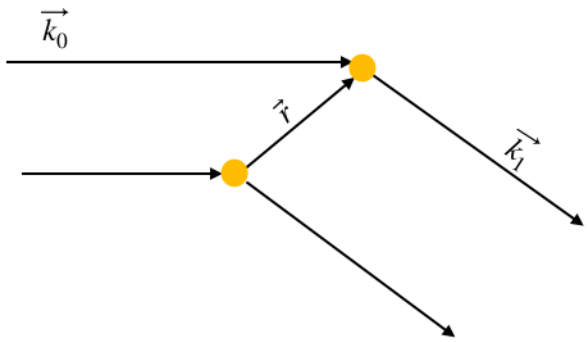

FIGURE 1.11: Figure depicting scattering from two scattering centres separated by a distance $\vec{r}$. $\vec{k_0}$ and $\vec{k_1}$ are the incident and scattered wave vector respectively.

The scattered wave amplitude ϕ_{sct} at a distance $\vec{R}$ where $\vec{R} >> |\vec{r}|$ is given by the equation

$$\phi_{sct} = (\phi_o s/R)e^{i(\kappa.R - \vec{q}.\vec{r})} \tag{1.19}$$

where s is the scattering length density and $\vec{q} = \vec{\kappa_1} - \vec{\kappa_o}$ is the scattering vector. $\vec{\kappa_1}$ is the scattering vector in the direction of $\vec{R}$. For a sample consisting of N scatterers, the total scattering amplitude can be given by

$$\phi_{tot} = (\phi_o s/R)e^{i\kappa R} \sum_{n=1}^{N} e^{-i\vec{q}.\vec{r_n}} \tag{1.20}$$

For a sample with an electron density $\rho(\vec{r}) = \sum_n \delta(\vec{r} - \vec{r_n})$, the scattering amplitude can be written as

$$\phi_{tot} = (\phi_o s/R)e^{i\kappa R} \int \rho(\vec{r})e^{-i\vec{q}.\vec{r}}dr \ . \tag{1.21}$$

This on the other hand is the Fourier transform of the electron density of

the scattering medium. Multiple scattering is assumed to be negligible. The scattered intensity is the square of the above equation and is given by

$$\begin{aligned} I(q) &= |\phi_{tot}|^2 = |[(\phi_o s/R)e^{ikR}\int \rho(\vec{r})e^{(-i\vec{q}\cdot\vec{r})}d\vec{r}]|^2 \\ &= A|F(q)|^2 \end{aligned} \tag{1.22}$$

where $F(q) = \int \rho(\vec{r})e^{-i\vec{q}\cdot\vec{r}}$ and A is a constant independent of q. A crystal has a periodic arrangement, which can be represented as the convolution of a lattice function ρ_l and a basis function ρ_b.

$$\rho(\vec{r}) = \rho_l \circledast \rho_b \tag{1.23}$$

The lattice structure can be defined as a set of delta functions given by,

$$\rho_l(\vec{r}) = \sum_k \sum_l \sum_m \delta(r - w\vec{a} - t\vec{b} - p\vec{c}) \tag{1.24}$$

where, $\vec{a}, \vec{b}, \vec{c}$ are the basis vectors and w, t, p are integers. Taking the Fourier transform of 1.23, we get

$$\begin{aligned} F(q) &= F_l(q)F_b(q) \\ I(q) &= A^2|F_l(q)|^2|F_b(q)|^2 \end{aligned} \tag{1.25}$$

where,

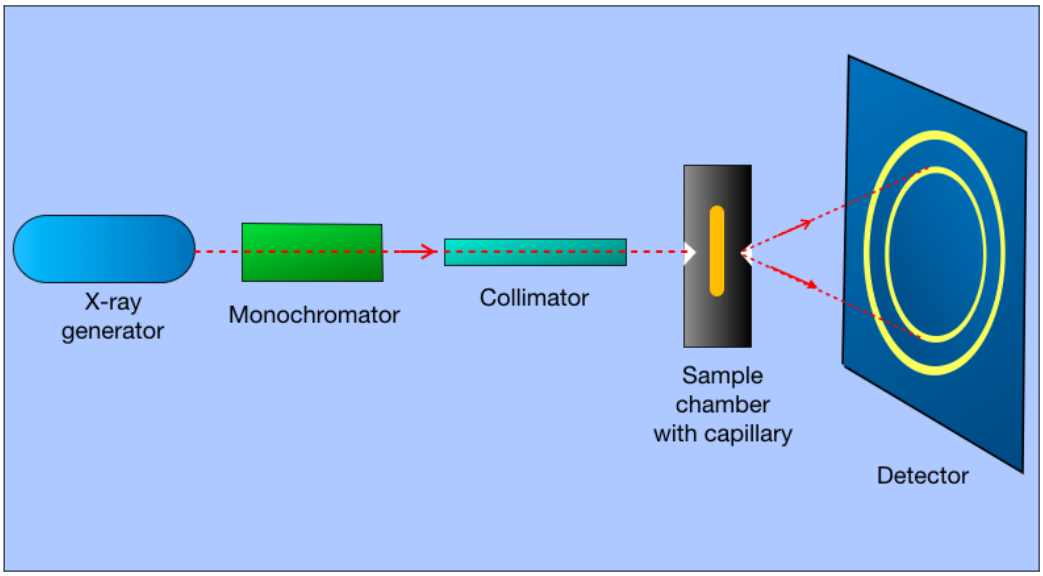

FIGURE 1.12: Schematic of the experimental set up used for x-ray diffraction study.

$$F_l(q) = \sum_h \sum_k \sum_l \delta(q - ha^* - kb^* - lc^*)$$
$$F_b(q) = \int e^{-i\vec{q}.\vec{r}} \rho_b(\vec{r}) d\vec{r} \tag{1.26}$$
.

$F_l(q)$ is the Fourier transform of the lattice and $F_b(q)$ is the Fourier transform of the basis. The square of the function $F_b(q)$ decides the intensity of the peaks of the diffraction pattern.

The observed intensity I_o is then corrected for factors like polarization and geometry. A polarization factor $P = (1 + Cos^2 2\theta)/2$ arises from the unpolarised nature of the incident beam. Yet another factor is related to the geometry of the detector and nature of the sample, which can be denoted as m. For unaligned samples, the intensity of peaks will be distributed in a shell of radius q. If the detector which collects the data is one dimensional,

then the observed intensity is multiplied by q^2 and if the detector is two dimensional (the spherical shell is cut along a plane, resulting in a ring), the observed intensity is obtained by circular integration of the intensity of the rings and then further multiplied by q. Thus the corrected intensity $I_{corr}(q)$ can be given by,

$$I_{corr}(q) = APmI_o(q) \tag{1.27}$$

where $m = q^2$ in the case of 1D detectors and $m = q$ in the case of 2D detectors.

For our studies, we used the Hecus S3-Micro small angle x-ray scattering system. Schematic diagram of a typical SAXS setup is given in Fig. 1.12. A one dimensional position sensitive detector (PSD) was used to collect the scattered rays. The sample to detector distance (D) was fixed at $\sim$ 26.6 cm and the beam path in the sample chamber is evaluated. Calibration was done using silver behanate which has a lamellar structure with a spacing of 5.84 nm. This system has a built-in temperature controller, which has a range from -20°C to 120°C. Typical exposure time was 30 to 90 minutes, depending on the scattering strength of the sample.

1.4.2 Polarising Optical Microscopy

Polarising optical microscope (POM) is used to identify several liquid crystalline phases. Since liquid crystals are anisotropic, they exhibit birefringence. The samples are generally taken in between a coverslip and glass slide or in a rectangular capillary. When such liquid crystal samples are

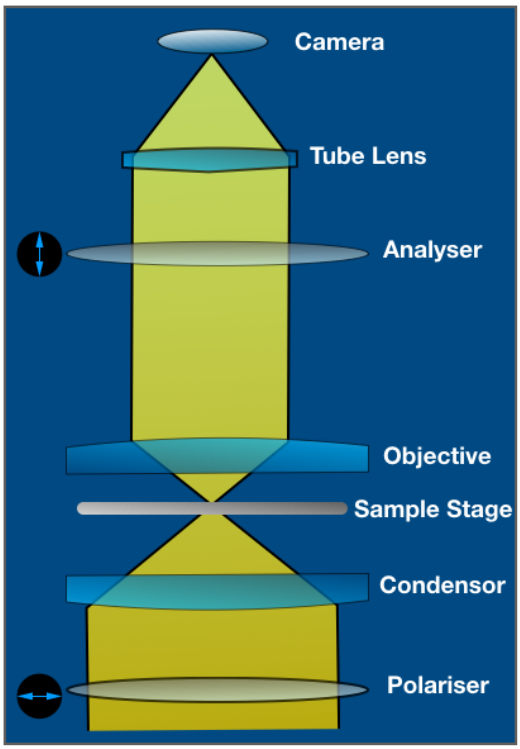

FIGURE 1.13: The schematic of a polarising optical microscope.

observed between crossed polarisers using POM, they exhibit characteristic textures. This arises from several defects present in the samples. This is discussed in detail in section 1.5.

POM is very useful to study optically anisotropic materials. Fig. 1.13 shows the schematic of a POM. The light from the bottom of the microscope, passes through a polariser above it. This linearly polarised light is then focused by the condenser onto the anisotropic liquid crystal material kept in the sample stage. The sample stage is connected to a temperature controller, enabling us to study phase transitions in the samples. The extraordinary and the ordinary waves emanating from the sample then pass through the objective, analyser and then an eye piece. For the study of liquid crystals, the polariser and analyser are kept in such a way that their optic axis is perpendicular to each other, or in other words, in crossed position as can be seen from Fig. 1.13. The microscope is equipped with objectives of different magnifications

(10X, 20X and 50X).

1.4.3 Cryogenic Scanning Electron Microscopy

Cryogenic scanning electron microscopy (cryo-SEM) is used for the characterisation of several soft matter and biological systems[14,15], which are ordinarily unstable in the high vacuum of the electron microscope. The cryogenic fixation (generally done by quenching in liquid nitrogen), preserves the sample in its fully hydrated and chemically unmodified state.

For the study, sample is transferred to a cuvette, attached to the sample holder and then quenched in nitrogen slush. This evacuated sample is then transferred to the preparation chamber. The sample is then sublimated to remove any ice and then fractured with a cold knife. The fractured sample is then sputter-coated with platinum and then transferred to the cold stage of the SEM chamber, which is cooled by nitrogen. The temperature is maintained below -170°C at all stages of sample preparation and at -190°C, in the SEM chamber.

The electron beam scans over the object and interacts with the surface of the object, inducing emission of secondary electrons from the surface of the specimen. A secondary electron detector collects the scattered electrons. The brightness of the image obtained, depends on the number of electrons that reach the detector. Additional sensors detect backscattered electrons (electrons that reflect off the specimen's surface) and X-rays (emitted from beneath the specimen's surface).

For our experiments, samples were quenched in liquid nitrogen for cryogenic scanning electron microscopy (cryo-SEM) studies. The frozen samples were then transferred to a PP3000T cryo unit (Quorum Technologies),

maintained at a temperature of -180°C, where they were fractured with a cold knife. The fractured samples were sublimated at -90°C for 5 min and then sputtered with platinum for 90 s to form a few nm thick coating on the fractured surface. Samples were imaged using a Zeiss Ultra Plus Cryo-SEM.

1.4.4 CHNS Elemental Analysis

CHNS elemental analyser helps in determining relative amounts of carbon, hydrogen, nitrogen and sulphur in organic and inorganic materials[16]. A CHNS analyser works in an oxygen-rich environment, based on the classical Pregl-Dumas method. This combustion can be carried out in two ways, static or dynamic. Under static conditions a fixed volume of oxygen is introduced in the combustion tube before the sample is placed in the chamber. In dynamic conditions, oxygen is allowed to flow continuously for a set period of time, while the sample is placed in the chamber.

During the process of combustion ($\sim$ 1100°C), carbon is converted to carbon dioxide, hydrogen to water, nitrogen to nitrogen gas/ oxides of nitrogen and sulphur to sulphur dioxide. Several kinds of absorbents are used to remove any additional combustion products or any of the principal elements, sulphur for example, whose determination is not required at the time. All these gases are then taken to a heated copper chamber using an inert gas medium, to remove any extra oxygen and also convert nitrogen oxides to nitrogen. The next set of absorbents allow passage of only carbon dioxide, water, nitrogen and sulphur dioxide. The gases are then detected using a gas chromatography separation technique. The amount of gas is quantified using thermal conductivity.

1.5 Identification of Lyotropic Liquid Crystalline (LLC) Phases

Liquid crystals are intermediate states of matter observed between the solid crystal phase and isotropic liquid phase, characterised by long range orientational order. Liquid crystals are anisotropic, because they exhibit different physical properties in different directions[17]. In the case of surfactants, they exhibit liquid crystalline phases when mixed in water. They are called Lyotropic Liquid Crystals (LLC). In the case of LLC, several phases are found. Some of the common phases exhibited by LLC materials are hexagonal phase, lamellar phase, inverted hexagonal phase etc. In certain cases they also exhibit nematic, sponge, cubic phases etc. These phases can be identified using several techniques like polarising optical microscopy, x-ray diffraction, cryo-SEM etc. as discussed in the previous section.

Nematic phase : They are characterised by long range orientational order but short range positional order. Fig. 1.14(a)[19] shows the 2 dimensional x-ray scattering data of an oriented nematic sample. If a_o and c_o, are two length scales present in the system (as shown in Fig. 1.14(a))[19] , the scattering data will have peaks corresponding to both of them. The corresponding scattering vectors are $q_1 = 2\pi/a_o$ and $q_2 = 2\pi/c_o$. In POM they exhibit the typical Schlieren texture as shown in Fig. 1.14[18].

Hexagonal phase : Also called columnar phase, they are made up of cylindrical micelles in LLC systems. It has long range translational order in two dimensions and also long range orientational order. In POM they are optically birefringent and often exhibit no sharp features in its texture (Fig. 1.15(b)). The hexagonal phases can be the regular hexagonal phase (H_I)

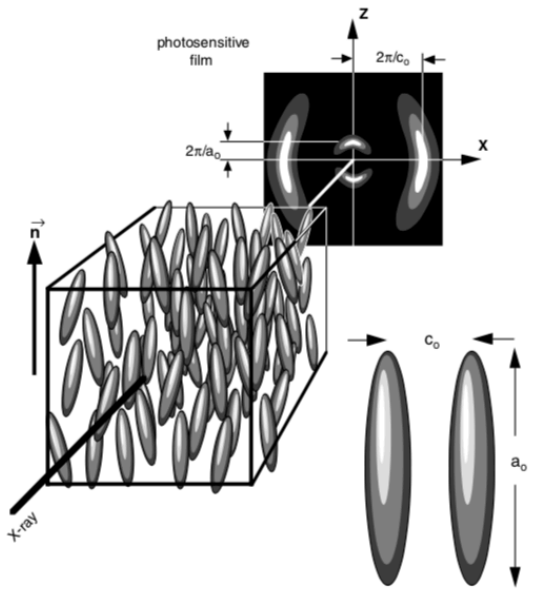

(a)

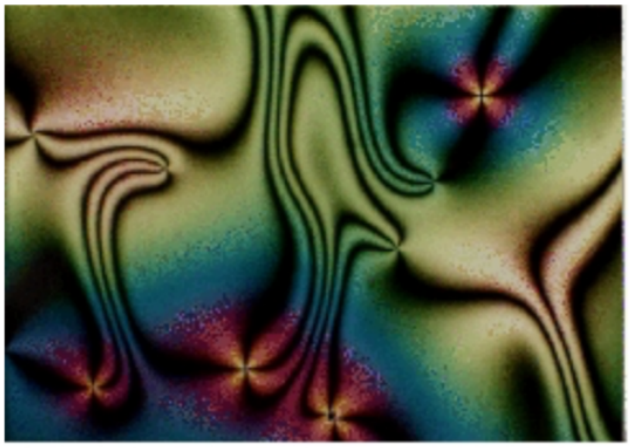

(b)

FIGURE 1.14: (a) SAXS data[19] and (b) POM texture of a nematic liquid crystal sample[18].

(positive curvature) or the inverted hexagonal phase (H_{II}) (negative curvature). In both the cases, x-ray scattering data show that the chains are molten with a broad wide angle peak, and the small-angle x-ray scattering contain Bragg peaks with magnitude of the scattering vector (q) in the ratio $1 : \sqrt{3} : 2$ (Fig. 1.15(a)).

Lamellar phase : These phases have long range translational order along one direction. The SAXS spectrum has peaks in the q ratio $1 : 2 : 3$ (Fig. 1.16(a)), and a broad peak in the wide angle region with a spacing of around 0.45 nm^{-1}, which correspond to the molten hydrophobic chains. Under crossed polarisers they exhibit birefringence with typical oily streak texture (Fig. 1.16(b)). The lamellar sheets can also curl up to form multilamellar vesicles (MLV) as shown in Fig.1.17, eradicating its edges. These MLVs exhibit Maltese cross texture. Cryo-SEM can reveal these structures and thus help identify the phases (Fig. 1.18).

Sponge phase : The sponge phase is optically isotropic and therefore doesn't exhibit any birefringence. The SAXS data can be modelled to that of scattering from randomly oriented discs. Fig. 1.19, shows a schematic and SAXS data from a sponge phase. The phase has a broad peak at small angles, whose value L, depends on the cell to cell distance. The details of the analysis will be discussed in section 1.6.2

1.6 Analysis of the scattering data of several soft matter phases

The SAXS data was analysed to obtain the structural parameters of the corresponding phases.

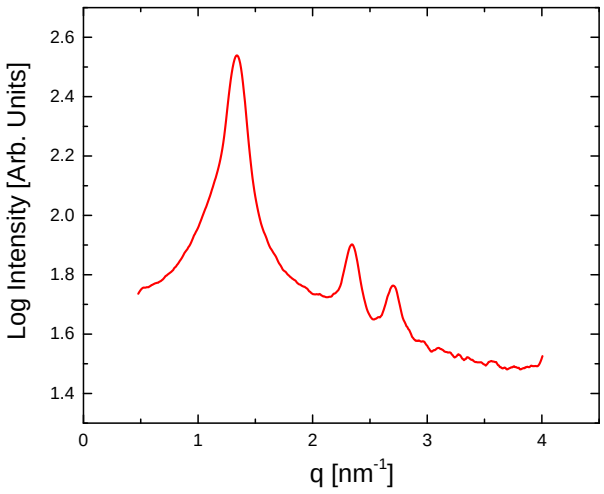

(a)

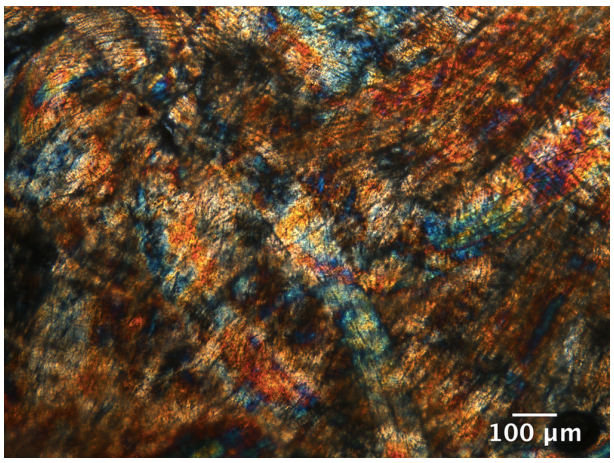

(b)

FIGURE 1.15: (a) SAXS data and (b) POM texture of a hexagonal phase[19].

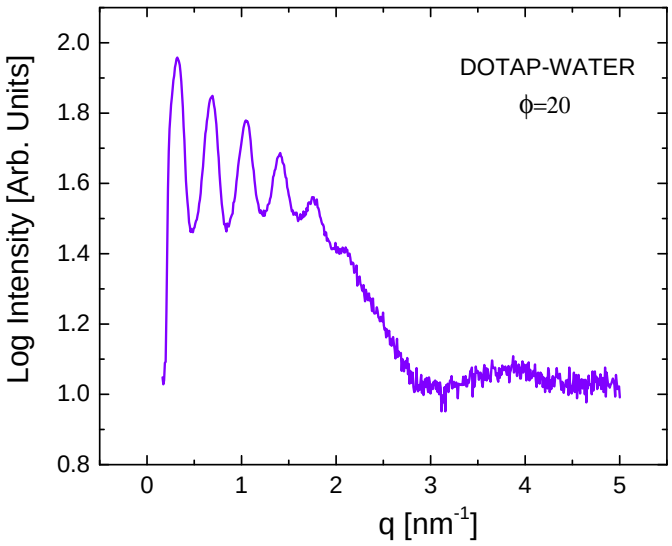

(a)

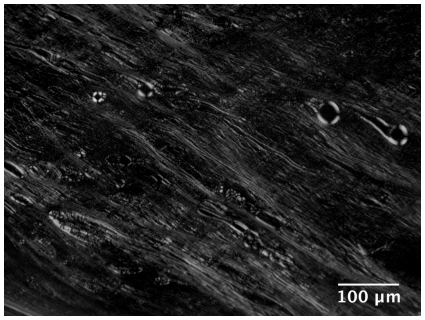

(b)

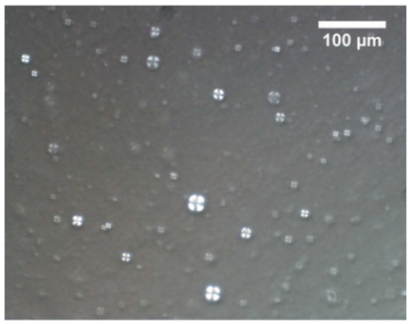

(c)

FIGURE 1.16: (a) SAXS data and (b) oily streak texture obtained from the POM for a lyotropic lamellar phase. (c) The maltese cross texture of multi lamellar vesicle dispersion[19].

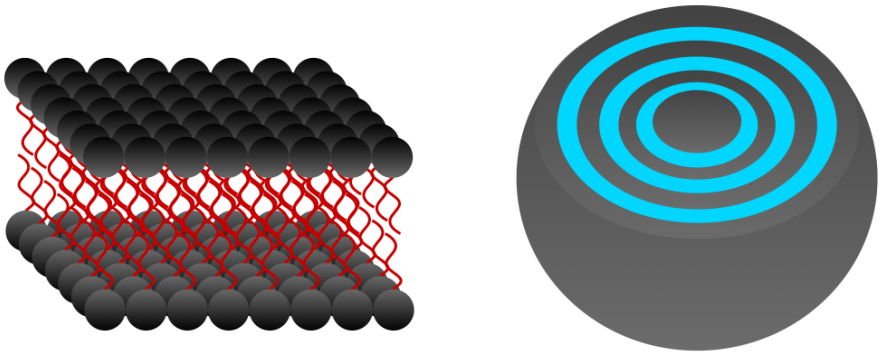

FIGURE 1.17: The structure of a bilayer, the building blocks of lamellar phase (*left*) and a cross section of a multilamellar vesicle (*right*) made up of alternate layers of bilayers and water.

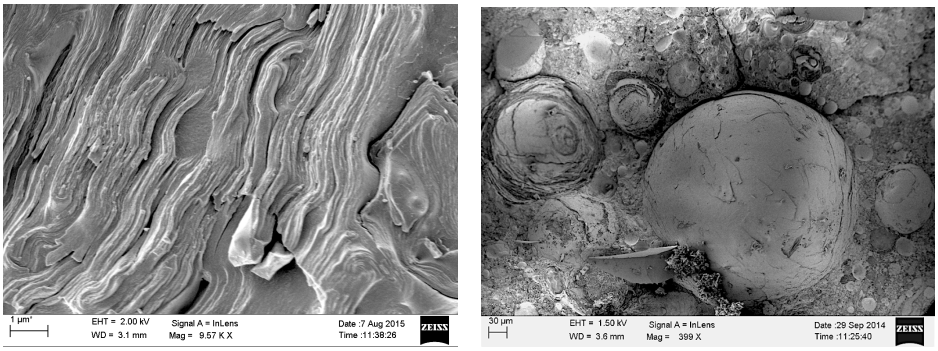

(a) (b)

FIGURE 1.18: Cryo-SEM image showing the layered morphology of (a) a lyotropic lamellar phase and (b) the multi-lamellar vesicles.

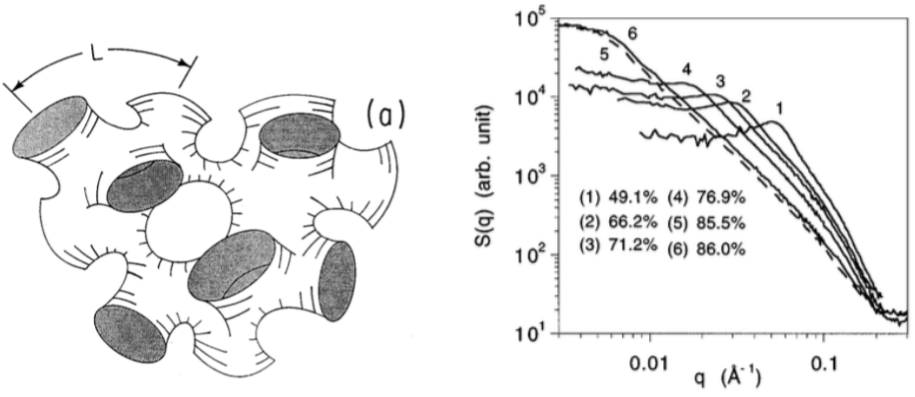

(a) (b)

FIGURE 1.19: The (a) schematic and (b) SAXS data of a sponge phase[20].

1.6.1 Analysis of Lamellar (L_α) phase

The scattering data of the lamellar (L_α) phase was analysed using the procedure described by Pabst et al[21]. They expressed the electron density of the bilayer $\rho(z)$ in terms of three Gaussians, two representing the head-group, with width σ_h, centred at $z = \pm z_h$, and the third one representing the methyl region of the bilayer with a width of σ_c at the bilayer centre, $z = 0$[21] (Fig. 1.20).

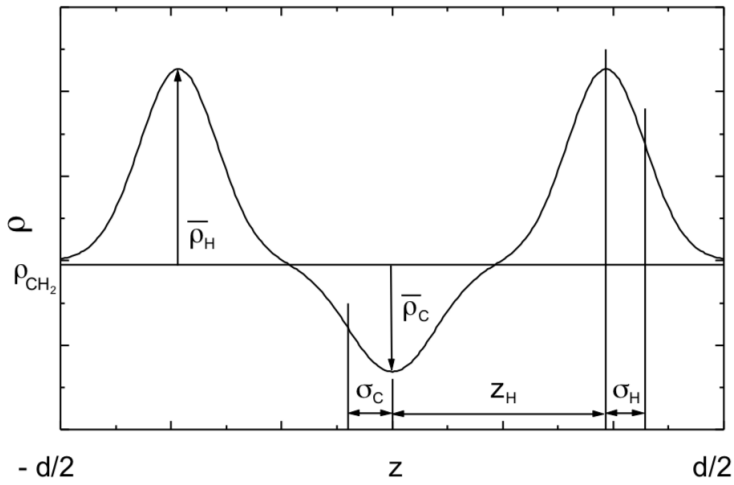

FIGURE 1.20: The three Gaussian model of the electron density profile of a bilayer[21].

$$\rho(z) = \rho_{CH_2} + \bar{\rho_h}[exp(-\frac{(z-z_h)^2}{2{\sigma_h}^2}) + exp(-\frac{(z+z_h)^2}{2{\sigma_h}^2})] + \bar{\rho_c}[exp(-\frac{z^2}{2{\sigma_c}^2})] \tag{1.28}$$

where the electron densities of the head group ρ_h and hydrocarbon region ρ_c are defined relative to the electron density of the methyl group, ρ_{CH_2}. The form factor $F(q)$ is obtained by taking the Fourier transform[21]

$$F(q) = 2\sqrt{2\pi}\sigma_h\bar{\rho_h}[exp(-\frac{{\sigma_h}^2q^2}{2})]Cos(qz_h) + \sqrt{2\pi}\sigma c\bar{\rho_c}[exp(-\frac{{\sigma_c}^2q^2}{2})] \tag{1.29}$$

According to modified Caillé theory, the structure factor S(q) is given by[22]

$$S(q) = N + 2\sum_{k=1}^{N-1}(N-k)Cos(kqd) \times e^{-(d/2\pi)^2q^2\eta\gamma}\pi k^{-(d/2\pi)^2q^2\eta} \tag{1.30}$$

where N is the mean number of coherent scattering bilayers, γ is the Euler's constant, and d the lamellar periodicity. The Caillé parameter, $\eta = q^2 K_B T/(8\pi\sqrt{KB})$, where K and B are the bending and bulk moduli of the lamellar stack, respectively. The model parameters such as σ_c, σ_h, ρ_c/ρ_h, z_h, η, N & N_d are adjusted to get the best fit between the observed and calculated intensity. N_d is the fraction of uncorrelated bilayers, which give rise to diffuse scattering. The scattered intensity is given by

$$I(q) = \frac{S(q)|F(q)|^2}{q^2} + \frac{N_d|F(q)|^2}{q^2} \tag{1.31}$$

where $S(q)$ is the structure factor and $F(q)$ is the form factor of the bilayers. The last term in eqn. 1.31 arises from the diffuse scattering from uncorrelated bilayers[21].

1.6.2 Analysis of Sponge phase

The analysis of the sponge phase was performed following the method of Porcar et al.[23]. The observed scattering intensity from a sponge phase can be expressed as,

$$I(q) = NS(q)P(q), \tag{1.32}$$

where $S(q)$ is the structure factor and $P(q)$ is the form factor of the bilayer discoids and N is the effective density of these discoids. These terms are detailed in the rest of this section. Diffraction data of the sponge (L_3) phase were analysed using the procedure described by Porcar[23]. The Structure factor of a sponge phase can be expressed as[23],

$$S(q) = 1 + C_1 \frac{arctan(\frac{q\xi_1}{2})}{q} + \frac{C_2}{\xi_2^2 + (q - q_c)^2} \tag{1.33}$$

ξ_1 is the correlation length associated with the in-out order parameter[23]. Third term describes the cell-cell correlation with correlation length ξ_2 and an average cell-cell distance $L = 2\pi/q_c$. The scattering data from the L_3 phase is characterised by a broad peak, whose position is given by the scattering vector q_c.

We have used the form factor $P(q)$ for scattering from membrane discoids of thickness (w) with a Gaussian distribution of transverse scattering length density characterised by a radius of gyration σ[23]. An analytical approximation for $P(q)$ of these discoids averaged over random orientations is given by[23],

$$P(q) \approx 4(\pi\sigma^2 Nm)^2 \frac{1 - Cos(qw)exp(\frac{-q^2w^2}{32})/q^2}{q^2\sigma^2 + 2exp(\frac{-q^2\sigma^2}{6})} \tag{1.34}$$

The model parameters such as C_1, ξ_1, C_2, ξ_2, w & σ are adjusted to get the best fit between the observed and calculated intensity.

Bibliography

[1] Jacob N. Israelachvili. *Intermolecular and surface forces*. Elsevier, Amsterdam, 3 edition, 2011.

[2] R.A.L. Jones. *Soft Condensed Matter*. Oxford Master Series in Physics. OUP Oxford, 2002.

[3] Domenico Lombardo; Mikhail A. Kiselev; Salvatore Magazú; and Pietro Calandra. Amphiphiles self-assembly: Basic concepts and future perspectives of supramolecular approaches. *Advances in Condensed Matter Physics*, 2015:151683, 2015.

[4] De Gennes, P.G., Pincus, P., Velasco, R.M., and Brochard, F. Remarks on polyelectrolyte conformation. *J. Phys. France*, 37(12):1461–1473, 1976.

[5] J. Des Cloizeaux. Statistics of Long Chains with Repulsive Interactions. *Physical Society of Japan Journal Supplement, Vol. 26. Proceedings of the International Conference on Statistical Mechanics held 9-14 September, 1968 in Koyto., p.42*, 26:42, 1969.

[6] M. Rubinstein and R.H. Colby. *Polymer Physics*. OUP Oxford, 2003.

[7] Fumio Oosawa. *Polyelectrolytes*. FIND, 1971.

[8] I. Szilagyi, G. Trefalt, A. Tiraferri, P. Maroni, and M. Borkovec. Polyelectrolyte adsorption, interparticle forces, and colloidal aggregation. *Soft Matter*, 10:2479–2502, 2014.

[9] David Andelman. Introduction to electrostatics in soft and biological matter. 01 2006.

[10] R. Dias and B. Lindman. *DNA Interactions with Polymers and Surfactants*. Wiley, 2008.

[11] W. Helfrich. Effect of thermal undulations on the rigidity of fluid membranes and interfaces. *Journal de Physique*, 46(7):1263–1268, 1985.

[12] P.M. Chaikin and T.C. Lubensky. *Principles of Condensed Matter Physics*. Cambridge University Press, 2000.

[13] D. Sherwood. *Crystals, X-rays, and proteins*. Wiley, 1976.

[14] Reinhard Strey, W. Jahn, G. Porte, and P. Bassereau. Freeze fracture electron microscopy of dilute lamellar and anomalous isotropic (l3) phases. *Langmuir*, 6(11):1635–1639, 1990.

[15] H.W Meyer and W Richter. Freeze-fracture studies on lipids and membranes. *Micron*, 32(6):615–644, 2001.

[16] E. Wachberger, A. Dirscherl and K. Pulver, *Microchemical Journal*, 1971, **16**, 318 – 328

[17] P. G. de Gennes and J. Prost. *The Physics of Liquid Crystals*. International Series of Monogr. Clarendon Press, 1995.

[18] D. Andrienko, *Journal of Molecular Liquids*, 2018

[19] P. Oswald and P. Pieranski. *Smectic and Columnar Liquid Crystals: Concepts and Physical Properties Illustrated by Experiments*. Liquid Crystals Book Series. CRC Press, 2005.

[20] Ning Lei, C. R. Safinya, D. Roux, and K. S. Liang. Synchrotron x-ray-scattering studies on the sodium dodecyl sulfate–water–pentanol–dodecane L_3 sponge phase. *Phys. Rev. E*, 56:608–613, Jul 1997.

[21] G. Pabst, M Rappolt, H Amenitsch, and P. Laggner. Structural information from multilamellar liposomes at full hydration: Full q-range fitting with high quality x-ray data. *Phys. Rev. E.*, 62(3):4000–4009, 2000.

[22] R. Zhang, R. M. Suter, and J. F. Nagle, *Phys. Rev. E*, **50**, 5047 (1994).

[23] L. Porcar, W. A. Hamilton, P. D. Butler, and G. G. Warr. Scaling of structural and rheological response of l3 sponge phases in the "sweetened" cetylpyridinium/hexanol/dextrose/brine system. *Langmuir*, 19 (26):10779–10794, 2003.

PART I

Interaction of a Linear Anionic Polyelectrolyte with the Lamellar Phase of a Cationic Surfactant

Chapter 2

Swelling Transition of a Lamellar Amphiphile - Polyelectrolyte Complex

2.1 Introduction

Amphiphilic molecules self-assemble in water into diverse structures due to the hydrophobicity of their hydrocarbon chains[2]. The shape of these aggregates is determined by the packing parameter of the amphiphile, which is discussed in the previous chapter. In the case of ionic amphiphiles the aggregates formed are charged and the spatial distribution of dissociated counterions is well described by the Poisson-Boltzmann theory[2]. In a similar fashion, polyelectrolytes, which are ionic macromolecules, also attain a charge in aqueous solutions by releasing their counterions. Strong polyelectrolytes dissociate completely in solution, whereas the degree of dissociation of weak polyelectrolytes depends on the pH of the solvent[3]. If the linear charge density of these polyions is more than one elementary charge (e) per Bjerrum length[2], $l_b = e^2/(4\pi\epsilon_o\epsilon_r kT)$, then a fraction of the counterions condense back on the polymer backbone[4]. The Bjerrum length is

the separation between two elementary charges in a medium of dielectric constant ϵ_r, at which their electrostatic interaction energy is equal to the thermal energy kT, where k is the Boltzmann constant and T the absolute temperature. In water at room temperature, $l_b = 0.7$ nm. When dispersed in water, ionic amphiphiles associate with oppositely charged polyelectrolytes to form complexes by releasing the condensed counterions.

2.2 Earlier Studies

The amphiphile - polyelectrolyte complex formation can be understood as a consequence of the gain in the translational entropy of the counterions released on complexation[5–8]. This complexation process is similar to coacervate formation, where a colloidal/polymer dispersion phase separates into two immiscible liquid phases, one of them being dense in colloidal/polymer components and the other a dilute aqueous phase. The coacervation process is often classified as simple or complex depending on whether the phase separation is induced by the addition of a simple salt or a macroion, respectively[9–12]. The resulting coacervates are usually disordered and hence optically isotropic. On the other hand, the amphiphile - polyelectrolyte complexes mentioned above are often characterised by long-range orientational order and hence exhibit birefringence.

Adsorption of polyelectrolyte chains onto oppositely charged surfaces is a related process that has been widely studied[13]. It is known to depend significantly on the charge density of the polymer chain, which influences not only the polyelectrolyte-surface interaction but also the mutual repulsion between the polymer chains[14,15]. Attraction between the polyelectrolyte and the adsorbing surface increases with increasing polyelectrolyte charge

density. However, higher charge density also leads to stronger lateral repulsion between the chains adsorbed on the surface. As a result, in the case of highly charged polyelectrolytes, adsorption saturates at very low adsorbed polyelectrolyte mass, resulting in the formation of a thin adsorbed layer[13,16]. The adsorption process often results in overcharging of the substrate by the polymer chains[17–19]. Salt is known to affect the adsorption process significantly. At low salt concentrations the electrostatic repulsion between the polyelectrolyte chains results in the adsorption process saturating at very low amounts of the adsorbed polyelectrolyte. As the salt concentration is gradually increased, more and more polyelectrolyte chains get adsorbed on the bilayer, due to the screening of the electrostatic repulsion between the chains[17,20–23]. This results in an abrupt increase in the adsorbed amount of the polyelectrolyte as its bulk concentration is increased[13,24]. These observations are well described by the DLVO theory which takes into account Van der Waals and electrostatic double layer interactions[18]. The importance of non-DLVO forces, such as steric and bridging interactions, in these systems has also been extensively studied[25,26].

In this chapter we discuss experiments on the influence of the anionic polyelectrolyte, sodium polyacrylate (PAANa), on the lamellar (L_α) phase of the cationic amphiphile, didodecyldimethyl ammonium chloride (DDAC), consisting of a stack of fluid bilayers[27]. Decreasing the water content at constant PAANa/DDAC ratio is found to lead to a collapsed $\rightarrow$ swollen $\rightarrow$ collapsed transition of the lamellar phase. We have studied the influence of several factors, such as the bulk salt concentration, molecular weight of the polyelectrolyte and the bending rigidity of the bilayers, on the phase behaviour of this system, using small angle x-ray scattering, polarising optical microscopy and cryogenic scanning electron microscopy. The phase

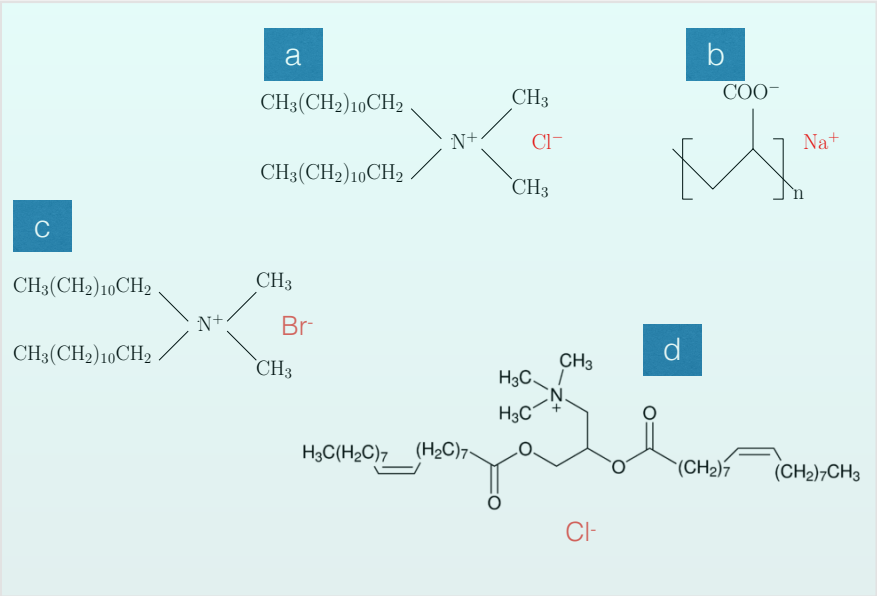

FIGURE 2.1: Chemical structures of (a) DDAC, (b) PAANa, (c) DDAB and (d) DOTAP.

behaviour of some other systems, such as the cationic amphiphile, didodecyldimethylammonium bromide (DDAB) and also a cationic phospholipid in the presence of PAANa, was also studied.

2.3 Materials and Methods

Sodium salt of poly acrylic acid (PAANa) (M_w = 2100, 5100 and 8000), DDAB, sodium bromide (NaBr) and sodium chloride (NaCl) were purchased from Sigma-Aldrich and were used without further purification. 1,2-dioleoyl-3-trimethylammonium-propane (chloride salt) (DOTAP) was obtained from Avanti Polar Lipids. For the preparation of DDAC, N,N dimethyldodecylamine (NND) and 1-chlorododecane (CDD) were obtained from TCI Chemicals and were used as received. DDAC was prepared by following the procedure discussed by A. Cipiciani et al.[28]. It was prepared by quarternizing NND with CDD in ethanol under reflux for four days and was recrystallised

from hexane[28]. Its purity was checked using elemental analysis. Samples were prepared in Millipore water. The polyelectrolyte/amphiphile weight ratio in the sample is denoted by R and the combined weight percentage of DDAC and PAANa in the solution by ϕ. The isoelectric point of the system was calculated to be around R$\sim$0.2, above which the sample is in excess polyelectrolyte regime. To study the effect of dilution, DDAC and PAANa were added to a vial, at a fixed ratio R. Millipore water was added to obtain the desired concentration. To study the effect of salt, samples were prepared in NaCl solutions of varying ionic strengths, at ϕ = 20 and R = 7. DDAB-PAANa2100 samples were also prepared without excess polyelectrolyte in NaCl solutions of varying ionic strengths at ϕ=20, where ϕ is the weight percentage of DDAB+PAANa. DOTAP samples were prepared at ϕ = 20 and R = 7 in the presence of polyelectrolyte and were studied as a function of NaCl concentration. In this case ϕ is the weight percentage of DOTAP+PAANa2100. Vials containing the samples were sealed and equilibrated at 40°C for at least a month. POM, cryo-SEM and SAXS studies were done. The results are discussed in the next section.

2.4 Results

2.4.1 Effect of dilution

DDAC - PAANa2100 mixtures were prepared with ϕ ranging from 20 to 70 at R = 7. At ϕ = 20 the sample contains a white precipitate floating on top of a dilute aqueous solution. A turbid dispersion with a precipitate is observed at ϕ = 25. Samples are also turbid at ϕ = 30 and 40, but without any precipitate. At ϕ = 50 and 60 the samples are phase separated with a clear viscous liquid on top and an aqueous layer at the bottom. The viscosity of

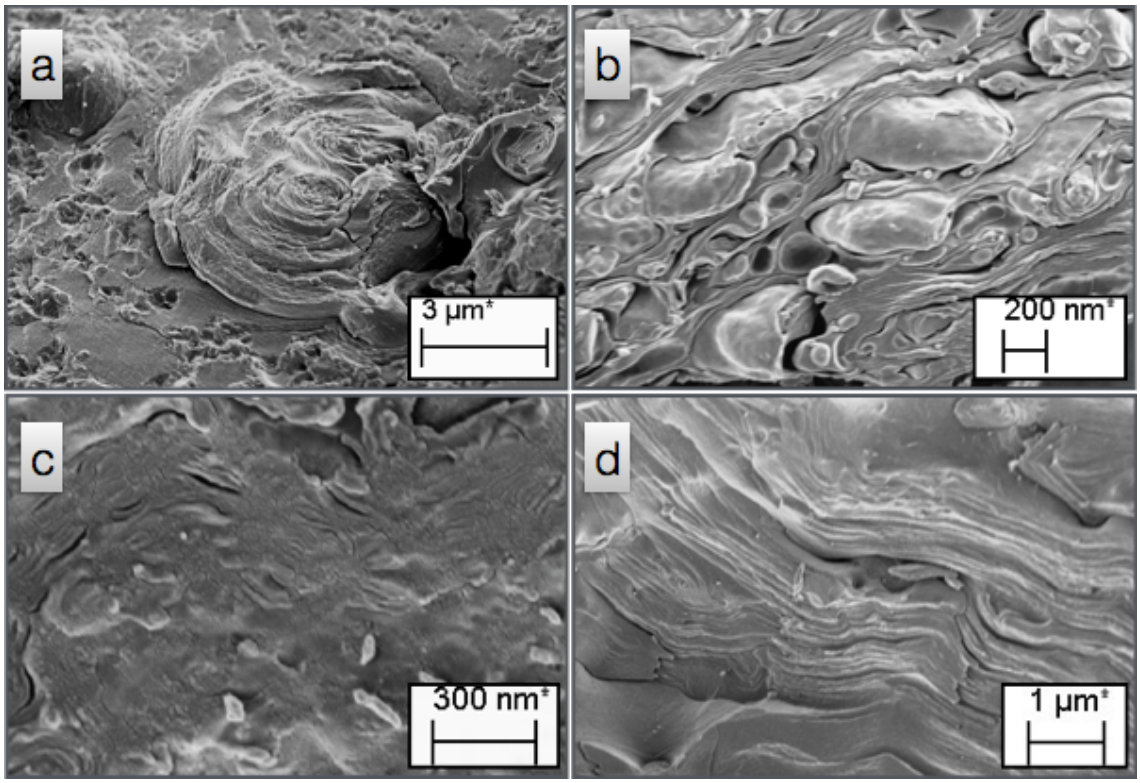

FIGURE 2.2: Cryo-SEM images of DDAC-PAANa2100 complexes, showing layered morphology typical of a lamellar phase at ϕ = 30 (a), 40 (b), 50 (c) and 60 (d).

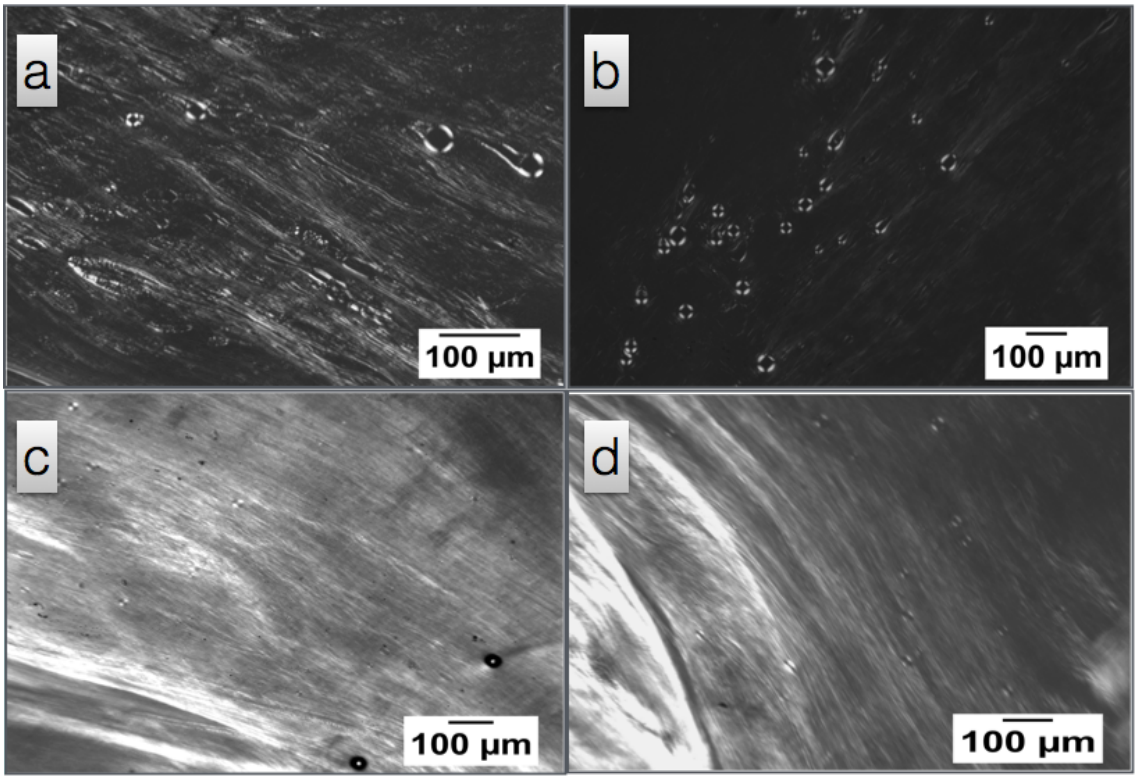

FIGURE 2.3: POM images of DDAC-PAANa2100 complexes showing Maltese cross and oily streak textures, typical of the lamellar phase, at ϕ = 30 (a), 40 (b), 50 (c) and 60 (d).

the top layer is seen to increase with increasing ϕ. At $\phi = 70$ there is a whitish viscous layer (on top) and a viscous aqueous solution of polyelectrolyte at the bottom. The aqueous solution seen in the bottom of the samples consists of excess polyelectrolyte in water (and devoid of any surfactant), since our samples are prepared in the excess polyelectrolyte regime.

Figs. 2.2 and 2.3 show cryo-SEM and POM images of DDAC - PAANa 2100 complexes at different values of ϕ for R = 7. Cryo-SEM images of all the complexes reveal a layered morphology. Their POM images exhibit either a Maltese cross or an oily streak texture, which are typical of the lamellar phase. From these observations we can conclude that the complexes possess a lamellar structure over the range of ϕ studied.

SAXS patterns of these complexes, presented in Fig. 2.4(a), are consistent with a lamellar structure. Values of the lamellar periodicity (d) of the complexes determined from these patterns are given in Fig. 2.5(a). At ϕ = 20 a lamellar phase with d= 3.48 nm is observed. Periodicity of this phase is only slightly higher than the bilayer thickness of DDAC membranes, which is about 2.35 nm[29]. We refer to this as the collapsed lamellar phase L_α^{c1}. At ϕ = 25 a highly swollen lamellar (L_α^s) phase with d= 27.25 nm is found to coexist with the L_α^{c1} phase. At ϕ = 30 the L_α^{c1} phase is not observed and the periodicity of the L_α^s phase is beyond the range accessible with our SAXS system. With further increase in ϕ, $d$gradually decreases from 36.30 nm at ϕ = 40 to 9.89 nm at ϕ = 60. A second collapsed phase (L_α^{c2}) with a slightly smaller periodicity of about 2.9 nm compared to that of the L_α^{c1} phase is observed to coexist with the L_α^s phase at ϕ = 70. These results clearly show the occurrence of a swelling transition of the complexes at $\phi \sim 25$ followed by a de-swelling transition at $\phi \sim 70$.

The samples, especially at low ϕ, are found to have an equilibration time

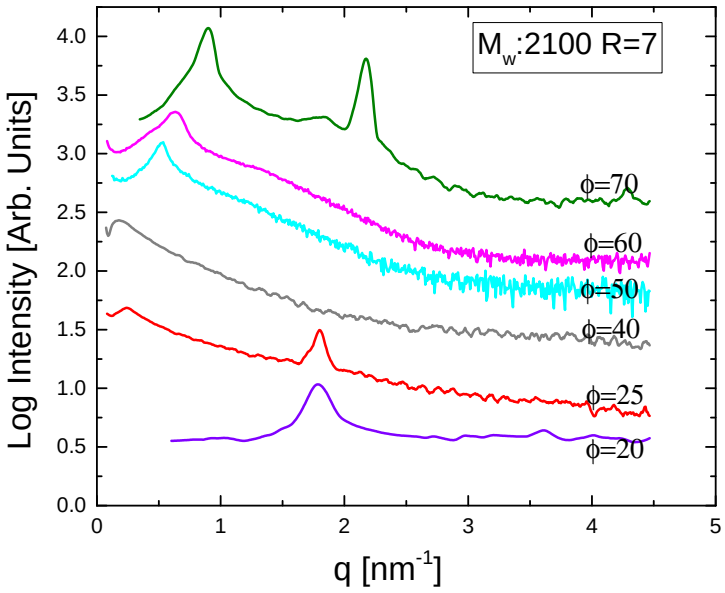

(a)

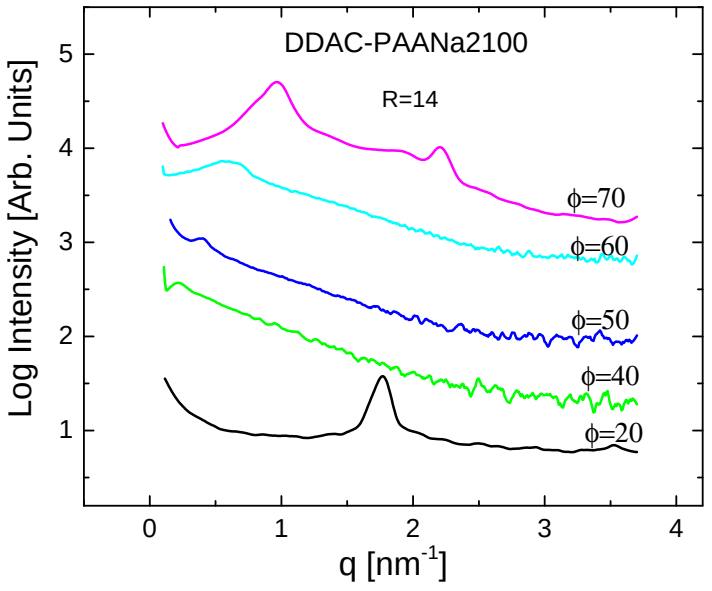

(b)

FIGURE 2.4: SAXS data of DDAC-PAANa2100 complexes in water obtained for different values of ϕ at (a) R = 7 and (b) R = 14.

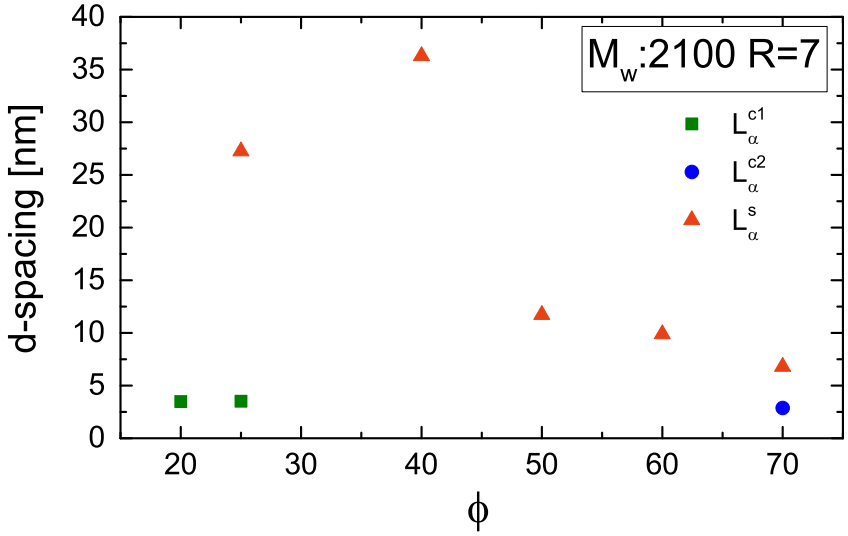

(a)

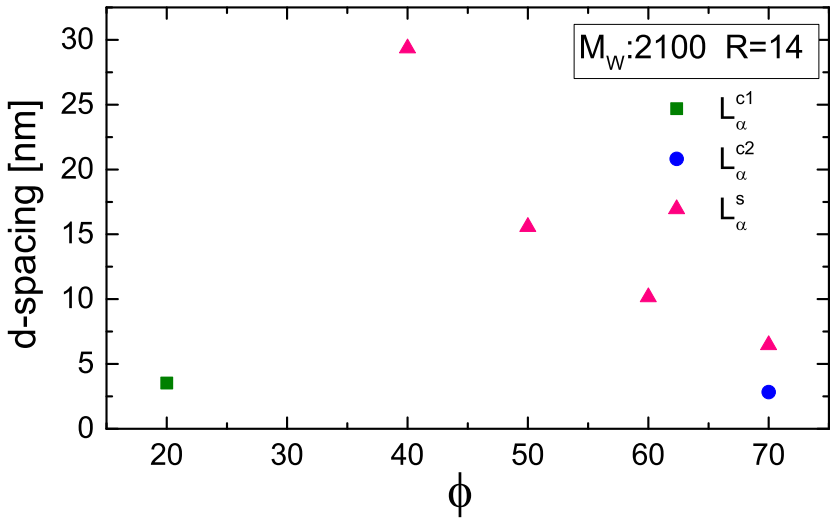

(b)

FIGURE 2.5: Lamellar periodicity, d of the DDAC-PAANa2100-water system, determined from SAXS data for different values of ϕ at (a) R = 7 and (b) R = 14.

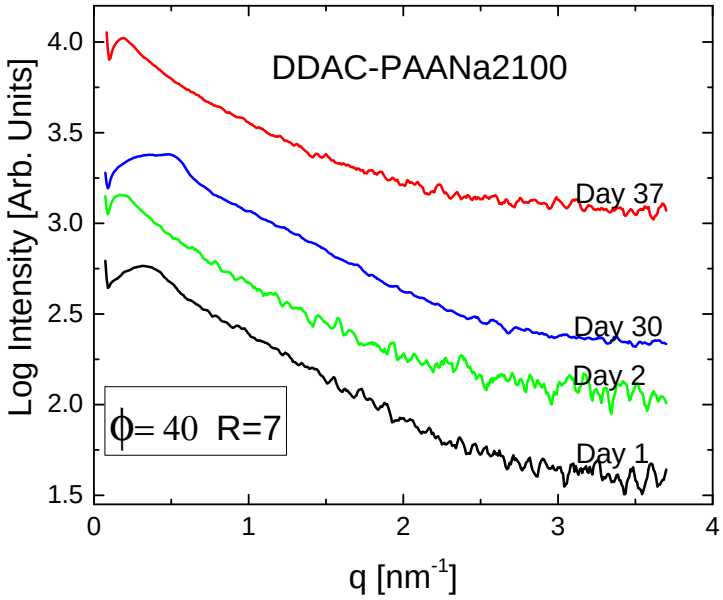

FIGURE 2.6: Time evolution of SAXS patterns of the DDAC-PAANa2100 complexes at R = 7 for ϕ=40 at T = 25 °C.

of around a month. Before the sample reaches equilibrium, the SAXS data of the L_α^s phase evolve slowly, with the peaks gradually becoming sharper (Fig. 2.6). Peak positions are also found to shift slightly over many days. The samples were therefore equilibrated for at least a month before data were collected.

Almost identical behaviour is observed at R = 14 (Fig. 2.4(b)). Variation of $d$with ϕ for these samples is shown in Fig. 2.5(b). Periodicities of some of the samples could not be determined, since the corresponding peaks were inaccessible with our SAXS system.

2.4.2 Effect of salt

As mentioned in the introduction, formation of DDAC-PAANa complexes is accompanied by the release of Na^+ and Cl^- counterions into the solution. Therefore, increasing ϕ at fixed R is essentially equivalent to increasing the

salt concentration in the solution. This suggests that the observed $L_\alpha^{c1} \rightarrow L_\alpha^s$ swelling transition and the $L_\alpha^s \rightarrow L_\alpha^{c2}$ de-swelling transition are consequences of increasing bulk salt concentration in the solution. In order to understand the influence of salt concentration on the swelling behaviour of the complexes two sets of experiments were carried out.

In the absence of excess polyelectrolyte:
In the first set of experiments, DDAC-PAANa complexes were prepared at R = 7 and ϕ = 20 in Millipore water and the precipitate formed was then transferred to NaCl solutions of ionic strength varying from 100 to 1000 mM. This protocol ensures that the salt solution has a negligible concentration of excess uncomplexed polyelectrolyte. SAXS studies were carried out on these samples (Fig. 2.7(a)) after equilibration and their lamellar periodicities are given in Fig. 2.8(a). As can be seen from the figure, the complexes exhibit the L_α^{c1} phase at all salt concentrations, with a periodicity of about 3.5 nm.

In the presence of excess polyelectrolyte:
In the second set of experiments, complexes were prepared in NaCl solutions of ionic strength varying from 75 to 500 mM at R = 7 and ϕ = 20. These samples, therefore, contain excess uncomplexed polyelectrolytes in the bulk. SAXS data is given in Fig. 2.7(b) and the corresponding lamellar periodicities of these samples are shown in Fig. 2.8(b). At 75 mM the L_α^{c1} phase, with d= 3.54 nm, is observed, which suddenly swells at 150 mM to form the L_α^s phase. At 300 mM, the sample is still swollen but we were not able to measure the d-spacing with our SAXS setup. As the NaCl concentration is increased to 400 mM, the complex transforms into the (L_α^{c2}) phase, with d= 3.39 nm.

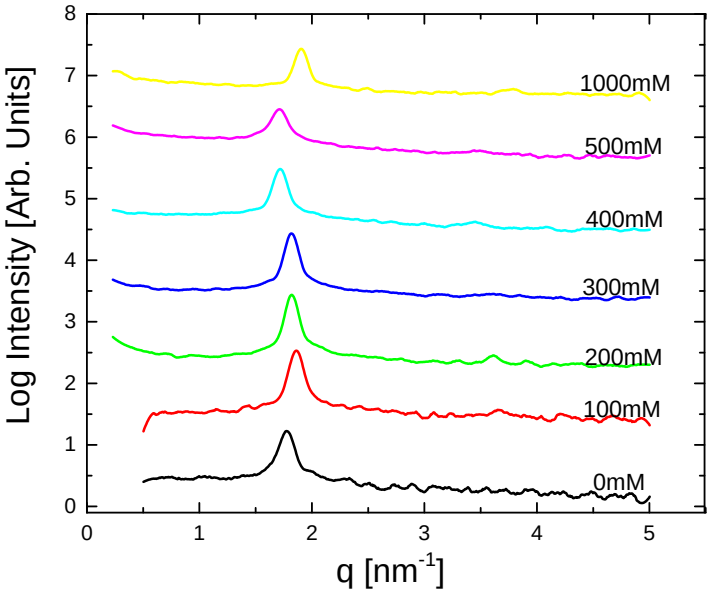

(a)

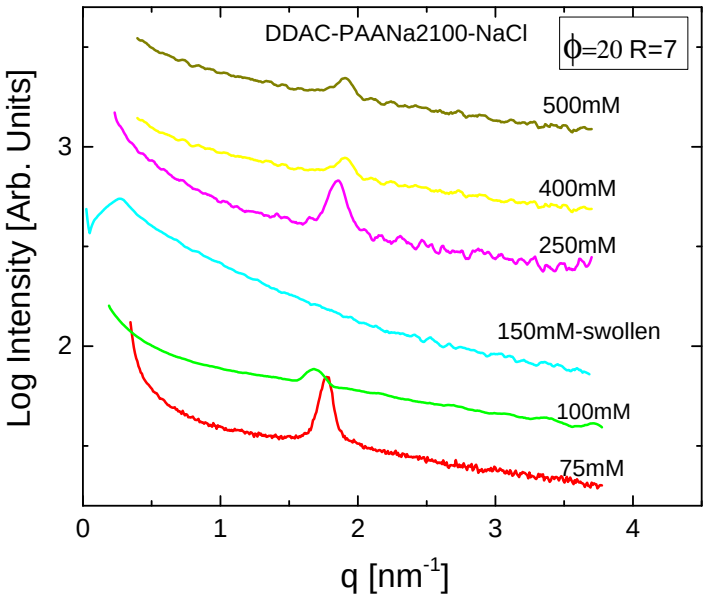

(b)

FIGURE 2.7: SAXS data of the DDAC-PAANa2100-NaCl system at R=7 (a) in the absence of excess polyelectrolyte and (b) in the presence of excess polyelectrolyte. T=25°C

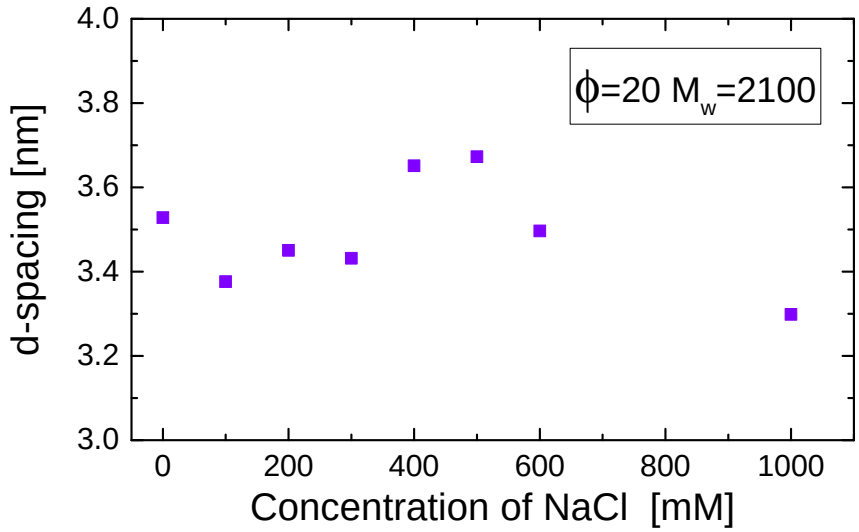

(a)

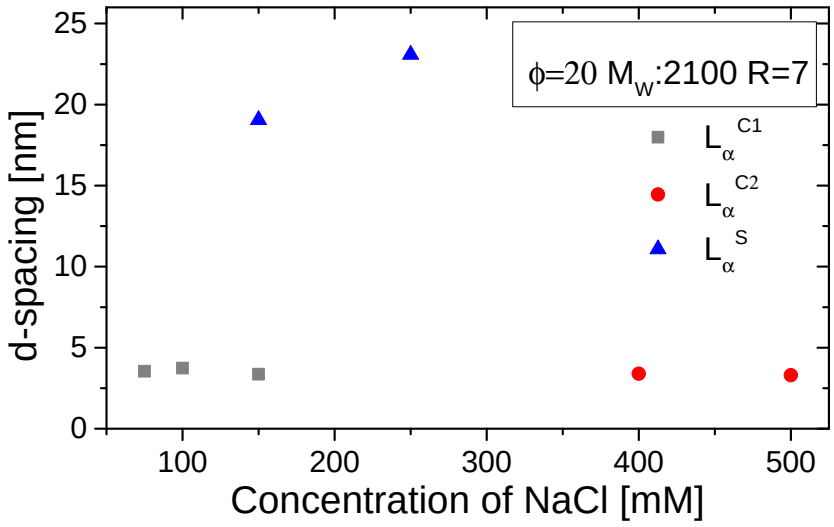

(b)

FIGURE 2.8: Variation of the lamellar periodicity, d of the DDAC-PAANa2100-NaCl system at R=7 (a) in the absence of excess polyelectrolyte and (b) in the presence of excess polyelectrolyte.T=25°C

2.4.3 Effect of molecular weight

In order to check the effect of molecular weight of the polyelectrolyte on the swelling behaviour, studies were carried out with PAANa of molecular weights 5100 and 8000. In the case of PAANa5100, samples were prepared in water with ϕ varying from 20 to 70 at R = 7. SAXS studies of the system (Fig.2.9(a)) show a swelling behaviour similar to that seen with PAANa2100. Lamellar periodicities of the samples obtained from SAXS are given in Fig. 2.10(a). In the case of PAANa8000, the polyelectrolyte was obtained as a 45 wt% solution in water, and hence samples were prepared in NaCl solutions of ionic strength varying from 0 mM to 900 mM at ϕ = 20 and R = 7. Interestingly, these samples exhibit only a collapsed lamellar phase at all salt concentrations as observed from SAXS studies (Fig.2.9(b)). The corresponding lamellar periodicity is depicted in Fig. 2.10(b).

2.4.4 Effect of variation of R

The isoelectric point of the DDAC-PAANa2100 system is estimated to be around around R = 0.2. In order to understand the influence of relative PAANa to DDAC concentration, the structure of DDAC-PAANa complexes was probed as a function of R at ϕ = 20 and 30. At ϕ = 20, SAXS patterns show that the complex remains in a collapsed lamellar phase, irrespective of the value of R. The d-spacing is found to vary from 3.48 nm to 3.68 nm, as R is increased from 7 to 20 (Fig. 2.11(a)). At ϕ = 30 the system is seen to evolve from a collapsed lamellar phase to a swollen lamellar phase as R is increased above the isoelectric point (Fig. 2.11(b)). At R = 0.18, the d-spacing is found to be 3.38 nm. The swollen and collapsed phases, with spacings of 10.44 nm and 3.43 nm, respectively, coexist as R is increased to 0.5. Since the concentration of counterions (Na^+ and Cl^-) released on complexation at ϕ =

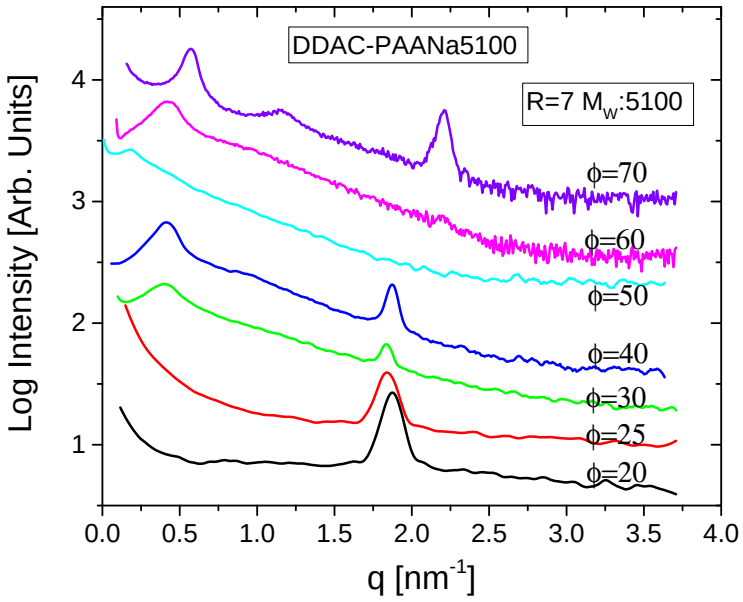

(a)

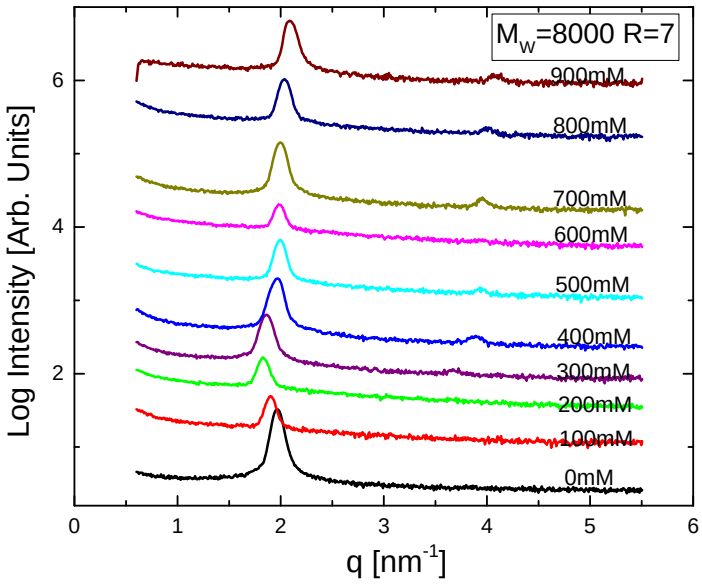

(b)

FIGURE 2.9: SAXS data of the (a) DDAC-PAANa5100-water system as a function of ϕ at R = 7, and the (b) DDAC-PAANa8000-water system as a function of NaCl concentration at R = 7. T=25 °C.

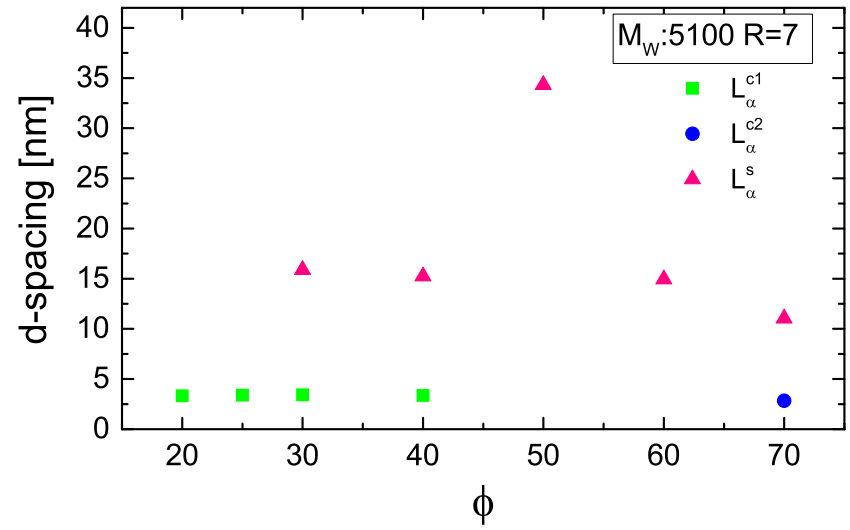

(a)

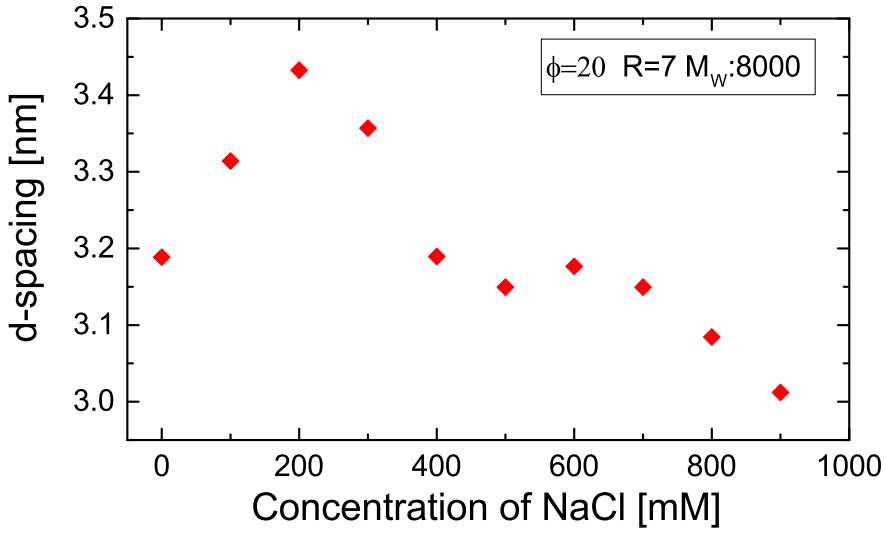

(b)

FIGURE 2.10: Lamellar periodicity, d of the (a) DDAC-PAANa5100-water system as a function of ϕ at R = 7, and (b) the DDAC-PAANa8000-water system as a function of NaCl concentration at R = 7. T=25 $^{\circ}C$.

20 is less than that at ϕ = 30, these observations once again demonstrate the important role of bulk salt concentration in driving the swelling transition.

2.5 Other systems

2.5.1 DOTAP-PAANa2100 system

Studies were also performed on the complexes of charged phospholipid, DOTAP and PAANa2100. The samples were prepared in NaCl solutions whose concentration ranged from 0 mM to 1 M for R=7 and their SAXS data were obtained at room temperature. Fig 2.12(a) and 2.12(b) show the obtained SAXS data and the corresponding d-spacing. The lipid-polyelectrolyte complex doesn't show any swelling in the d-spacing. The isoelectric point for this system was found to be $R \sim 3.0$. At 0 mM, the peak position is around 5.15 nm. As the NaCl concentration is gradually increased from 100 mM to 300 mM, the d-spacing is found to increase from 5.08 nm to 5.22 nm. At 400 mM, the d-spacing slightly decrease to 5.11 nm. At very high concentration of NaCl of 1 M, the d-spacing is found to decrease to 4.85 nm.

2.5.2 Effect of salt in DDAB-PAANa2100 complexes: In the absence of excess polyelectrolyte

Studies were done previously on DDAB-PAANa complexes[1]. A phase diagram[1] from the study is given in Fig. 2.13. At molecular weights 2100 and 5100 of the polyelectrolyte, the complex exhibit a collapsed lamellar phase at high dilution and a swollen sponge phase at low dilution. We have already discussed the importance of excess polyelectrolyte in inducing swelling in the case of DDAC-PAANa complexes. To study the same

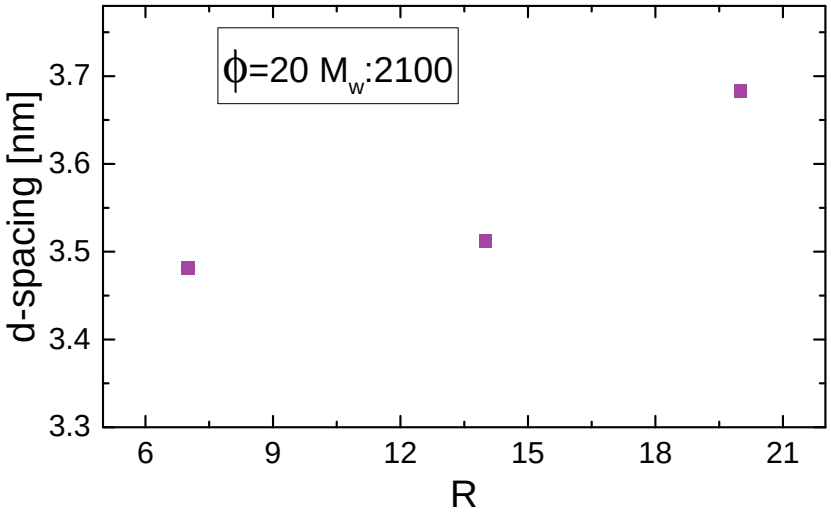

(a)

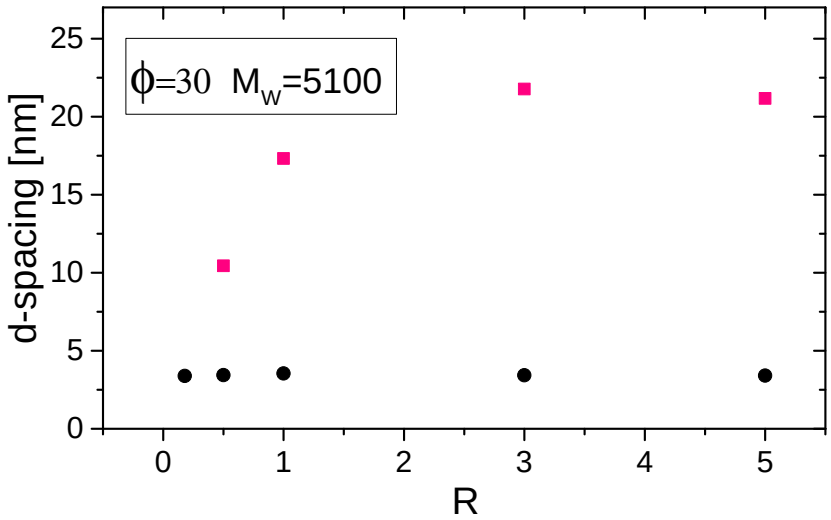

(b)

FIGURE 2.11: Variation with R of the d-spacings of (a) DDAC-PAANa2100 complexes at ϕ=20 and (b) DDAC-PAANa5100 complexes at ϕ=30. T = 25 °C.

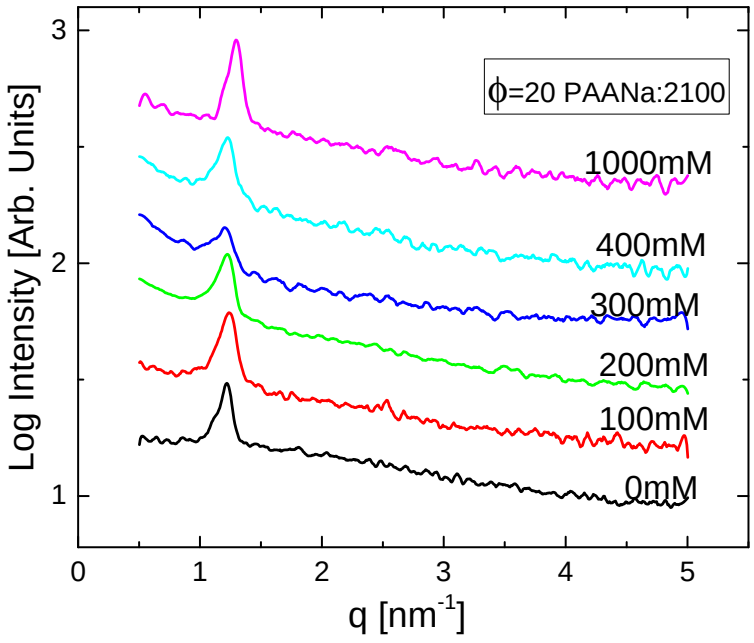

(a)

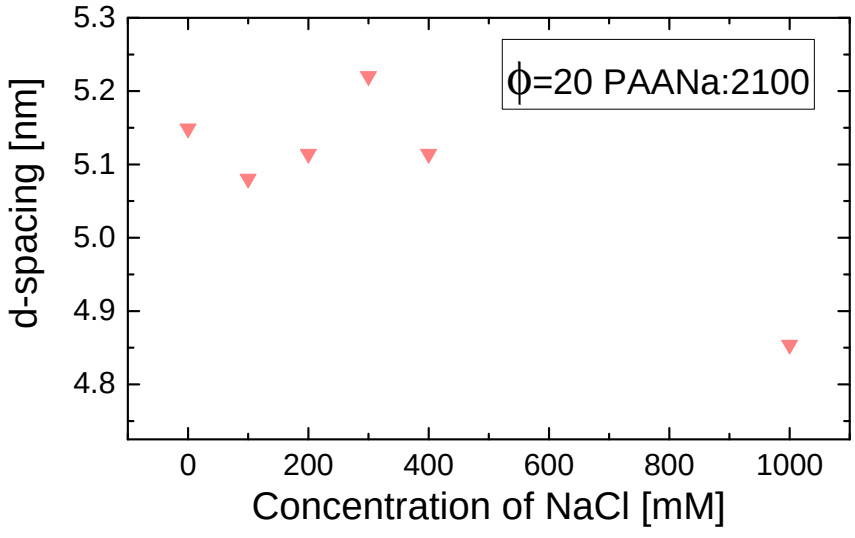

(b)

FIGURE 2.12: (a) SAXS data and (b) the corresponding d-spacings obtained for the DOTAP-PAANa2100 complexes at ϕ=20 at T = 25 °C.

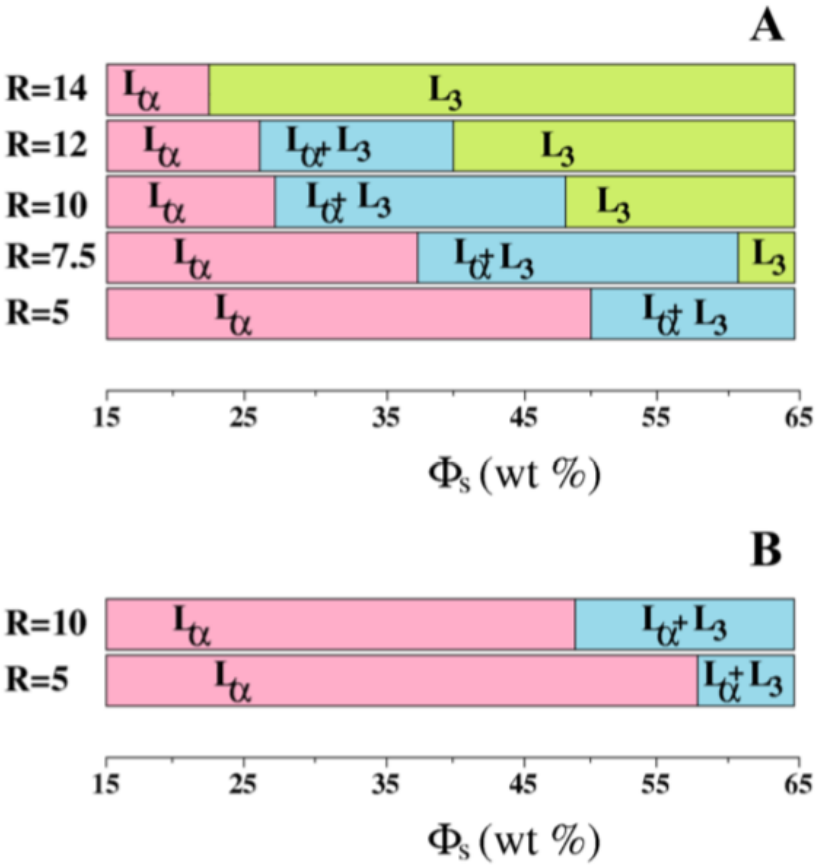

FIGURE 2.13: Partial phase diagrams for DDAB-PAANa systems in water for molecular weights (a) 2100 and (b) 5100, at different values of R[1]

in DDAB-PAANa2100 case, samples were made in NaBr solutions of varying concentrations. The SAXS data and the corresponding variation in the lamellar phase d-spacings are given in Figs. 2.14(a) and (b) respectively. A collapsed lamellar phase of d-spacing of around 3.4 nm is observed at low ionic strengths. At 200 mM, the d-spacing is found to increase to around 3.6 nm. On further increase of salt, the d-spacing is found to reduce gradually and at very high ionic strength of 1 M, the d-spacing is found to be around 2.95 nm. This phase behaviour is similar to the DDAC-PAANa2100 case. It is also interesting to note that the d-spacing at very high salt is slightly lower than that at low salt concentrations.

2.6 Discussion

The DDAC - water system is known to exhibit a highly swollen lamellar phase over a very wide range of compositions, which is stabilised by electrostatic repulsion between the bilayers[30]. When an oppositely charged polyelectrolyte, such as PAANa, is added to the system, a complex is formed, as described in the introduction. In most of the studies reported here the PAANa to DDAC weight ratio (R) was fixed at either 7 or 14. Since the isoelectric point of the system is around R = 0.2, these complexes are in equilibrium with excess polyelectrolyte in the solution. All the complexes are found to exhibit a collapsed lamellar phase L_{α}^{c1} in very dilute solutions, irrespective of the molecular weight of the PAANa used. In this case the separation between the bilayers is sufficient to accommodate a very thin layer of the polyelectrolyte. As mentioned in the introduction, strong polyelectrolytes are known to adsorb on oppositely charged surfaces, forming thin adsorption layers. At complete dissociation, PAANa and DDAC bilayers have one unit charge per 0.25 nm[31] and 0.68 nm^2[29], respectively. Therefore,

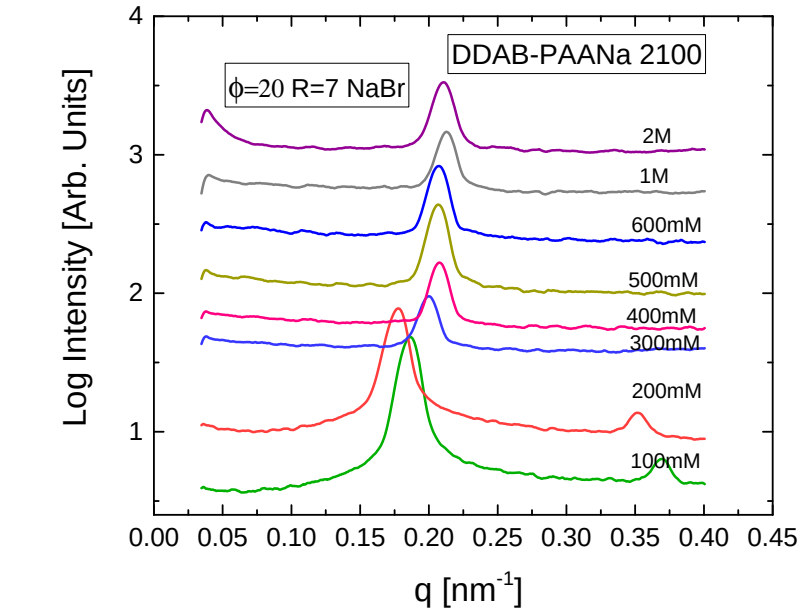

(a)

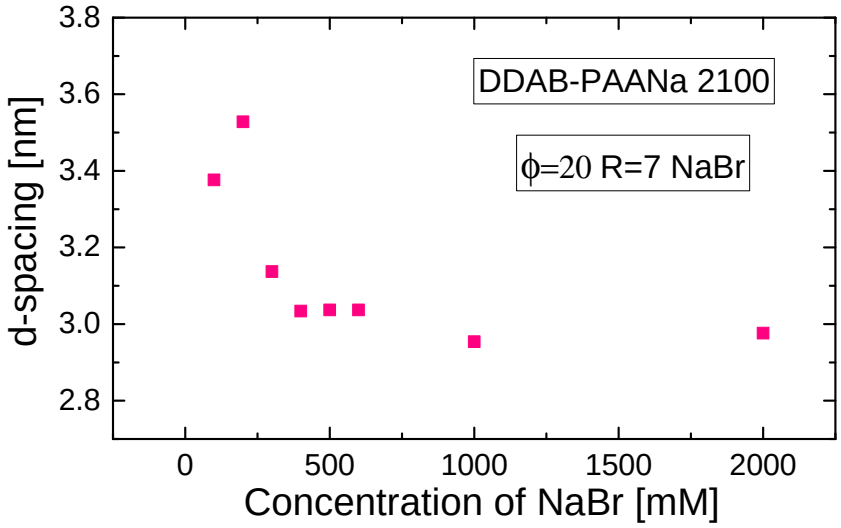

(b)

FIGURE 2.14: (a) SAXS data and (b) the corresponding variation in the d-spacing obtained for the DDAB-PAANa2100 complexes at R=7 and ϕ=20 in NaBr solutions, in the absence of excess polyelectrolyte.

even if the polyelectrolyte chains are fully stretched out on the bilayer surface, the charges on them cannot be fully neutralised by those on the bilayer. This can result in patch-charge attraction between adjacent bilayers[32], stabilizing the L_α^{c1} phase. Under these conditions bridging of adjacent bilayers by polyelectrolyte chains[33,34] can also give rise to an attractive interaction between the bilayers. Detailed experiments on the dependence of the attractive interaction on the separation between the surfaces are required to distinguish between these two possibilities.

Data presented in Figs. 2.8(a) and 2.8(b) confirm that the $L_\alpha^{c1} \rightarrow L_\alpha^{s}$ swelling transition is related to an abrupt increase in the amount of adsorbed polyelectrolyte on increasing the salt concentration. This behaviour is reminiscent of adsorption of strong polyelectrolytes on oppositely charged surfaces, where the amount of adsorbed polyelectrolyte is known to show a rather abrupt increase on increasing the ionic strength of the solution[13,20]. According to the random sequential adsorption (RSA) model[13,35], strong polyelectrolytes adsorbed on an oppositely charged surface form a very thin heterogeneous layer at low salt concentration. Further adsorption is prevented by inter-chain repulsion. Increasing the salt concentration results in the screening of this repulsion and leads to enhanced adsorption. The increase in the adsorption takes place over a rather narrow range of salt concentration and results in a much thicker and more homogeneous adsorbed layer. The swelling transition observed in DDAC-PAANa complexes can be attributed to a similar enhanced adsorption on increasing the ionic strength of the solution. Our studies with DDAC-PAANa2100 and DDAB-PAANa2100 complexes at ϕ=20, in the absence of excess polyelectrolyte do not show any swelling behaviour. This confirms that excess polyelectrolyte is a necessary criterion to induce the observed swelling transition.

Having established the fact that the $L_\alpha^{c1} \rightarrow L_\alpha^{s}$ swelling transition is driven

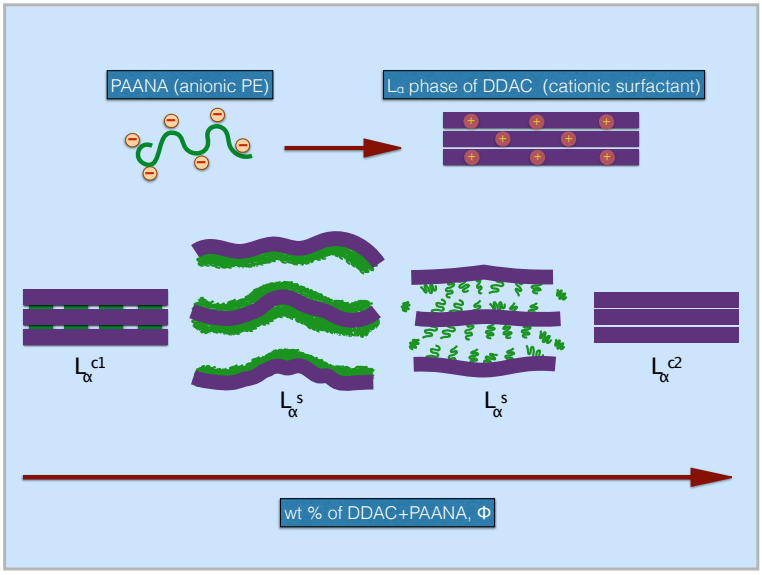

FIGURE 2.15: Schematic of the swelling behaviour of DDAC-PAANa complexes at low molecular weight of PAANa.

by salt-induced enhancement in the amount of adsorbed polyelectrolyte, let us consider possible interactions stabilizing the swollen lamellar phase. Electrostatic repulsion can be ruled out due to the high salt concentration in the solution; the resulting Debye screening length being very much smaller than the thickness of the water layer separating the bilayers. Steric repulsion between polymer brushes adsorbed on adjacent bilayers can also be discounted, since the water layer thickness is larger than twice the contour length ($\sim$7 nm for M_w=2100) of the polyelectrolyte chains. Another possibility is steric repulsion due to thermal undulations of the bilayers[36]. Bending rigidity modulus K of charged bilayers has a significant contribution from electrostatic interactions[37]. In order to estimate the bare value of K, the electrostatic contribution has to be eliminated by screening the electrostatic repulsion between the head groups. This study is discussed in detail in Chapter 3, for the lamellar phase of DDAC. A brief description is given here. Fig. 3.4(b) shows variation of the lamellar periodicity of a ϕ_s = 20 wt% solution of DDAC in water as a function of NaCl concentration. At very low

salt concentrations the diffraction patterns show a set of sharp peaks, as expected from a lamellar phase stabilised by electrostatic repulsion[37]. Sharpness of the peaks is a reflection of negligible thermal undulations of the bilayers, due to their high bending rigidity. At higher salt concentrations only one or two broad peaks are observed in the diffraction pattern, indicating that this phase is stabilised by steric repulsion arising from thermal undulations of the bilayers[37]. The large periodicity of this phase is consistent with a value of K of the order of a few kT. We have analysed the diffraction data using the protocol described in Chapter 1, following ref. 38. The Caillé parameter, η which is related to both bending rigidity modulus and bulk modulus ($\eta \propto 1/\sqrt{KB}$) is found to increase from 0.06 to 0.51 as the salt concentration is varied from 0 to 200 mM, confirming that the electrostatically stabilised lamellar phase in the absence of salt gets transformed into an undulation stabilised phase at high salt concentration. Adsorption of polymers on a bilayer is expected to decrease the value of K[39]. Hence a swollen lamellar phase can be stabilised by thermal undulations even in the case of DDAC bilayers with adsorbed polyelectrolytes, consistent with our observations. This conclusion is also supported by the fact that the swelling transition is not observed in complexes of PAANa2100 with the cationic lipid DOTAP (Fig. 2.12), which has a much higher value of bare K, as follows from the observation that the lamellar periodicity of this system at high salt concentrations is only slightly higher than its bilayer thickness.

In addition to the swelling transition at intermediate salt concentration, DDAC-PAANa2100 and DDAC-PAANa5100 complexes also show a $L_\alpha^s \rightarrow L_\alpha^{c2}$ de-swelling transition at very high salt concentrations. Interestingly, even in complexes that do not exhibit the swelling transition, such as DDAC-PAANa 8000 and DOTAP-PAANa2100, the lamellar periodicity decreases

slightly at very high salt concentrations. Studies on the adsorption of polyelectrolytes on oppositely charged surfaces indicate that the polyelectrolyte chains desorb from the surface at very high salt concentrations of ~ 1.0 M[40]. A similar behaviour can be expected in the present case. Further, at these high salt concentrations the interbilayer interactions are dominated by the Van der Waals attraction, leading to the de-swelling transition and the formation of the collapsed L_α^{c2} phase. The absence of adsorbed polyelectrolytes result in the slightly lower lamellar periodicity of this phase compared to that of the L_α^{c1} phase. This proposal is supported by the observation of a de-swelling transition in the DDAC-water system, in the absence of PAANa, at around 400 mM (Fig. 3.4). A schematic of the proposed mechanism for the observed swelling behaviour is given in Fig. 2.15.

DDAC-PAANa8000 complexes do not exhibit the swelling transitions. However, the lamellar periodicity shows a slight increase over an intermediate range of salt concentration, over which both DDAC-PAANa2100 and DDAC-PAANa5100 complexes show the swollen phase. This observation suggests a salt-induced increase in the adsorbed amount of the polyelectrolyte is present in the case of PAANa8000 also, but without resulting in a swelling transition. This might point to a substantial increase in the strength of the patch-charge attraction with the molecular weight of the polyelectrolyte[41,42]. Interestingly, in conformity with such a scenario, the lamellar periodicity of the L_α^{c1} phase at $\phi = 20$ is found to decrease monotonically with increasing molecular weight of PAANa; d= 3.48 nm, 3.32 nm and 3.19 nm for PAANa2100, PAANa5100 and PAANa8000, respectively. Yet another candidate is bridging interaction. The above observation can also result from increased attractive bridging interaction with increase in the molecular weight of the polyelectrolyte[33,43]. Further work is needed to unambiguously establish this possibility.

Although we have provided a qualitative explanation for some aspects of the observed swelling behaviour of DDAC-PAANa complexes, certain others remain not fully addressed. As mentioned earlier, the lamellar periodicity of the swollen L_α^s phase is found to evolve over time and also shows a large scatter. This is most probably a consequence of osmotic pressure applied by small vesicles in the solution, whose concentration will vary from sample to sample and also over time, as reported in some other systems[44]. Therefore the samples were equilibrated at least for a month. The value of d-spacing initially increases sharply with salt concentration, reaching a maximum at around 300 mM, and then decreases gradually at higher salt concentrations. As discussed earlier, the only long-range repulsion that stabilises the swollen L_α^s phase arises from thermal undulations of the bilayers. Hence the observed non-monotonic dependence of d on salt concentration is consistent with a non-monotonic dependence of K on salt concentration. Interestingly, the change in K due to adsorption of polymers has been predicted to depend on the morphology of the adsorbed layer. In the case of polymers forming a thin adsorbed layer, K is found to decrease[39,45], whereas for anchored polymers forming a thick brush, it is expected to increase[46]. It is conceivable that such a change, from a thin adsorbed layer to a brush-like morphology, takes place in the present system as the polyelectrolyte chains become gradually detached from the bilayer surface with increasing salt concentration. A detailed study of the dependence of the structure of the absorbed layer on salt concentration is required to establish such a scenario.

In the case of DOTAP-PAANa2100 complexes, no swelling behaviour is observed. The complex always remains in a collapsed lamellar phase. This is expected from the fact that the charged lipid bilayer is more rigid than the bilayers formed by the ionic amphiphiles[47]. Further studies on the DOTAP

lamellar phase in the presence of NaCl solutions show a gradual decrease in d-spacing (which in turn imply a gradual decrease in Debye length), with increase in ionic strength. This is discussed in detail in Chapter 3.

As already mentioned the swelling transition requires excess polyelectrolyte in the system. Studies on DDAB-PAANa2100 complexes confirm the importance of excess polyelectrolyte in the swelling transition. Further, the formation of a swollen sponge phase in this system, indicates that both the bending rigidity modulus (K) and the Gaussian rigidity modulus ($\bar{K}$) are affected by the adsorbed layer. In fact theories predict that $\bar{K}$ should become more positive in the presence of an adsorption layer[39] which is in agreement with the formation of the sponge phase.

2.7 Conclusions

DDAC-PAANa complexes are found to exhibit consecutive swelling and de-swelling transitions with decreasing water content for low molecular weights of the polyelectrolyte. This behaviour is shown to result from increasing bulk concentration of the counterions released during the complexation process, with decreasing water content. Our observations suggest that the L_α^{c1} at low salt content is stabilised by either patch-charge attraction or polyelectrolyte bridging between the bilayers due to the presence of a thin heterogeneous adsorption layer of the polyelectrolyte on the bilayer surface. The L_α^{c2} phase is formed at high salt regime due to Van der Waals attraction. The swelling transition reported is driven by the abrupt uptake of polyelectrolyte chains from the aqueous solution by the complex above a threshold salt concentration.

Bibliography

[1] Santosh Kumar Gupta. *Studies on novel phase behavior of ionic amphiphile - water systems*. PhD thesis, Raman Research Institute, Jawaharlal Nehru University, New Delhi, 2007.

[2] Jacob N. Israelachvili. *Intermolecular and surface forces*. Elsevier, Amsterdam, 3 edition, 2011.

[3] G. J. M. Koper and M. Borkovec. Proton binding by linear, branched, and hyperbranched polyelectrolytes. *Polymer*, 51:5649–5662, 2010.

[4] G. Manning. Limiting laws and counterion condensation in polyelectrolyte solutions i. colligative properties. *J. Chem. Phys.*, 51:924–933, 1969.

[5] I. Michaeli, J. T. G. Overbeek, and M. J. Voorn. Phase separation of polyelectrolyte solutions. *Journal of Polymer Science*, 23:443–450, 1957.

[6] J. T. G. Overbeek and M. J. Voorn. Phase separation in polyelectrolyte solutions. theory of complex coacervation. *J. Cell.Comp. Physiol.*, 49(S1): 7–26, 1957.

[7] A Veis. Phase separation in polyelectrolyte solutions ii. interaction effects. *J. Phys. Chem.*, 65(10):1798–1803, 1961.

[8] A. Veis, E. Bodor, and S. Mussell. Molecular weight fractionation and the self-suppression of complex coacervation. *Biopolymers*, 5(1):421–430, 1967.

[9] H. G. Bungenberg de Jong and H. R. Kruyt. *Colloid Science*. Elsevier, Amsterdam, 1949.

[10] F. Oosawa. A simple theory of thermodynamic properties of polyelectrolyte solutions. *J. Polym. Sci.*, 23:421–430, 1957.

[11] R. Bruinsma. Electrostatics of DNA-cationic lipid complexes: Isoelectric instability. *Euro Phys. J. B.*, 4:75–88, 1998.

[12] M. Wang and Y. Wang. Development of amphiphile coacervation in aqueous solution. *Soft Matter*, 10:7909–7919, 2014.

[13] I. Szilagyi, G. Trefalt, A. Tiraferri, P. Maroni, and M. Borkovec. Polyelectrolyte adsorption, interparticle forces, and colloidal aggregation. *Soft Matter*, 10:2479–2502, 2014.

[14] M. R. Böhmer, O. A. Evers, and J. M. H. M. Scheutjens. Weak polyelectrolytes between two surfaces: adsorption and stabilization. *Macromolecules*, 23:2288–2301, 1990.

[15] J. Blaakmeer, M. R. Böhmer, M. A. Cohen Stuart, and G. J. Fleer. Adsorption of weak polyelectrolytes on highly charged surfaces. poly(acrylic acid) on polystyrene latex with strong cationic groups. *Marcomolecules*, 23(8):2301–2309, 1990.

[16] M. A. Cohen Stuart. Polyelectrolyte adsorption. *J. Phys. France*, 49: 1001–1008, 1988.

[17] J. Kleimann, C. Gehin-Delval, H. Auweter, and M. Borkovec. Superstoichiometric charge neutralization in particle-polyelectrolyte systems. *Langmuir*, 21:3688–3698, 2005.

[18] M. Finessi, P. Sinha, I. Szìlagyi, I. Popa, P. Maroni, and M. Borkovec. Charge reversal of sulfate latex particles by adsorbed linear

poly(ethylene imine) probed by multiparticle colloidal probe technique. *J. Phys. Chem. B*, 115:9098–9105, 2011.

[19] M. Borkovec, I. Szilàgyi, I. Popa, M. Finessi, P. Sinha, P. Maroni, and G. Papastavrou. Investigating forces between charged particles in the presence of oppositely charged polyelectrolytes with the multi-particle colloidal probe technique. *Advances in Colloid and Interface Science*, 179: 85–98, 2012.

[20] I. Popa, B. P. Cahill, P. Maroni, G. Papastavrou, and M. Borkovec. Thin adsorbed films of a strong cationic polyelectrolyte on silica substrates. *J. Colloid Interface Sci.*, 309:28–35, 2007.

[21] G. J. Fleer, M. A. Cohen Stuart, J. M. H. M. Scheutjens, T. Cosgrove, and B. Vincent. *Polymers at Interfaces (Chapter 7)*. Chapman and Hall: New York, 1993.

[22] M. Muthukumar. Adsorption of a polyelectrolyte chain to a charged surface. *J. Chem. Phys.*, 86:7230–7235, 1987.

[23] R. R. Netz and J. F. Joanny. Adsorption of semiflexible polyelectrolytes on charged planar surfaces: Charge compensation, charge reversal, and multilayer formation. *Macromolecules*, 32:9013–9025, 1999.

[24] M. Porus, P. Maroni, and M. Borkovec. Structure of adsorbed polyelectrolyte monolayers investigated by combining optical reflectometry and piezoelectric techniques. *Langmuir*, 28:5642–5651, 2012.

[25] P. M. Claesson, E. Poptoshev, E. Blomberg, and A. Dedinaite. Polyelectrolyte-mediated surface interactions. *Adv. Colloid Interface Sci.*, 114:173–187, 2005.

[26] R. Podgornik and M. Licer. Polyelectrolyte bridging interactions between charged macromolecules. *Curr. Opin. Colloid Interface Sci.*, 11(5):

273–279, 2006.

[27] M. Thomas, K. Swamynathan and V. A. Raghunathan, *The Journal of Chemical Physics*, 2019, **150**, 094903

[28] A Cipiciani, R. Germani, G. Saveili, C. A. Bunton, M. Mhala, and J. R. Moffatt. The effects of single and twin tailed ionic amphiphiles upon aromatic nucleophilic substitution. *J. Chem. Soc. Perkin Trans II*, 5:541–546, 1987.

[29] G Brotons, M. Dubois, I. Belloni L, Grillo, T. Narayanan, and T. Zemb. The role of counterions on the elasticity of highly charged lamellar phases: A small-angle x-ray and neutron-scattering determination. *J. Chem. Phys.*, 123:024704, 2005.

[30] C. Kang and A. J. Khan. Self-assembly in systems of didodecyldimethylammonium surfactants: Binary and ternary phase equilibria and phase structures with sulphate, hydroxide, acetate, and chloride counterions. *Coll. Int. Sci.*, 156:218–228, 1993.

[31] K. Kogez and J Skerjanc. Binding of cetylpyridenium cation by poly (acrylic acid): Effect of polymer charge density. *Acta Chim. Slov.*, 46(2): 269–279, 1999.

[32] S. Perkin, N. Kampf, and J. Klein. Long-range attraction between charge-mosaic surfaces across water. *Phys. Rev. Lett.*, 96:038301, 2006.

[33] Rudi Podgornik. Self consistent field theory for confined polyelectrolyte chains. *The Journal of Physical Chemistry*, 96(2):884–896, 1992.

[34] Rudi Podgornik. Polyelectrolyte-mediated bridging interactions. *Journal of Polymer Science Part B: Polymer Physics*, 42(19):3539–3556, 2004.

[35] J. W. Evans. Random and cooperative sequential adsorption. *Rev. Mod. Phys.*, 65:1281–1329, 1993.

[36] W. Helfrich. Elastic properties of lipid bilayers: Theory and possible experiments. *Z. Naturforsch. C*, 28:693–703, 1973.

[37] D. Roux and C. R. Safinya. A synchrotron x-ray study of competing undulation and electrostatic interlayer interactions in fluid multimembrane lyotropic phases. *Journal de Physique*, 49:307–318, 1988.

[38] G. Pabst, M Rappolt, H Amenitsch, and P. Laggner. Structural information from multilamellar liposomes at full hydration: Full q-range fitting with high quality x-ray data. *Phys. Rev. E.*, 62(3):4000–4009, 2000.

[39] J. T. Brooks, C. M. Marques, and M. E. Cates. The effect of adsorbed polymer on the elastic moduli of surfactant bilayers. *J. Phys. II*, 1:673–690, 1991.

[40] F. Xie, T. Nylander, L. Piculell, S. Utsel, L. Wøagberg, T. øAkesson, and J. Forsman. Polyelectrolyte adsorption on solid surfaces: theoretical predictions and experimental measurements. *Langmuir*, 94:12421–12431, 2013.

[41] I. Popa, G. Gillies, G. Papastavrou, and M. Borkovec. Attractive and repulsive electrostatic forces between positively charged latex particles in the presence of anionic linear polyelectrolytes. *J. Phys. Chem. B*, 114: 3170–3177, 2010.

[42] R. M. Adar, D. Andelman, and H. Diamant. Electrostatic attraction between overall neutral surfaces. *Phys. Rev. E*, 94:022803, 2016.

[43] R. Podgornik, *The Journal of Physical Chemistry*, 1992, **96**, 884–896

[44] B. S. Lu, S. Gupta, M. Belička, R. Podgornik, and G. Pabst. Modulation of elasticity and interactions in charged lipid multibilayers: monovalent salt solutions. *Langmuir*, 32:13546–13555, 2016.

[45] M. Maugey and A. M. Bellocq. Effect of adsorbed and anchored polymers on membrane flexibility: a light scattering study of sponge phases. *Langmuir*, 17:6740–6742, 2001.

[46] C. Hiergeist and R. Lipowsky. Elastic properties of polymer-decorated membranes. *J. Phys. II*, 6:1465–1481, 1996.

[47] Bing-Sui Lu, Santosh Prasad Gupta, Michal Belička, Rudolf Podgornik, and Georg Pabst. Modulation of elasticity and interactions in charged lipid multibilayers: Monovalent salt solutions. *Langmuir*, 32(50):13546–13555, 2016.

Chapter 3

Effect of Salt on the Lamellar Phase of Some Cationic Surfactants and Lipids

3.1 Introduction

In the previous chapter, we saw the anomalous swelling behaviour of the lamellar phase of DDAC, in the presence of a polyelectrolyte. Several parameters like counterion concentration (salt), degree of adsorption of the polyelectrolyte can contribute to this swelling transition. In this chapter we study the effect of salt on the bending rigidity of the lamellar bilayers and try to understand the swelling transition observed for the DDAC-PAANa system. The influence of salt on some other lamellar phase forming systems are also studied.

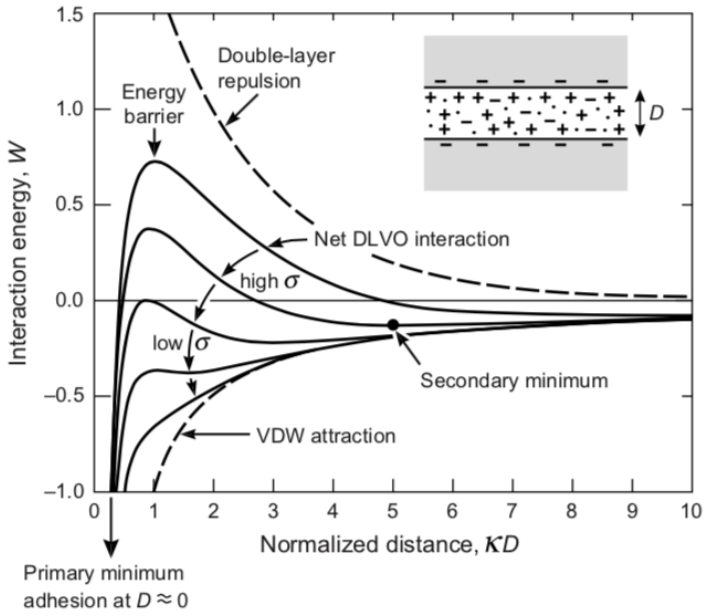

FIGURE 3.1: The energy versus distance profiles of the DLVO interaction[3].

3.2 Earlier Studies

Double tailed cationic surfactants such as DDAC can form lamellar phase over a wide range of concentrations[1,2]. The equilibrium spacing in these lamellar phases is determined by the balance of several forces, such as electric double layer repulsion, Van der Waals attraction, undulation repulsion and hydration repulsion. The first three interactions are discussed in detail in the introduction. The DLVO (Derjaguin, Landau, Verwey and Overbeek) theory describes interaction between two surfaces through electric double layer repulsion and Van der Waals attraction in the presence and absence of added electrolytes[3]. The hydration force is short-ranged and arises from the ordering of water molecules at the bilayer surface and from thermally excited protrusion of molecules out of the bilayer[3]. As the water content in a lamellar phase forming system is gradually increased, the thickness of the water layer increases. Once it reaches the maximum swelling, any excess water separates out. This d-spacing corresponds to the minimum of the

interaction energy.

In the presence of electrolytes, screening by the counterions also comes into picture. In this context it is worthwhile to discuss briefly the DLVO theory[3]. Fig. 3.1, shows the behaviour of interaction energy with distance, as the electrolyte concentration is gradually increased. In the absence of any electrolyte, there is a strong long-range repulsion that peaks at short distances (1-5 nm). This also implies that the Debye length is very large. As the electrolyte concentration is gradually increased, a secondary minima develops (> 3 nm), which becomes more and more significant with increasing electrolyte concentration. The primary minimum as shown in the figure is where the particles are touching each other. But approaching it is difficult because of the high energy barrier. In this case the charged particles may either be in the secondary minima or be dispersed in the solution. At very high electrolyte concentration, the energy barrier disappears and only Van der Waals attraction remains.

The phase behaviour of double tailed cationic surfactants didodecyldimethyl ammonium bromide (DDAB) and didodecyldimethyl ammonium chloride (DDAC) has been studied extensively. Phase diagrams of DDAB and DDAC[1] obtained from these studies[2] are given in Fig. 3.2. In the case of DDAB, we can see that at very low concentrations and very high temperatures, there is an isotropic phase L_1. As the DDAB concentration is gradually increased transition to a lamellar phase, L_α is found. At yet higher concentrations there is a region where a coexistence of L_α, with a collapsed lamellar phase, $L_{\alpha'}$ is found. In the case of DDAC, only a single lamellar phase L_α is found throughout a large range of concentrations. The effect of addition of some organic and inorganic salts on the lamellar phase of DDAB was also studied by Ghosh et al[4]. They discuss in detail the lamellar - lamellar coexistense, present in the DDAB - water system and also the effect of addition of salt.

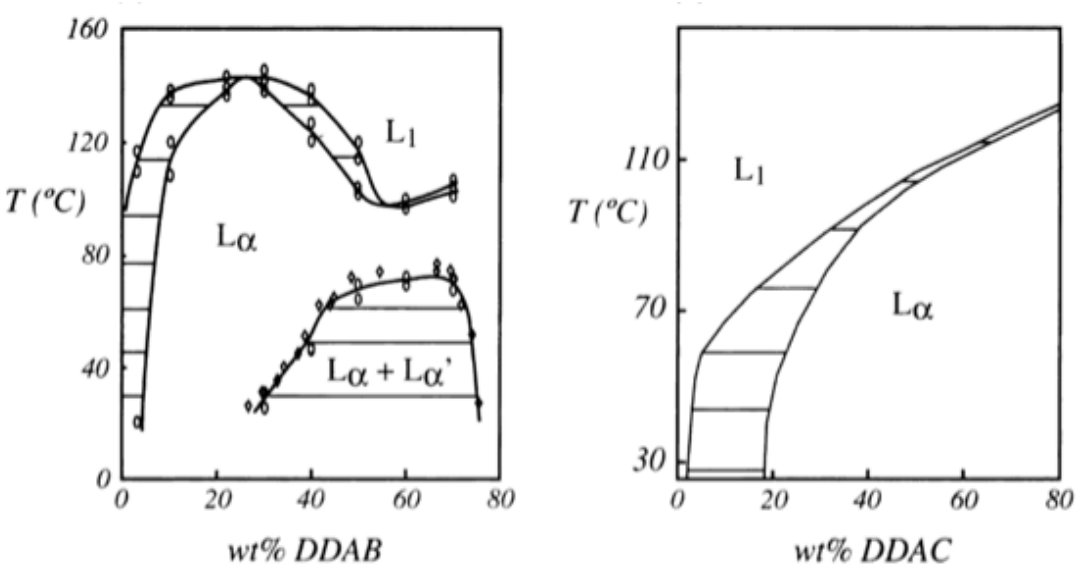

FIGURE 3.2: The partial phase diagrams of DDAB and DDAC surfactants in water[1].

Roux and Safinya have studied in detail the competing electrostatic and undulation forces in SDS - pentanol - dodecane water/brine system[7]. The lamellar phase was found to be stable over a large dilution range. Also the structure factor was seen to follow a power law behaviour, with a characteristic exponent value η, called the Caillé parameter. The asymptotic behaviour of the structure factor in the directions parallel ($||$) and perpendicular ($\perp$) to the layer normal is given by simple power laws

$$\begin{aligned} S(0, q_{||}) &\propto 1/|q_{||} - q_m|^{2-\eta_m} \\ S(q_\perp, q_m) &\propto 1/q_\perp^{4-2\eta_m} \end{aligned} \tag{3.1}$$

where q_m is the position of the mth harmonic of the structure factor ($q_m = mq_0$, $m = 1, 2, ...$ and $q_0 = 2\pi/d$, d being lamellar periodicity). The Caillé parameter, η_m is related to the membrane bending modulus (K) and compressibility modulus (B) through the relation $\eta_m = mq_0^2 KT/8\pi\sqrt{KB}$. They also show that, in the case of water dilution, η saturates at a value of 0.3 and

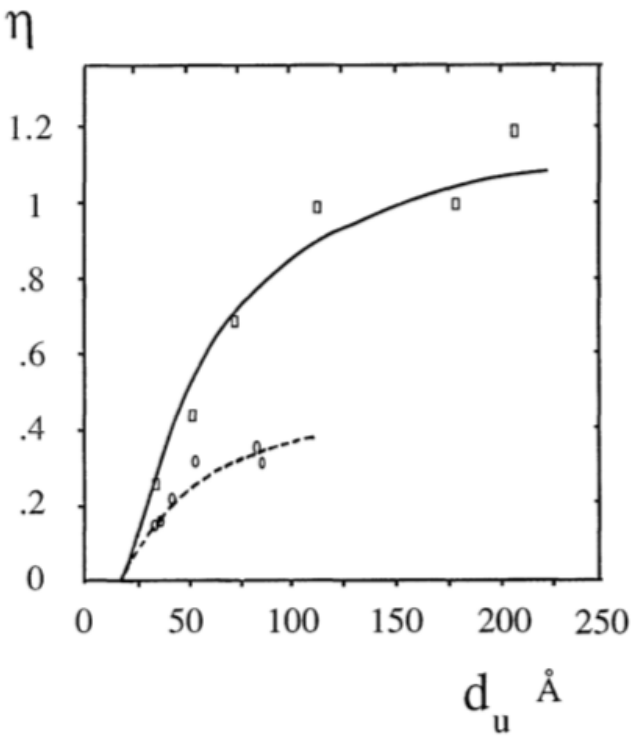

FIGURE 3.3: Variation of the Caillé parameter as a function of the repeat distance d_u for the water dilution (open circles) and for the brine dilution (open square)[7].

that in the brine dilution case, it increases and saturates at a value ∼1.0 (Fig. 3.3). From the above relation, it is clear that the value of η is high when the membranes are flexible and is less when the membranes are rigid. In case of charged membranes, the η value is small, because of the high rigidity. From Fig. 3.3 it can be seen that as the water concentration is gradually increased, η saturates at ∼0.3[7]. In the case of brine dilution, as the salt concentration is gradually increased, the counterions screen the charges, reducing the charges on the surface. This makes the membrane more flexible and results in a large η value as shown in the Fig. 3.3.

3.3 Materials and Methods

For the studies we have used surfactants, didodecyldimethyl ammonium bromide (DDAB) and didodecyldimethyl ammonium chloride (DDAC). DDAB along with NaCl and NaBr were obtained from Sigma. N,N dimethyldodecylamine (NND) and 1-chlorododecane (CDD) were obtained from TCI Chemicals and were used as received, for the preparation of DDAC. 1,2 dioleoyl-3-trimethylammonium propane (chloride salt) (DOTAP) was obtained from Avanti Polar Lipids. DDAC was prepared following the procedure discussed by Cipiciani et al.[6]. Samples were prepared in Millipore water. For sample preparation, DDAC and DDAB samples at weight percentage, ϕ=20 were made in NaCl/ NaBr solutions of different ionic strengths. In the case of charged lipid, DOTAP samples were prepared at a weight percentage ϕ=20 in NaCl solutions with varying ionic strengths. In both the cases, ϕ is the weight percentage of the surfactant or lipid and is defined as $W_s/(W_s+W_b)$, where W_s and W_b are the weights of surfactant (lipid) and brine respectively. All studies were done at room temperature.

3.4 Results

3.4.1 Effect of salt on the lamellar phase of DDAC

DDAC forms lamellar phase in water over a wide range of concentrations. DDAC samples for the study were prepared at ϕ=20 in NaCl solutions whose concentrations varied from 0 mM to 700 mM. The SAXS data of the samples at ϕ=20, is shown in Fig. 3.4(a). In water and at very low ionic strengths, the SAXS data show a set of sharp peaks corresponding to a lamellar L_α phase. In water the L_α phase has a d-spacing of 11.9 nm, which reduces to 10.8 nm

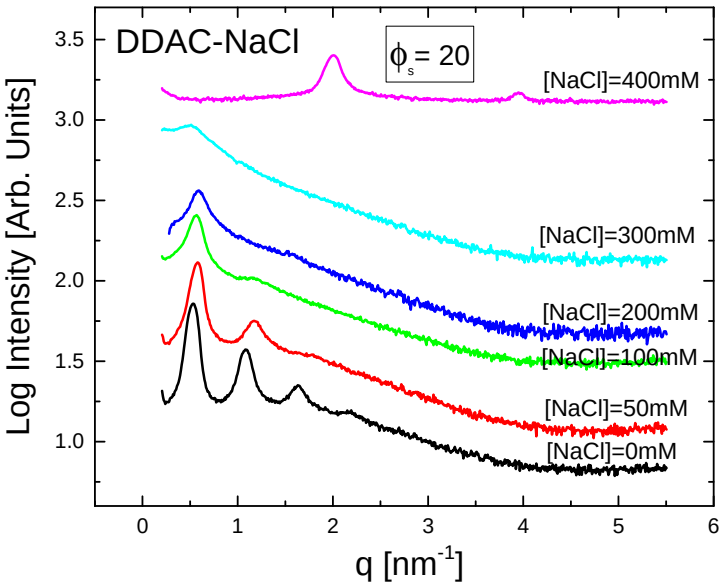

(a)

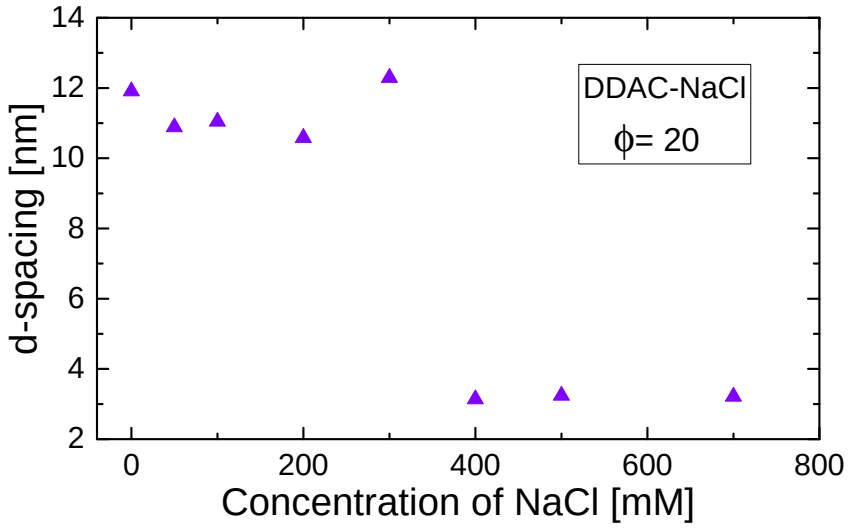

(b)

FIGURE 3.4: (a) SAXS data and (b) corresponding *d*-spacing of the DDAC-NaCl system.

at 50 mM and to 11.0 nm at 100 mM NaCl (Fig. 3.4(b)). As the ionic strength of the sample is gradually increased, the peaks are seen to broaden and the number of peaks reduce. It is also observed that the peak position remains the same at low ionic strengths. The phase has a spacing of 10.6 nm in 200 mM and 12.29 nm in 300 mM solutions. As the ionic strength is further increased to 400 mM, a collapsed lamellar phase with a d-spacing of 3.13 nm is observed.

3.4.2 Effect of salt on the lamellar phase of DDAB

DDAB samples were prepared at ϕ=20 with the NaCl concentration ranging from 15 mM to 2M. The SAXS data of the DDAB-NaCl system show a similar behaviour as the DDAC-NaCl system. In the absence of salt, the sample showed a set of sharp peaks corresponding to a lamellar phase with d-spacing, 12.1 nm as shown in Fig. 3.5(a). As the ionic strength of the sample is increased to 30mM, peaks broaden and higher orders disappear. The sample has a d-spacing of 13.1 nm. However at 100 mM, the d-spacing reduces drastically and the sample is seen to form a collapsed lamellar phase, with much smaller d-spacing of 3.1 nm. The d-spacings obtained from the SAXS studies are depicted in Fig. 3.5(b). The d-spacings at higher concentrations of NaCl, remain unchanged at around 3.1 nm.

In the case of DDAB-NaBr system, the SAXS data and the corresponding d-spacings are shown in Fig. 3.6(a) and 3.6(b). At low ionic strengths of NaBr, the system show L_α phase. At [NaBr]= 15 mM, the sample has a d-spacing of 11.5 nm which increases to 12.29 nm at 30 mM. At 100 mM, the sample shows a collapsed lamellar phase with much lower d-spacing of 3.0 nm. The collapsed lamellar phase is seen to exist upto an ionic strength of 1 M.

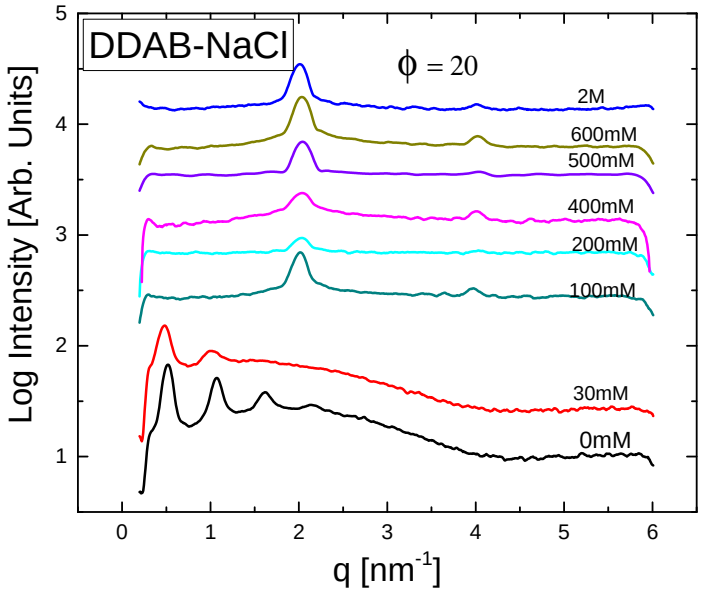

(a)

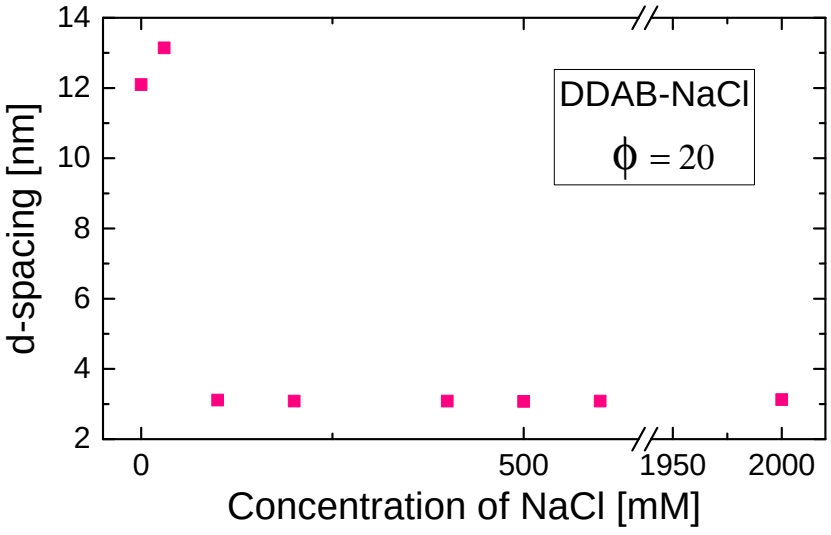

(b)

FIGURE 3.5: (a) SAXS data and (b) corresponding *d*-spacing, obtained for the DDAB-NaCl system.

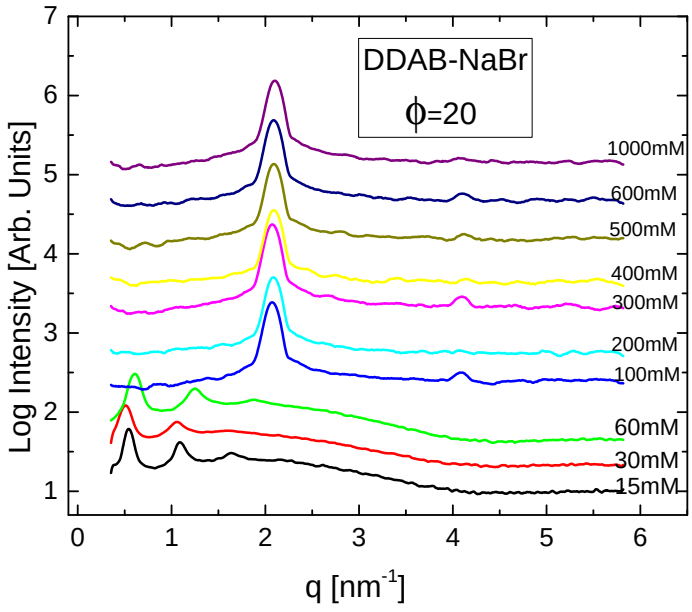

(a)

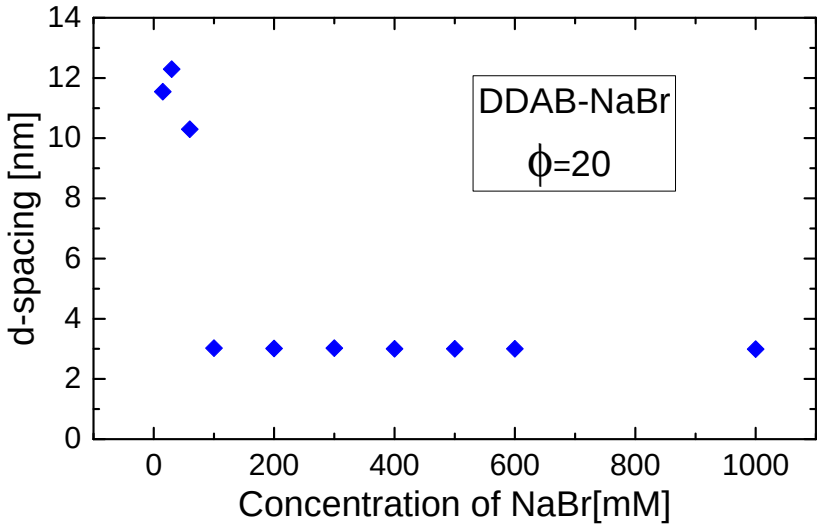

(b)

FIGURE 3.6: (a) SAXS data and (b) the corresponding *d*-spacing obtained for the DDAB-NaBr system.

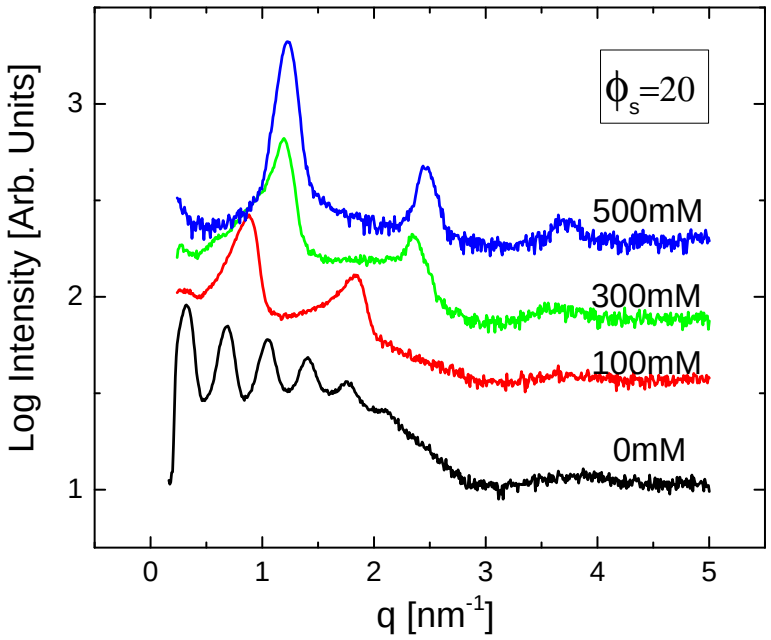

FIGURE 3.7: SAXS diffraction data for the DOTAP system in NaCl solutions of varying ionic strengths.

3.4.3 Effect of salt on a charged lipid (DOTAP) system

DOTAP is a charged lipid. In aqueous medium, it releases the chloride ion and the positively charged lipid molecule self assemble to form bilayers. In the absence of any added salt, SAXS data is as shown in Fig. 3.7, which corresponds to a lamellar phase. This arises from the long range translational order present in the system due to the long range electrostatic repulsion. As the ionic concentration is gradually increased, the *d*-spacing is seen to decrease gradually (Fig. 3.8). In water, the sample shows a *d*-spacing of 19.5 nm, which reduces to 7.1 nm at 100 mM to 5.1 nm at 500 mM.

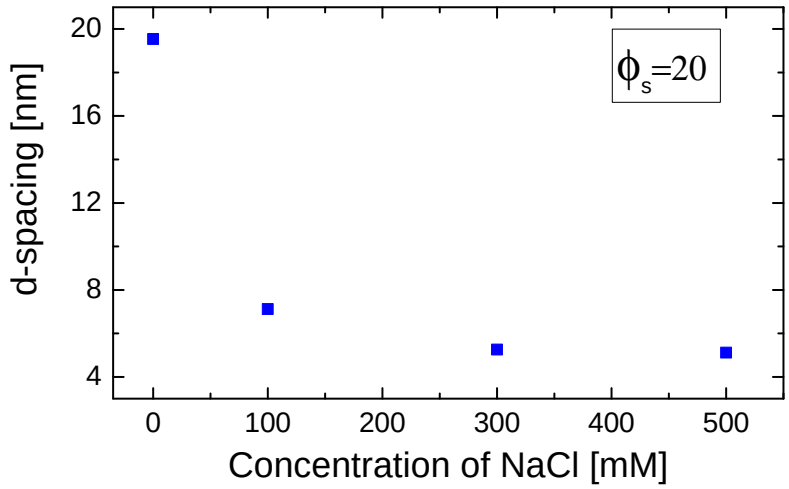

FIGURE 3.8: The variation in the lamellar periodicity for the DOTAP system in NaCl solutions of varying ionic strengths.

3.5 Discussion

Effect of salt on the lamellar phase of DDAC

DDAC shows lamellar phase in water over a wide range of concentrations. Bending rigidity of charged bilayers has a significant contribution from electrostatic interactions[7]. As the ionic concentration is gradually increased, the counterions screen the charges on the bilayer and therefore the electrostatic repulsion interaction is screened. This in turn reduces the Debye length in the sample and therefore we expect a gradual decrease in the *d*-spacing. As can be seen from Fig. 3.4(a) and 3.4(b), the lamellar periodicity of this system is around 12 nm, and does not vary significantly as the salt concentration is increased up to around 350 mM. However, the diffraction patterns show significant changes over this range of salt concentration (Fig. 3.4a).

At very low salt concentrations the diffraction patterns show a set of sharp peaks, as expected from a lamellar phase stabilised by electrostatic repulsion[7]. Sharpness of the peak is a reflection of negligible thermal undulations

of the bilayers, due to their high bending rigidity. At higher salt concentrations only one or two broad peaks are observed in the diffraction pattern, indicating that this phase is stabilised by steric repulsion arising from thermal undulations of the bilayers[5,7]. We have analysed the diffraction data using the protocol described in ref. 10, which is discussed in Chapter 1, and the obtained fits are given in Fig. 3.9. The Caillé parameter η is found to increase from 0.06 to 0.51 as the salt concentration is varied from 0 to 200 mM, confirming that the electrostatically stabilised lamellar phase in the absence of salt gets transformed into an undulation stabilised phase at high salt concentration.

At much higher ionic concentrations, a collapsed lamellar phase with a d-spacing of around 3.1 nm is observed. At such high concentrations of salt, the Debye length reduces significantly due to the screening of the surface charges by counterions. So the appearance of this collapsed lamellar phase can be attributed to Van der Waals attraction.

Effect of salt on the lamellar phase of DDAB

The SAXS data of DDAB-NaBr/NaCl system is very similar to the DDAC-NaCl system discussed above. However the swollen phase is seen to exist only at low ionic strengths. At 100 mM, both the samples show a collapsed lamellar phase. At low ionic strengths the samples show a set of sharp peaks, corresponding to an electrostatically stabilised lamellar phase.

With increasing ionic strength, it is observed that the peaks broaden and higher order reflections disappear. However no significant change in d-spacing is observed. The sample undergoes a transition from an electrostatically stabilised regime to an undulation stabilised regime. At still higher ionic concentration, a collapsed lamellar phase is observed. Transition from the swollen lamellar to collapsed lamellar phase is seen at around 100 mM.

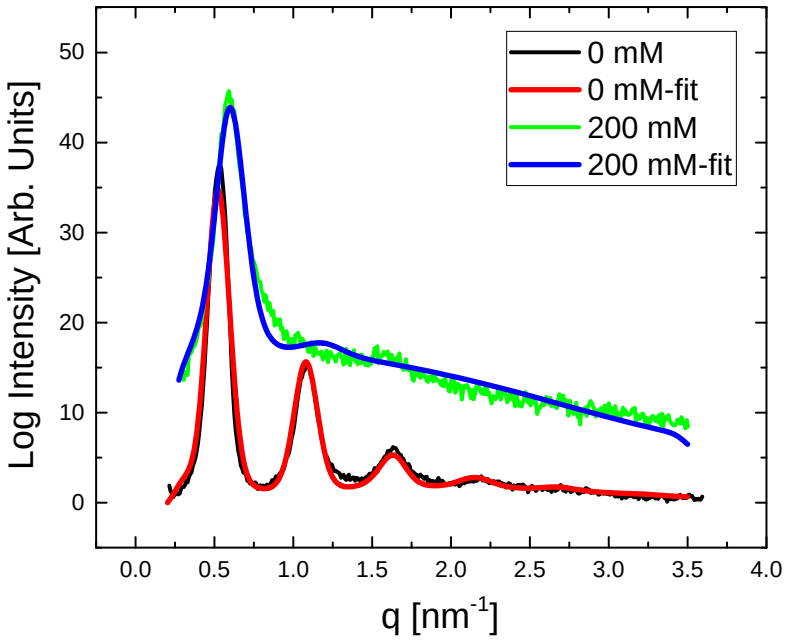

FIGURE 3.9: Fits obtained for the SAXS data of DDAC-NaCl system at ϕ=20. T=25°C

Unlike DDAC, a coexistence of collapsed and swollen lamellar phases are seen in the case of DDAB in the absence of salt. A detailed comparison of these systems is given in section 3.2. DDAB-PAANa complexes with PAANa2100 and PAANa5100 show a swollen sponge phase[9] (instead of a swollen lamellar phase in the DDAC case). Clearly the lamellar phase formed by DDA^+ ion in the presence of Br^- and Cl^- counterion show very different phase behaviour in the presence of low molecular weight PAANa.

Effect of salt on the lamellar phase of DOTAP

If the phospholipid membrane is not electro-neutral, then its bilayer bending rigidity will have contributions from the surface charges. Bilayers formed by charged lipids form lamellar phase, stabilised by electrostatic interaction. They have very high bending rigidity of $100kT$[8], in comparison to an uncharged fluid lipid bilayer ($30kT$)[11]. SAXS data shows a gradual decrease in the d-spacing with increasing ionic strength. As the ionic strength is gradually increased, the Debye length decreases due to the screening of charges by the counterions. Bing-Sui Lu et al.[8] have reported that, in the case of a charged lipid, dipalmitoylphosphatidyl glycerol (DPPG) the bending rigidity decreases with increase in the ionic concentration of the salt solution. They show that at [NaCl]$\sim$100 mM, the bending rigidity is around $100kT$ and at 500 mM it is around $50kT$[8]. This implies that, as the concentration of salt in the system is increased, the membranes soften.

DOTAP is a charged lipid, just like DPPG. With increase in the ionic strength, Debye length steadily reduces due to the screening thereby reducing the extent of electrostatic repulsion[3]. Also in this case, K is very high and therefore the undulation amplitude is very low. This explains the absence of undulation repulsion and therefore the absence of swelling in the DOTAP-PAANa system previously discussed in Chapter 2. The complexes show a d-spacing of around 5.0 nm, irrespective of the ionic concentration, which is similar to the DOTAP-NaCl system.

3.6 Conclusions

In this chapter we study the effect of salt in several lamellar phase forming surfactants. DDAC exhibits lamellar phase over a wide range of salt

concentrations. As the ionic strength of the brine solution is gradually increased lamellar phase is observed to undergo transition from an electrostatically stabilised (large d-spacing and high bending rigidity) $\rightarrow$ undulation stabilised (large d-spacing and low bending rigidity) $\rightarrow$ Van der Waals stabilised (low d-spacing) phase. The DDAB-NaCl system also shows a similar behaviour, though the transition to the Van der Waals stabilised phase happens at a much lower ionic strength. However in the case of a charged phospholipid DOTAP, the d-spacing steadily decreases with salt. Though a softening of the membranes might be occurring, the bare rigidity of these bilayers is high, as in the case of zwitterionic double chain lipids[12].

From the above studies we can conclude that the swelling behaviour of DDAC-PAANa complexes at low molecular weight of polyelectrolyte arises from the long range undulation repulsion interaction. This repulsive interaction arises from the thermally fluctuating bilayers of very low bending rigidity. Screening of charges by the counterions present in the system leads to the low bending rigidity of the membranes.

Bibliography

[1] I.D. Robb. *Specialist Surfactants*. Springer Netherlands, 1996.

[2] Changjiang Kang and Ali Khan. Self-assembly in systems of didodecyldimethylammonium surfactants: Binary and ternary phase equilibria and phase structures with sulphate, hydroxide, acetate, and chloride counterions. *Journal of Colloid and Interface Science*, 156"(1):218 – 228, 1993.

[3] Jacob N. Israelachvili. *Intermolecular and surface forces*. Elsevier, Amsterdam, 3 edition, 2011.

[4] Sajal Kumar Ghosh. *Influence of strongly bound counterions on the phase behaviour of ionic amphiphiles*. PhD thesis, Raman Research Institute, Jawaharlal Nehru University, New Delhi, 2007.

[5] W. Helfrich. Steric interaction of fluid membranes in multilayer systems. *Zeitschrift fur Naturforschung*, 33(3):305–315, 1978.

[6] A Cipiciani, R. Germani, G. Saveili, C. A. Bunton, M. Mhala, and J. R. Moffatt. The effects of single and twin tailed ionic amphiphiles upon aromatic nucleophilic substitution. *J. Chem. Soc. Perkin Trans II*, 5:541–546, 1987.

[7] D. Roux and C. R. Safinya. A synchrotron x-ray study of competing undulation and electrostatic interlayer interactions in fluid multimembrane lyotropic phases. *Journal de Physique*, 49:307–318, 1988.

[8] Bing-Sui Lu, Santosh Prasad Gupta, Michal Belička, Rudolf Podgornik, and Georg Pabst. Modulation of elasticity and interactions in charged lipid multibilayers: Monovalent salt solutions. *Langmuir*, 32(50):13546–13555, 2016.

[9] Santosh Kumar Gupta. *Studies on novel phase behavior of ionic amphiphile - water systems*. PhD thesis, Raman Research Institute, Jawaharlal Nehru University, New Delhi, 2007.

[10] G. Pabst, M Rappolt, H Amenitsch, and P. Laggner. Structural information from multilamellar liposomes at full hydration: Full q-range fitting with high quality x-ray data. *Phys. Rev. E.*, 62(3):4000–4009, 2000.

[11] Rumiana Dimova. Recent developments in the field of bending rigidity measurements on membranes. *Advances in Colloid and Interface Science*, 208:225 – 234, 2014.

[12] S. Purushothaman, P. Cicuta, O. Ces and N. J. Brooks, *The Journal of Physical Chemistry B*, 2015, **119**, 9805–9810

PART II

Interaction of Cationic Surfactants with DNA

Chapter 4

MTAB-DNA Complexes

4.1 Introduction

In the second part of the thesis we present studies on the structural polymorphism of surfactant micelle-DNA complexes. DNA, the carrier of hereditary information in living organisms, is an anionic polyelectrolyte. DNA and oppositely charged surfactant micelles can self-assemble into 2-dimensional crystalline structures in water, which mimic 2-dimensional ionic crystals. This self-assembly is driven mainly by the release of counterions that are initially condensed on DNA and the surfactant micelles[1–3]. These complexes exhibit various structures and their stability has been studied in the past by varying several factors, such as the relative DNA concentration, salt concentration, and type of surfactant counterion.

4.2 Earlier Studies

Surfactant-DNA complexes[4–11], show several kinds of phases like intercalated hexagonal phase, inverted hexagonal phase, lamellar phase etc. Rädler et al.[12] and Safinya[13] have discussed how DNA intercalates in between the

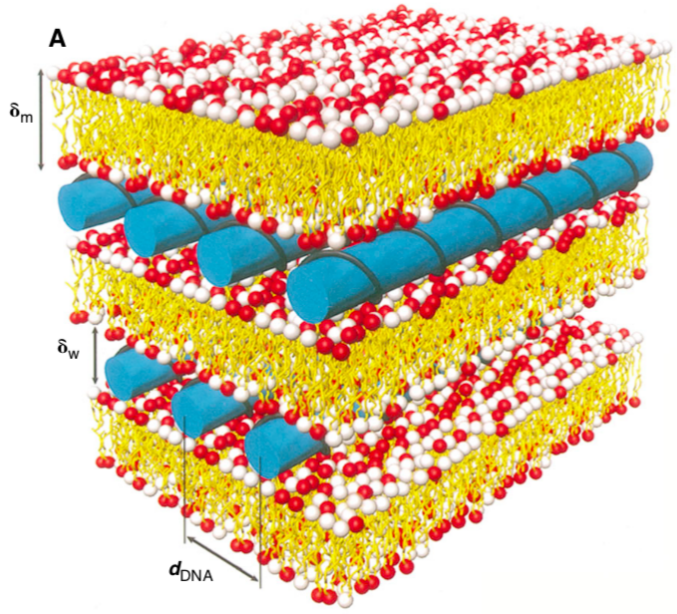

(a)

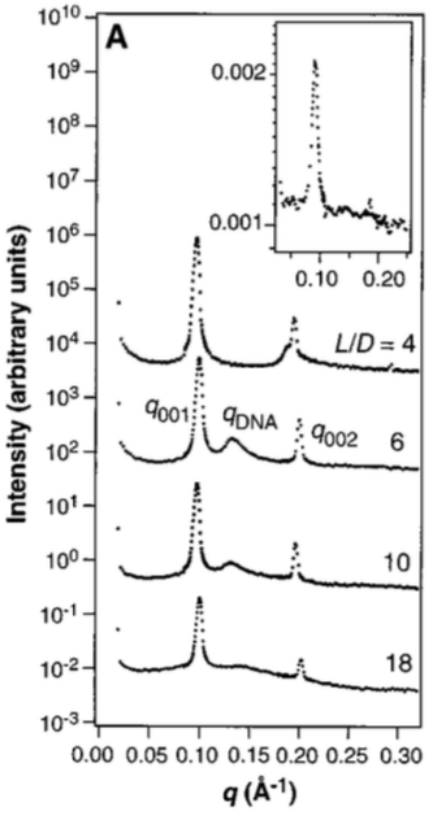

(b)

FIGURE 4.1: (a) Schematic of lipid-DNA complexes forming lamellar phase[4].(b) Diffraction patterns of cationic lipid-DNA complexes as a function of different lipid (L) to DNA (D) weight ratio (L/D)[4].

multimembrane lamellar stack made up of binary mixture of a neutral lipid and a charged lipid. Safinya et al.[4] studied lamellar complexes formed by the lipid mixtures DOPC/DOTAP or DOPE/DOTAP, in the presence of DNA. They observed a DNA-DNA correlation peak present in the SAXS data, arising from the DNA monolayer intercalated in the lamellar phase (Fig. 4.1a and b).

Bruinsma has proposed a Poisson - Boltzmann theory for the lipid-DNA complexes.[3]. There are also several other studies discussing the structure of cationic lipid - DNA complexes, because of its relevance in gene therapy[14–16]. Harries et al[17] developed a model to understand the phase behaviour of complexes of DNA with cationic lipids, as a function of charged to neutral lipid ratio and charged lipid to DNA ratio. They have discussed in detail the self assembly and electrostatics of intercalated DNA- lamellar complex. They found that at low ρ (excess DNA) and high ρ (excess liposome) the DNA-DNA spacing (d) was a constant. Over the intermediate region, d was found to increase linearly with ρ.

Cylindrical micelle forming surfactants can also form complexes with DNA, which mimic 2D ionic crystals. Fig. 4.2 is a figurative representation of such an intercalated hexagonal H_I^c and inverted hexagonal H_{II}^c phase formed by surfactant micelles and DNA. These phases have been studied by several groups[4–11,18]. Krishnaswamy et al.[9] showed the transition between hexagonal, lamellar and inverted hexagonal phases in CTAB-DNA complex by tuning the concentration of hexanol (cosurfactant) in the system.

In the following part of this section, structures formed by single chained surfactants of different alkyl chain lengths and counterions such as, cetyl trimethylammonium bromide (CTAB - with 16 carbons in the hydrophobic part), cetyltrimethylammonium tosylate (CTAT - with 16 carbons in the

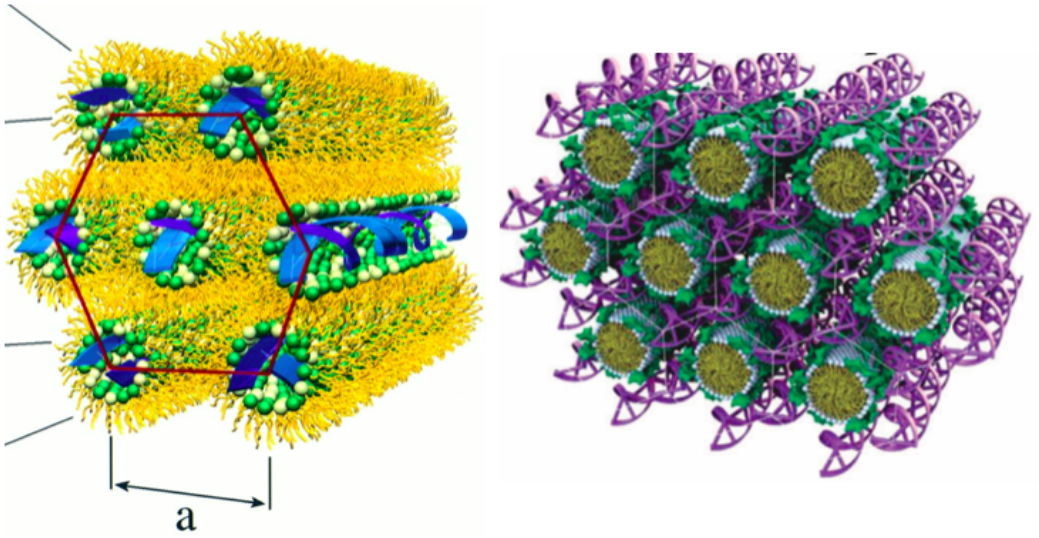

FIGURE 4.2: The inverted hexagonal phase (H_{II}^c) (*left*) and intercalated hexagonal phase (H_I^c) (*right*) 18.

hydrophobic part), dodecyltrimethylammonium bromide (DTAB) (with 12 carbons in the hydrophobic part) etc. with DNA, which are relevant to our present study are discussed briefly.

Fig. 4.3 shows the SAXS data obtained for CTAB-DNA complexes in water[5]. CTAB-DNA complexes were found to form an intercalated hexagonal (H_I^c) phase, with the scattering vectors of the peaks in the ratio $1 : \sqrt{3} : 2$[7]. Fig. 4.4a shows the polymorphic phase behaviour of the complexes of CTAT with DNA in water[6]. At low values of surfactant to DNA base molar ratio, ρ<1.5, as the [CTAT] is gradually increased, transition from an intercalated hexagonal (H_I^c) phase to a super hexagonal ($H_{I,s}^c$) phase is observed, the structures of which are discussed in detail in ref 6. At higher values of ρ and for [CTAT] > 50 mM, a square (S_I^c) phase is observed. The SAXS data of the above phases from ref. 6 is given in Fig. 4.4b. The $H_{I,s}^c$ phase is the $\sqrt{3}$ $\times$ $\sqrt{3}$ super lattice of the hexagonal phase, with the first order i.e. the (10) peak absent. The structure of the C_x phase shown in the phase diagram, is unknown.

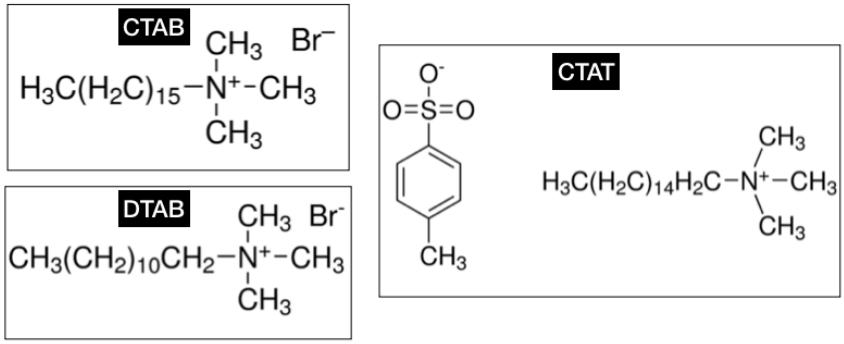

(a)

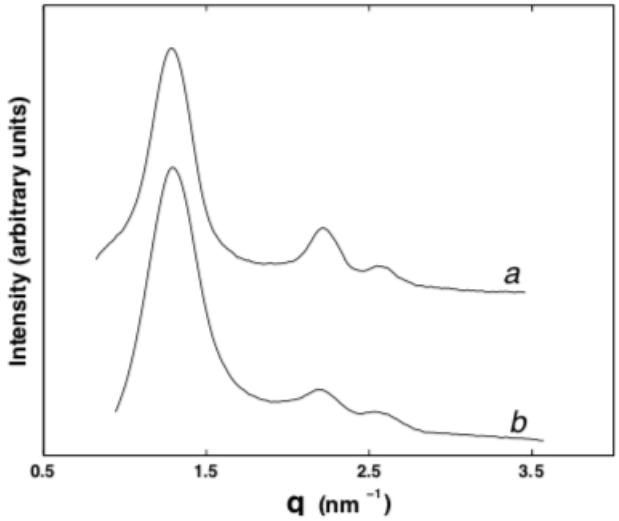

(b)

FIGURE 4.3: The (a) structure of surfactants CTAB, DTAB and CTAT (b) SAXS data of CTAB-DNA complexes in water at ρ=1 (a) and ρ=7.2 (b). [CTAB]=10 mM. T=30°C from ref 5.

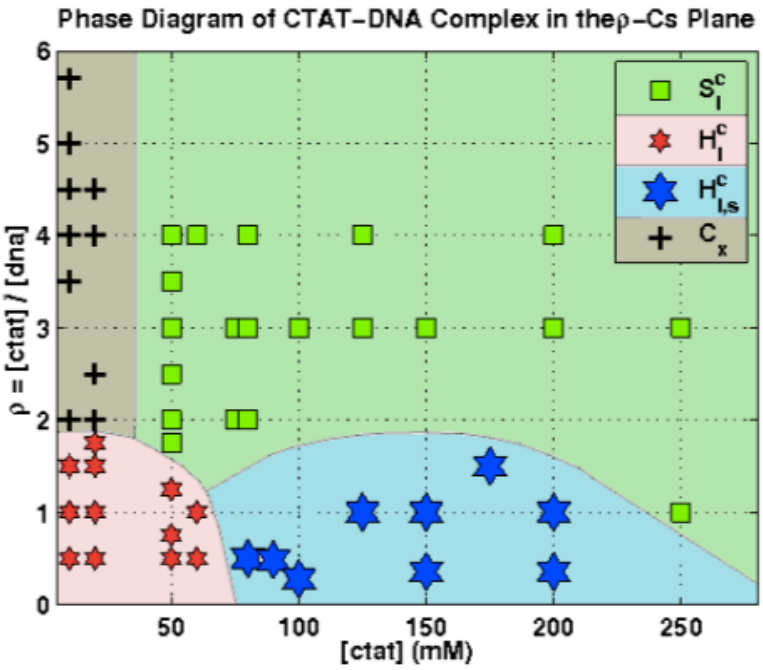

(a)

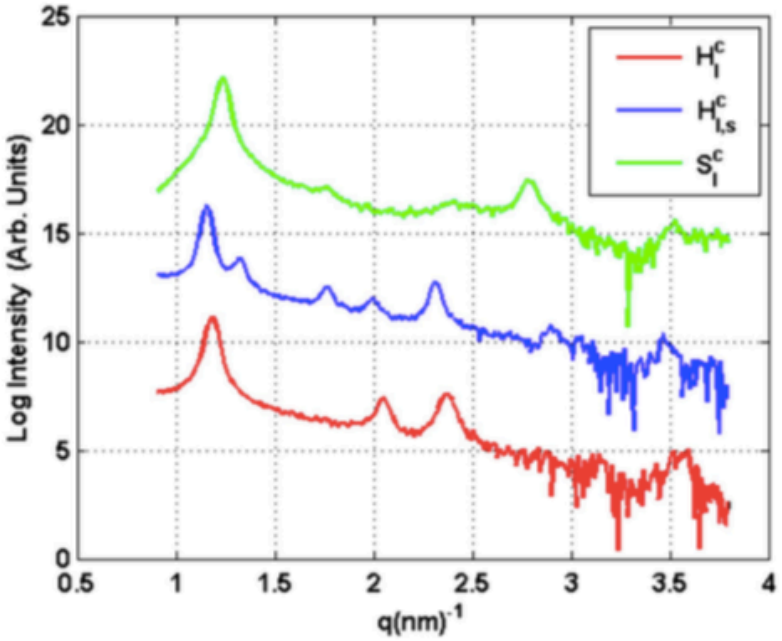

(b)

FIGURE 4.4: (a) Phase diagram of the CTAT-DNA complex in water constructed at 30°C from ref. 6; (b) Diffraction patterns of the three different structures of CTAT-DNA complexes from ref. 6.

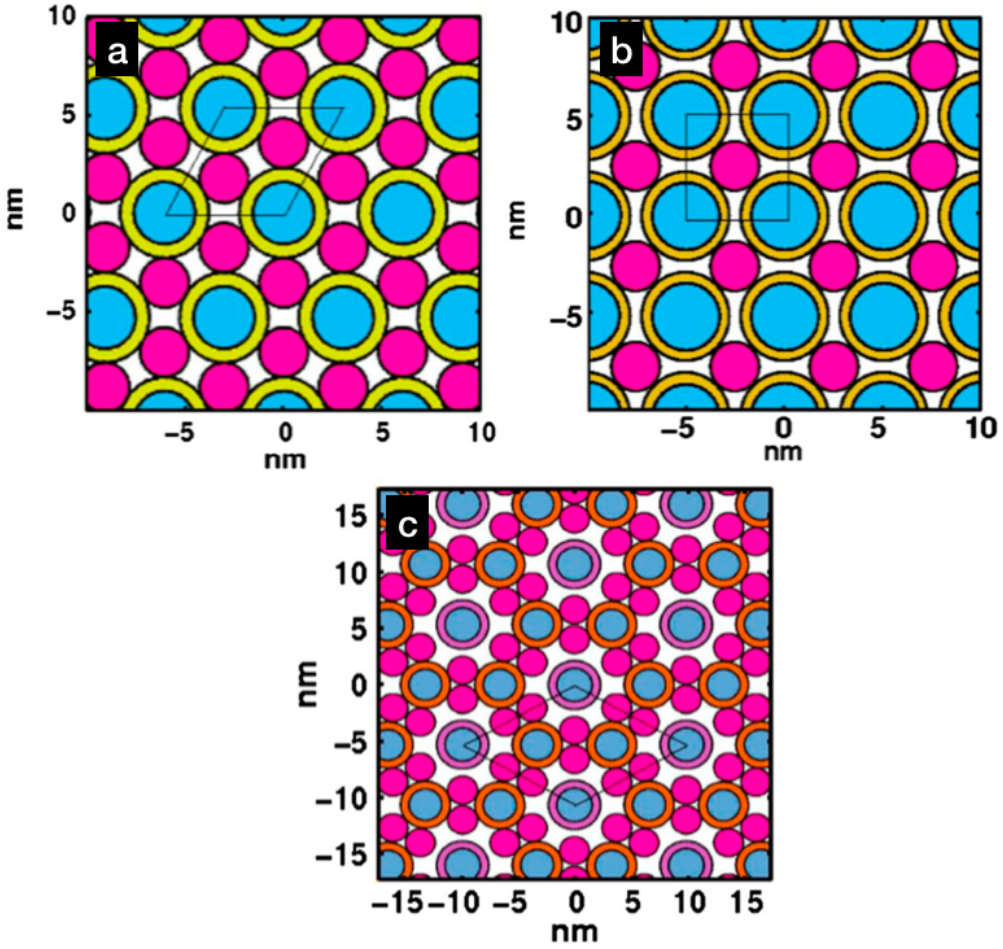

FIGURE 4.5: The (a) H_I^c, (b) S_I^c and (c) $H_{I,s}^c$ structures developed from the electron density model of CTAT-DNA complexes in water[6,7].

NaCl can induce the growth of CTAB cylindrical micelle to worm like micelles (WLMs). The complex is found to be stable in the H_I^c phase, even on addition of NaCl. Unlike NaCl, KBr which is more efficient for micellar growth was able to induce a phase transition from H_I^c phase to a $H_{I,s}^c$ phase[7]. At low ρ, in the presence of a strongly binding counterion containing salt like sodium tosylate (NaT) with concentrations ranging from 20 mM to 80 mM, a $H_I^c \rightarrow H_{I,s}^c \rightarrow S_I^c$ is observed. However, only a S_I^c phase is observed for a similar concentration of salt at high ρ[7].

Tosylate counterion can strongly adsorb on to surfactant micelle. In the case of a H_I^c phase, there are two DNA corresponding to one micelle. In the case

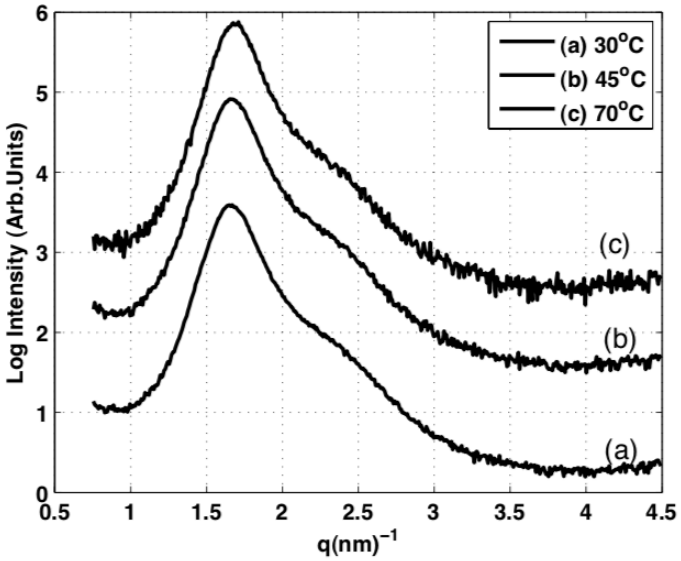

FIGURE 4.6: SAXS data of DTAB-DNA complexes at ρ=0.5 and [DTAB]=10 mM at different temperatures taken from ref. 7.

of S_I^c there is one DNA corresponding to one micelle. At low ρ and low values of CTAT concentration the complex forms an intercalated hexagonal phase (H_I^c). As the CTAT concentration is gradually increased, more tosylate counterions get adsorbed on the micelle. The DNA and the tosylate counterion compete to adsorb on the micelle. Since the square phase (S_I^c) demand release of only half the number of counterions in comparison to the hexagonal phase, at high CTAT concentrations S_I^c is observed. However an intermediate CTAT concentrations, $H_{I,s}^c$ phase is seen. Its structure correspond the $\sqrt{3} \times \sqrt{3}$ superlattice of the H_I^c structure, as shown in Fig. 4.5. Osmotic pressure studies on the samples prepared in the $H_{I,s}^c$ phase of the CTAT-DNA complexes in water showed that the complex undergo phase transition to an H_I^c phase on increasing the PEG8000 concentration[11], which confirms the proposed structure of the $H_{I,s}^c$ phase.

In case of DTAB-DNA complexes in water, SAXS data has broad peaks for different values of ρ and POM studies show birefringent textures[7]. The broad peaks indicate a short range translational order in the system, whereas

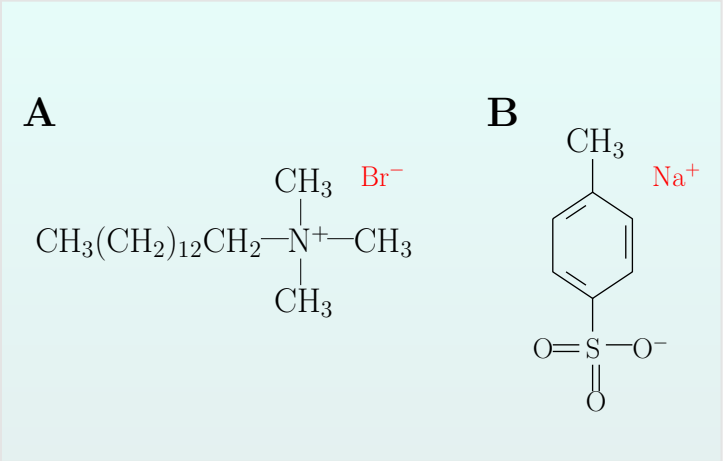

FIGURE 4.7: Chemical structure of surfactants, (A) myristyltrimethylammonium bromide (MTAB) and (B) sodium tosylate (NaT).

optical birefringence implies long range orientational order. Fig. 4.6, shows the SAXS pattern of this phase. The effect of addition of strongly binding tosylate counterion was also studied for the above complexes[7]. At ρ=0.5, a transition from $H^c_{I,s}$ phase to S^c_I phase is observed. Similar to the case of CTAT and CTAB, this $H^c_{I,s}$ phase also has a missing (10) reflection. On addition of NaCl to the complex at [DTAB]=10 mM, $H^c_{I,s}$ is observed at low values of ρ. At higher values of ρ an S^c_I phase is observed[11].

In this chapter, our motivation is to see the effect of surfactant chain length on the structure of the complex. Towards this end we study the structural polymorphism exhibited by the complexes of surfactant myristyltrimethylammonium bromide (MTAB) with DNA.

4.3 Materials and Methods

Myristyltrimethylammonium bromide (MTAB), deoxyribonucleic acid sodium salt (DNA) from calf thymus, sodium chloride (NaCl) and sodium tosylate

(NaT) shown in Fig. 4.7, were obtained from Sigma Aldrich and used without any further purification.

For sample preparation, DNA fibres were added to surfactant solutions of desired concentrations. The molar ratio of MTAB, to that of DNA base, n_s/n_b is defined as ρ. DNA fibres(w_{DNA}=5 mg), are added to MTAB samples prepared at 20 mM and 50 mM and left for equilibration (T= 40°C). Various techniques like polarising optical microscopy (POM), small angle x-ray scattering (SAXS), cryogenic scanning electron microscopy (cryo-SEM), elemental analysis (Carbon Hydrogen Nitrogen Sulphur (CHNS)) were performed to understand the structure of the complexes. For a square (S_I^c) phase, the peaks follow the ratio $1{:}\sqrt{2}{:}\sqrt{4}{:}\sqrt{5}$ and for a hexagonal (H_I^c) phase, the peaks follow the ratio $1{:}\sqrt{3}{:}\sqrt{4}$.

The samples for CHNS analysis were prepared the same way as for SAXS and POM. For the study, complex from the sample was transferred to tin cups and left to dry in a desiccator overnight. The weight of the dried samples were determined and placed into the carousel of the automatic sample feeder. The weight of the dried sample was around 1-5 mg after drying. The obtained percentages of carbon and nitrogen were used to determine the molar ratio of surfactant to base, i.e. n_s/n_b, in the complex.

4.4 Results

4.4.1 SAXS studies

Effect of surfactant concentration on the structure of complexes

DNA was added to MTAB solutions of concentration 50 mM, prepared at different ρ varying from 0.5 to 5 in Millipore water. At ρ=0.5, SAXS data

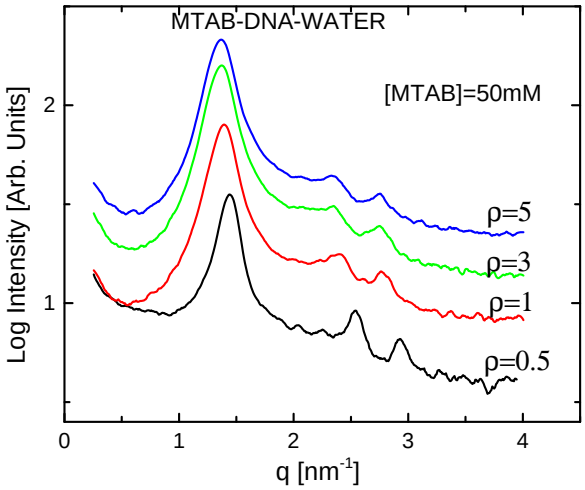

(a)

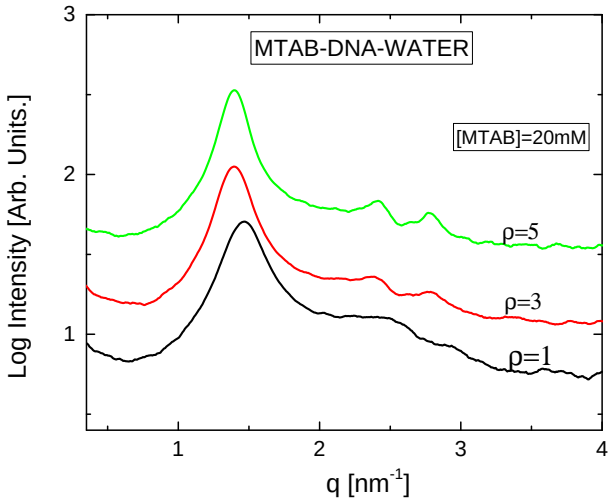

(b)

FIGURE 4.8: SAXS data of MTAB-DNA complexes in water with (a) [MTAB]=50 mM and ρ=0.5, 1, 3 and 5 and (b) [MTAB]=20 mM for ρ=1, 3 and 5 at T=30°C.

correspond to a hexagonal phase. The lattice parameter was found to be 5.01 nm. Fig. 4.8a, shows the SAXS data of these complexes at different values of ρ. Further, as we increase the value to ρ=5, the lattice parameter increased to 5.30 nm. This shift in the lattice parameter is a consequence of increase in the micellar size with increase in MTAB concentration. Table 4.1, shows the variation of *d*-spacing with ρ in water. The system continues to remain in the hexagonal phase on increasing ρ from 0.5 to 5.0.

TABLE 4.1: The lattice parameters of MTAB-DNA complexes in water obtained from SAXS data at [MTAB]=50 mM and 20 mM.

[MTAB]=50 mM			[MTAB]=20 mM		
ρ	a [nm]	Phase	ρ	a [nm]	Phase
0.5	5.01	H_I^c	-	-	-
1	5.21	H_I^c	1	4.94	H_I^c
3	5.27	H_I^c	3	5.21	H_I^c
5	5.30	H_I^c	5	5.18	H_I^c

To study the effect of surfactant concentration, a series of MTAB samples were also prepared at [MTAB]=20 mM. SAXS data correspond to a hexagonal phase similar to [MTAB]=50 mM, indicating that hexagonal phase is stable at different MTAB concentrations (Fig. 4.8b). Since the system shows similar phase behaviour at high and low values of MTAB concentrations, further experiments are done with [MTAB]=50 mM, unless mentioned otherwise.

Effect of salt on the structure of complexes

To study the effect of salt on the MTAB-DNA complexes, samples were made in NaCl solutions of varying concentrations, fixing [MTAB]=50 mM. NaCl concentration varied from 0 to 500 mM, with ρ = 0.5, 1, 3 and 5. The SAXS data correspond to a hexagonal phase. The sharpness of the peak

TABLE 4.2: The lattice parameters obtained for the MTAB-DNA-NaCl complexes from SAXS data at different ρ for [MTAB]=50 mM.

ρ=0.5			ρ=5		
NaCl [mM]	a [nm]	Phase	NaCl [mM]	a [nm]	Phase
0	5.01	H_I^c	0	5.30	H_I^c
200	5.10	H_I^c	200	5.27	H_I^c
400	5.38	H_I^c	400	5.43	H_I^c

is also increasing with increase in the salt concentration. As concentration of NaCl is gradually increased, initially a translucent complex is observed with SAXS study showing a broad peak. However at very high concentration of salt the system forms an isotropic phase. A similar behaviour is also observed at higher values of ρ i.e. at 1, 3 and 5. Figs. 4.9a, 4.9b, 4.10a and 4.10b show the SAXS data obtained for ρ=0.5, 1, 3 and 5 respectively, at different NaCl concentrations. Table. 4.2 shows the variation in lattice parameter at ρ=0.5 and 5. The lattice spacings of complexes at ρ=0.5, 1, 3 and 5 are depicted in Fig. 4.11.

The effect of addition of a strongly binding counterion (NaT) on the structure of complexes

At ρ=0.5, the samples were prepared with NaT solutions, whose concentration varied from 40 mM to 100 mM. As the [NaT] is gradually increased, transition from a hexagonal phase to a square phase was observed, with lattice parameters 5.64 nm and 5.05 nm respectively. In the square phase only the first order and the fourth order peaks are observed. They correspond to the (hk) planes (10) and (21). The phase behaviour of the sample is given in Fig. 4.12a. However, at higher concentrations of NaT, the system goes to an isotropic phase.

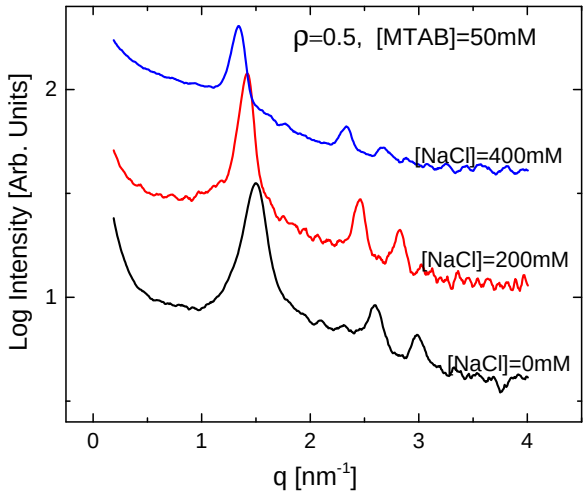

(a)

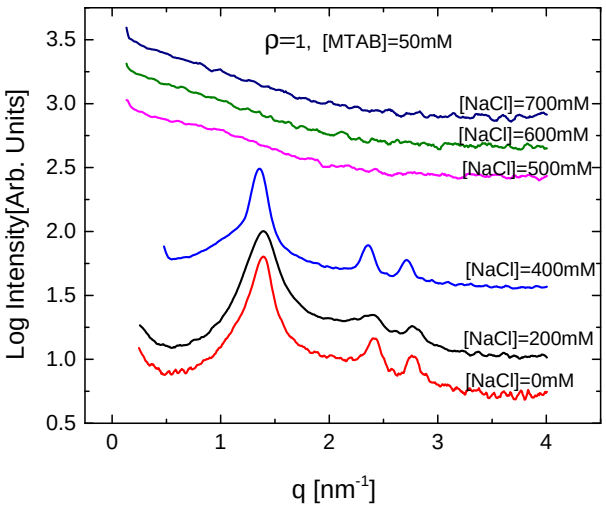

(b)

FIGURE 4.9: SAXS data of MTAB-DNA-NaCl complexes with [MTAB]=50 mM at (a) ρ=0.5 and (b) ρ=1. T=30°C.

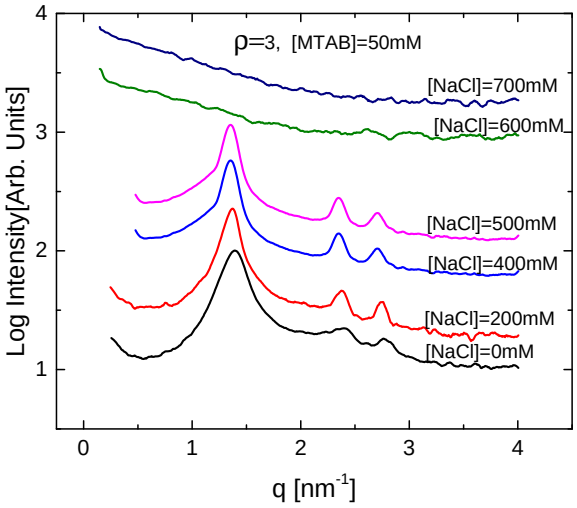

(a)

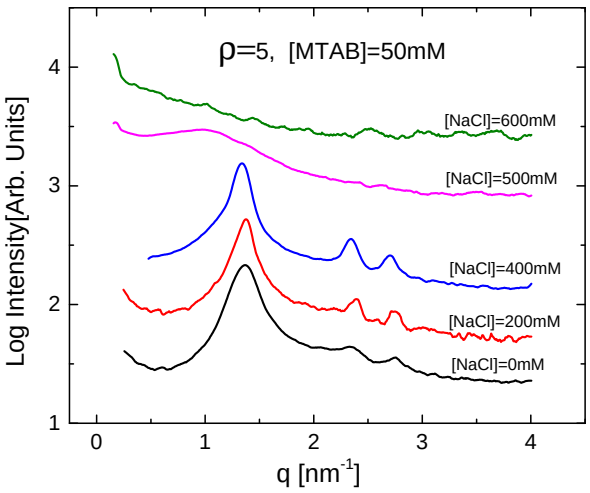

(b)

FIGURE 4.10: SAXS data of MTAB-DNA-NaCl complexes with [MTAB]=50 mM at (a) ρ=3 and (b) ρ=5. T=30°C.

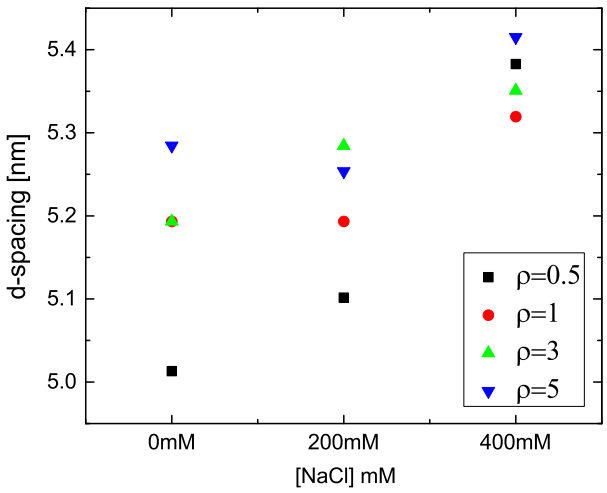

FIGURE 4.11: The lattice parameter of MTAB-DNA-NaCl complexes obtained from the SAXS data. [MTAB]=50 mM, ρ=0.5, 1, 3 and 5. T=30°C.

We also studied the phase behaviour at ρ=4, which also behaved similar to ρ=0.5. The SAXS data is depicted in Fig. 4.12b. In this case the hexagon to square phase transition was observed as the [NaT] was increased from 20 mM to 40 mM, with lattice parameters 5.43 nm and 4.7 nm respectively. At 60 mM, the square phase has a lattice parameter of 4.82 nm. As the NaT concentration is gradually increased, peaks broaden. At 150 mM the system is isotropic.

4.4.2 POM and Cryo-SEM studies of MTAB-DNA complexes

Optical microscopy studies of the MTAB-DNA complexes at [MTAB] = 50 mM were also performed. The complex in the hexagonal phase is a white, opaque precipitate. As the salt concentration is increased, the complex become translucent, which corresponds to nematic phase. The hexagonal and nematic phases show birefringence, indicating order in the system.

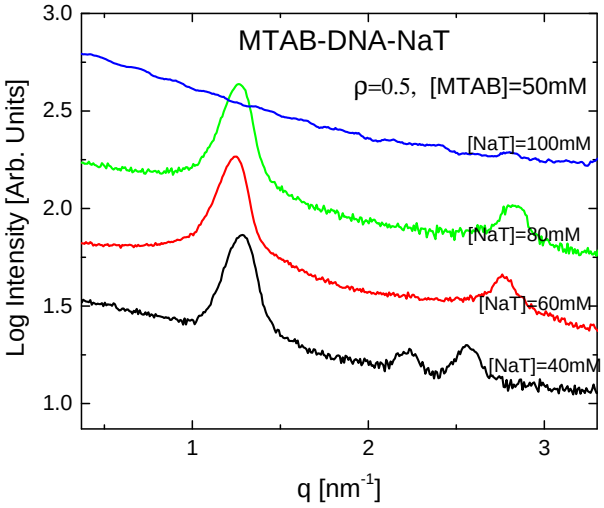

(a)

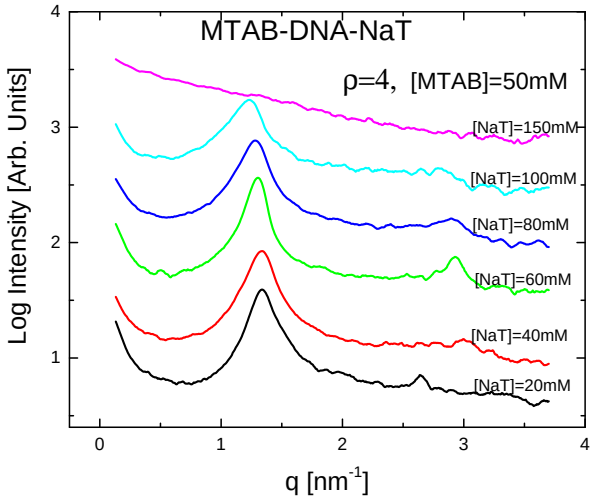

(b)

FIGURE 4.12: SAXS data of MTAB-DNA-NaT complexes at [MTAB]=50 mM, (a) ρ = 0.5 and (b) ρ=4. T=30°C.

Fig. 4.13a, shows the hexagonal phase of the complex at ρ=1 and [NaCl]= 400 mM. A highly birefringent coloured mosaic texture is obtained, typical of a hexagonal phase. Fig. 4.13b, shows the nematic phase of the complex obtained at ρ=5 and [NaCl] = 550 mM. A less birefringent texture indicating the nematic phase is observed. In this case, though long range translational order is lost, long range orientational order is still present which gives rise to the birefringent textures.

Fig. 4.14 and Fig. 4.15, show the cryo-SEM images at high and low DNA regimes. Both show bundles of rod like structures. In the case of ρ=0.5 and ρ = 5.0, each bundle has a diameter of around 44 ± 2 nm.

4.4.3 Cryo-SEM studies of complexes of CTAB and CTAT with DNA

CTAB forms 2D hexagonal lattice with DNA in water as discussed in section 4.2. On addition of salts, it can either stay in the hexagonal phase or can form super hexagonal phase depending on the kind of counterion. In the case of CTAT, it can form a square, hexagon or a super hexagon lattice under various conditions[6]. In this section, direct imaging of these structures are done by using cryo-SEM. In figures Fig. 4.16 and 4.17, we show the cryo-SEM images of these complexes. CTAB-DNA complexes show a large number of bundles. The bundle diameter is around 57 ± 5 nm for ρ=1 (Fig. 4.16(a)) and around 43 ± 5 nm for ρ=4 (Fig. 4.16(b)). Similarly, cryo-SEM images of CTAT-DNA complexes also show identical morphology. At ρ=1, the bundle size in this case is found to be around 64 ± 5 nm and at ρ=4, the size is around 56 ± 3 nm.

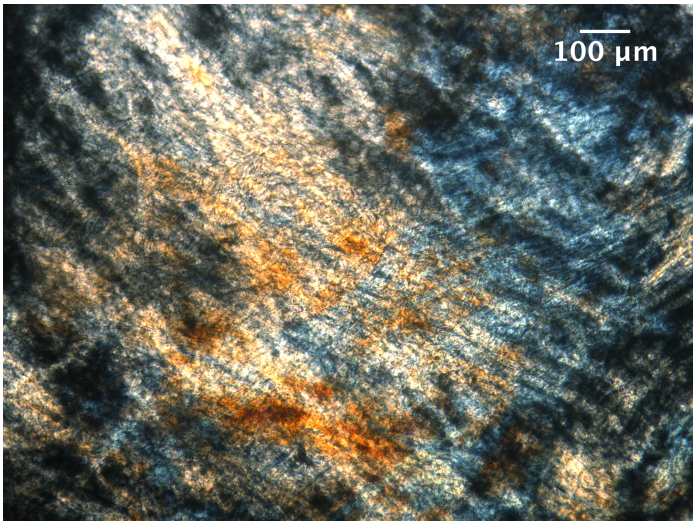

(a)

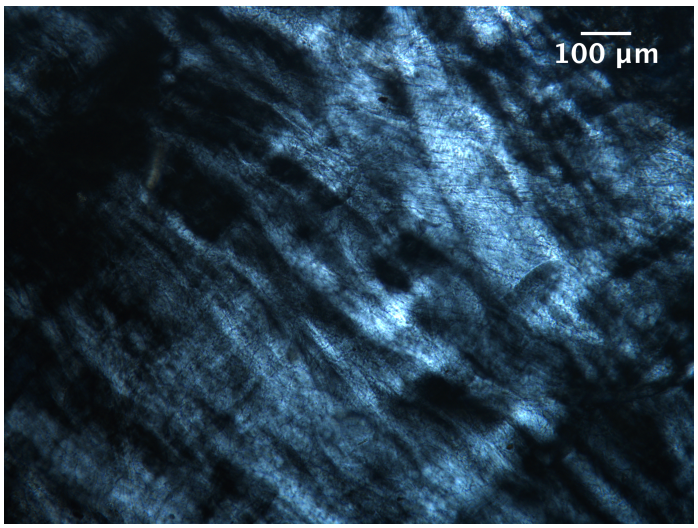

(b)

FIGURE 4.13: POM textures of MTAB-DNA complexes in (a) hexagonal phase ($\rho = 1$ [NaCl]=400 mM) and (b) nematic phase ($\rho = 5$ [NaCl]=550 mM) at [MTAB]=50 mM. T=30°C.

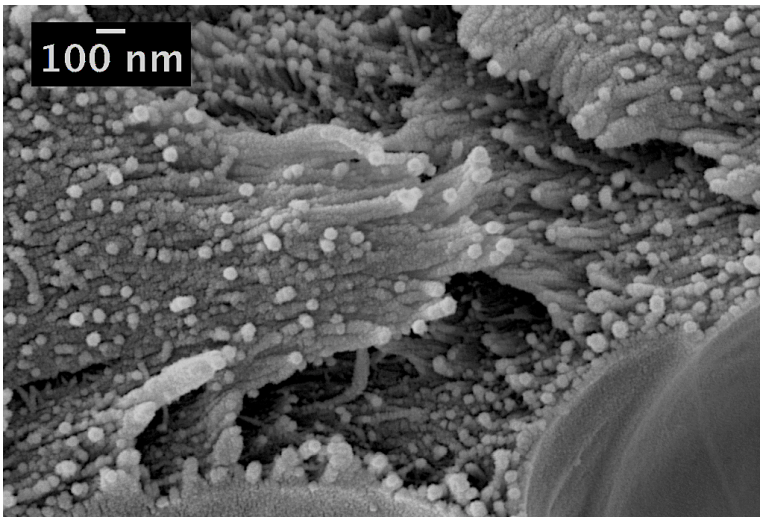

(a)

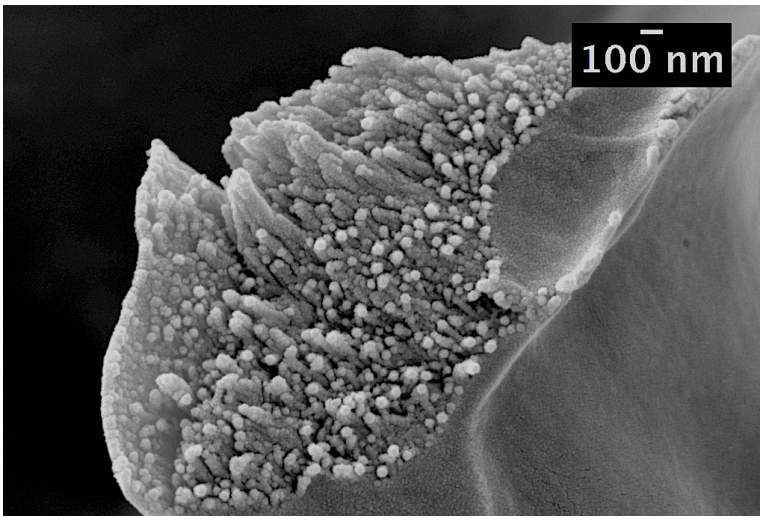

(b)

FIGURE 4.14: Cryo-SEM images of MTAB-DNA complexes in the hexagonal phase at ρ=1 and [MTAB]=50 mM. T=30°C.

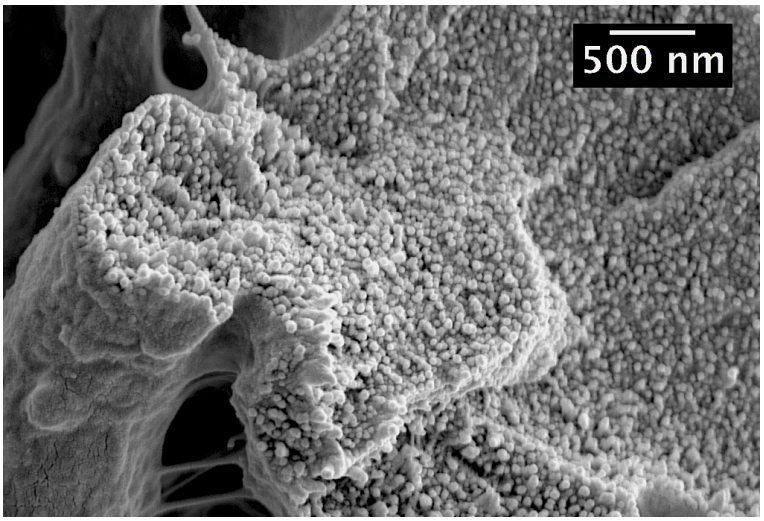

(a)

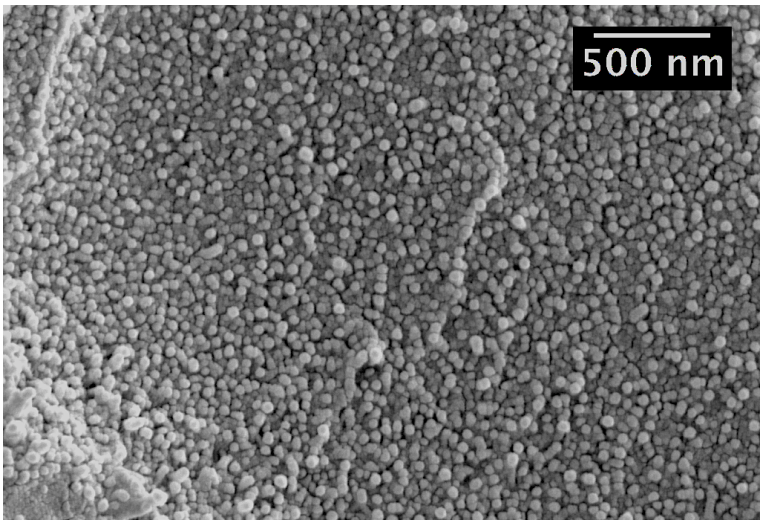

(b)

FIGURE 4.15: Cryo-SEM images of MTAB-DNA sample in the hexagonal phase at ρ=5 and [MTAB]=50 mM. T=30°C.

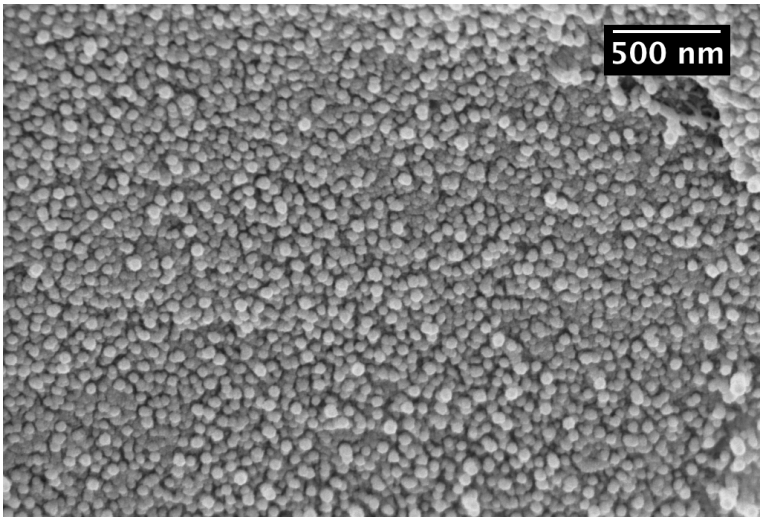

(a)

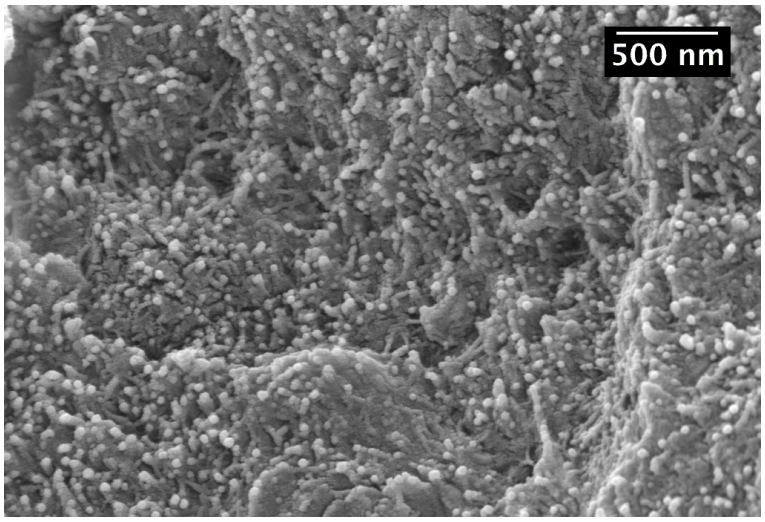

(b)

FIGURE 4.16: Cryo-SEM images of CTAB-DNA complex in the hexagonal phase at (a) $\rho = 1$ and (b) $\rho = 4$. [CTAB]= 20 mM. T=30°C.

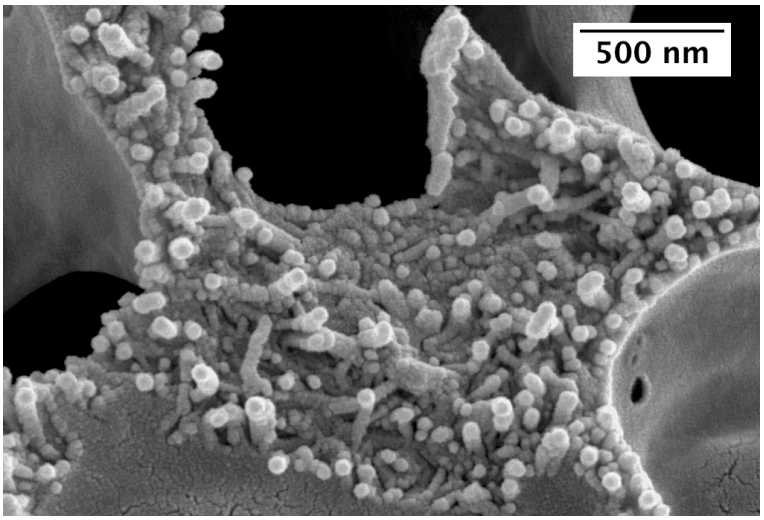

(a)

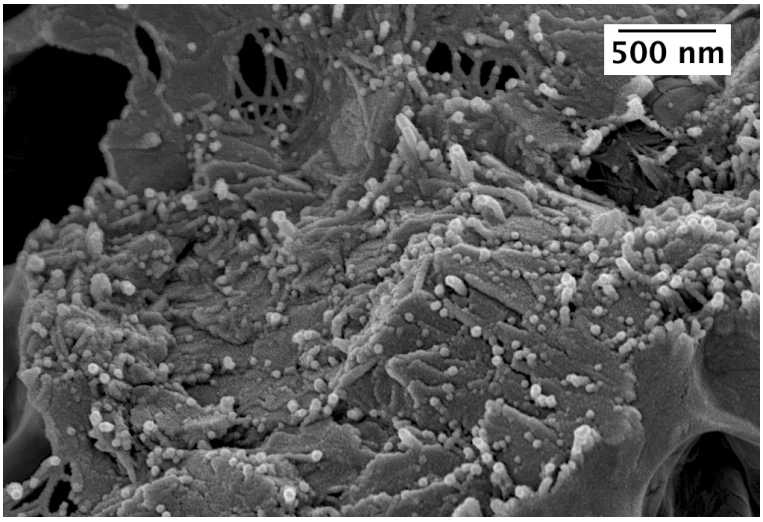

(b)

FIGURE 4.17: Cryo-SEM images of CTAT-DNA complex in the hexagonal phase at (a) $\rho = 1$ and (b) $\rho = 4$ at [CTAT]= 50 mM.

4.4.4 CHNS Analysis

In the previous section we found from small angle x-ray scattering and polarising microscopy studies that, the MTAB - DNA complexes form a 2 dimensional hexagonal lattice. CHNS analysis can provide us a quantitative information regarding the amount of surfactant and DNA (n_s/n_b) in the complex. This can then be compared with ρ in the bulk.

MTAB-DNA-Water: Samples with ρ ranging from 0.5 to 5, were used for the study. For the analysis, the complex was weighed and dried in the tin cups used in CHNS analysis. From the CHNS data we obtained the composition of Carbon and Nitrogen in the complex. We have the following relations,

$$\begin{aligned} n_b C_b + n_s C_s &= C_t \\ n_b N_b + n_s N_s &= N_t \end{aligned} \tag{4.1}$$

where n_b is the number of DNA bases, n_s is the number of surfactant molecules, C_b is number of carbons per base, C_s is number of carbons per surfactant molecule, N_b is number of nitrogen molecules per base, N_s number of nitrogen molecules per surfactant. C_t and N_t are the total number of carbon and nitrogen molecules present in the sample. The unknowns are n_b and n_s. Solving the above equations, the value of n_s/n_b is found.

From the CHNS data depicted in Fig. 4.18a, it can be seen that as ρ is gradually increased from 0.5 to 3, the corresponding n_s/n_b also increases to 1.5. However on further increasing ρ from 3 to 5, the n_s/n_b ratio remains unchanged and is saturated at the value 1.5. SAXS data (Fig. 4.8a) has shown that the system remain in a hexagonal phase at ρ values ranging from 0.5 to 5.

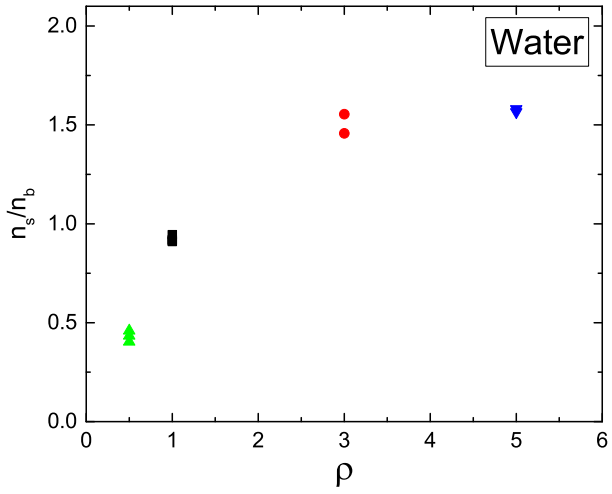

(a)

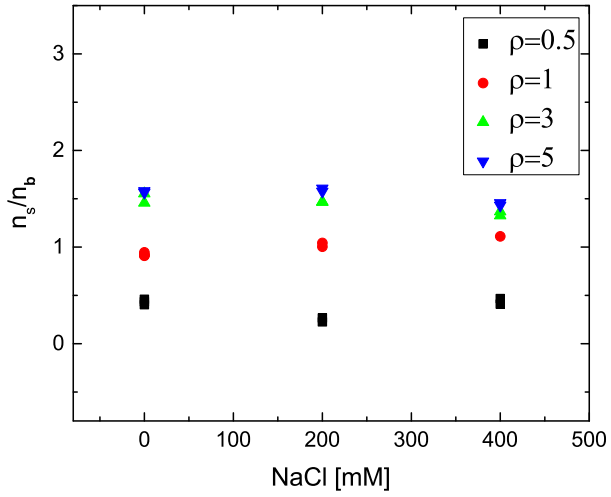

(b)

FIGURE 4.18: n_s/n_b of the MTAB-DNA complexes obtained from CHNS analysis in (a) water and (b) [NaCl] with ρ varying from 0.5 to 5.0. [MTAB]=50 mM. T=30°C.

Therefore from the CHNS experiment, it becomes evident that in a hexagonal phase, the maximum value of the molar ratio of MTAB to DNA, in the complex is 1.5. The CHNS data obtained is therefore in agreement with the theoretical value of the hexagonal phase as discussed below. The obtained result is shown in Fig. 4.18a.

MTAB-DNA-NaCl: CHNS analysis was also done with MTAB-DNA complexes in NaCl solutions with concentrations ranging from 200 mM to 400 mM and for ρ = 1, 3 and 5. The CHNS analysis depicted in Fig. 4.18b shows similar behaviour as the water samples. At ρ=0.5, as the ionic strength of NaCl is increased from 0 to 400 mM, n_s/n_b ratio is found to be around 0.5. At ρ=1, n_s/n_b is around 0.9 to 1.1 approximately. At ρ=3 and 5, n_s/n_b is around 1.5. From SAXS, it is found that the micelles and DNA arrange themselves in a 2D hexagonal lattice. The obtained value of n_s/n_b, is similar to that in water, with its maximum value at 1.5, which is what is expected for well packed cylindrical micelles with DNA, the calculation of which is given below[11].

The head group area of the alkyltrimethylammonium surfactant in the micellar phase is about 0.65nm^2[22]. For the calculation we assume DNA and micelle to be infinitely long. In hexagonal phase, corresponding to every micelle there are two DNA. The corresponding stoichiometric ratio is therefore 1:2. Taking the micellar radius to be $\sim$2.0 nm[23], the micellar surface area corresponding to the height of a base pair along the DNA strand (0.332 nm[24]) is $\sim$4.17 nm^2. This corresponds to 3.2 surfactant molecules for every DNA base. Hence n_s/n_b = 1.6.

4.5 Discussion

MTAB-DNA-water: MTAB-DNA complexes form a 2D hexagonal lattice. It is evident from the studies that this lattice structure is stable over a large range of surfactant concentrations. Figs. 4.8a and 4.8b, show the SAXS data of MTAB-DNA complexes. The studies were done for ρ=0.5, 1, 3 and 5. It can be seen that as the surfactant concentration is gradually increased (i.e. ρ is increasing), the peaks become sharper (eg. in Fig. 4.8(b)). As ρ is increased from 1 to 5, the higher order peaks grow from broad to sharp ones. CHNS data also show that as the value of ρ is gradually increased from 0.5 to 5, the n_s/n_b ratio also increase gradually and saturates at a value of 1.5. Up to ρ = 1.5, the global ρ and the n_s/n_b in the complex are the same. This is consistent with increasing length of the micelles with increasing ρ. Hence, there is no excess DNA in the solution. At higher global ρ, the n_s/n_b saturates at 1.5.

MTAB-DNA-NaCl system: The Na^+ and Cl^- ions present in the sample screen the charges on the DNA and MTAB micelles. The head group of MTAB carries a positive charge. As a result, the head groups repel each other. Addition of a monovalent salt like NaCl, reduces the strong electrostatic repulsion between the head groups reducing the spontaneous curvature and favouring micellar growth[19–21]. The long cylindrical micelles induce cross-linking with DNA more efficiently, thereby developing long range translational correlations across the system. The evidence can be seen in the increase of the sharpness of the peaks on addition of salt.

MTAB-DNA-NaT system: At low ρ and high ρ, the MTAB-DNA-NaT complexes show a hexagonal to square transition. In the case of a hexagonal lattice, there is 1 micelle corresponding to 2 DNA. In the case of a square lattice, there is 1 micelle corresponding to 1 DNA. So for the complex to

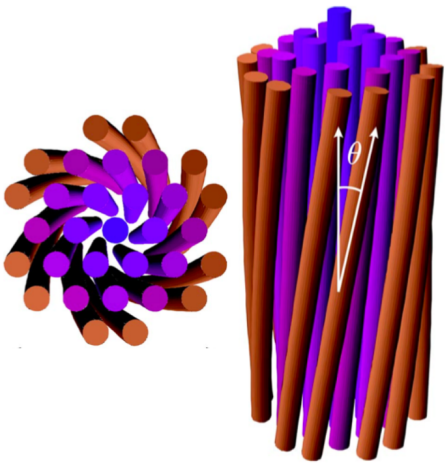

FIGURE 4.19: The twisting of bundles arising from microscopic chirality 25.

form a hexagonal phase, twice the number of counterions need to be released, in comparison to that of that of square phase. In the case of MTAB in water or NaCl solution, the counterions are not strongly adsorbing. So they release easily for the complex formation, leading to the formation of hexagonal phase. However, in the case of tosylate counterion, due to its strong adsorption in comparison to the Cl^- ions, a competition arises with DNA during the complex formation. On the other hand, for the formation of square phase, the amount of counterions needed to be released is only half as that required for the formation of a hexagonal phase as discussed already. So as the tosylate concentration is increased, more and more tosylate counterions strongly absorb into the micelle. Due to their reluctance to release into the solution, i.e. to reduce the amount of counterions released, the system undergoes a phase transition from a hexagon to a square phase. Thus a hexagon to a square phase transition is observed as we increase the NaT concentration in the case of MTAB-DNA-NaT system.

Cryo-SEM and POM studies: The POM of the MTAB-DNA complexes show birefringence. The cryo-SEM studies show bundles of rod like structures, with a preferential orientation. DNA is a chiral molecule. When it forms

complex with MTAB, the microscopic chirality can manifest macroscopically by inducing a twist as shown in Fig. 4.19. This may be the reason for the formation of bundles as discussed in 25 and shown in Fig. 4.19.

4.6 Conclusions

The SAXS and POM studies of MTAB-DNA complexes show an intercalated 2 dimensional hexagonal phase made up of MTAB micelles and DNA in water and also NaCl solutions. On addition of strongly binding salts like sodium tosylate, a hexagon to a square phase transition is observed. Cryo-SEM images revealed interesting bundle like morphology in these complexes. CHN studies indicate the growth of micelles with increasing surfactant concentration.

Bibliography

[1] F. Oosawa. A simple theory of thermodynamic properties of polyelectrolyte solutions. *J. Polym. Sci.*, 23:421–430, 1957.

[2] G. Manning. Limiting laws and counterion condensation in polyelectrolyte solutions i. colligative properties. *J. Chem. Phys.*, 51:924–933, 1969.

[3] R. Bruinsma. Electrostatics of dna-cationic lipid complexes: isoelectric instability. *The European Physical Journal B - Condensed Matter and Complex Systems*, 4(1):75–88, Jul 1998.

[4] Joachim O. Rädler, Ilya Koltover, Tim Salditt, and Cyrus R. Safinya. Structure of dna-cationic liposome complexes: Dna intercalation in multilamellar membranes in distinct interhelical packing regimes. *Science*, 275:810–4, 03 1997.

[5] Rema Krishnaswamy. *Structure of surfactant-polyelectrolyte complexes.* PhD thesis, Raman Research Institute, Jawaharlal Nehru University, New Delhi, 2003.

[6] A. V. Radhakrishnan, S. K. Ghosh, G. Pabst, V. A. Raghunathan, and A. K. Sood. Tuning dna - amphiphile condensate architecture with strongly binding counterions. *Proceedings of the National Academy of Sciences*, 109(17):6394–6398, 2012.

[7] A. V. Radhakrishnan. PhD thesis, Raman Research Institute, Jawaharlal Nehru University, New Delhi, 2012.

[8] Rema Krishnaswamy, Georg Pabst, Michael Rappolt, V. A. Raghunathan, and A. K. Sood. Structure of dna-ctab-hexanol complexes. *Phys. Rev. E*, 73:031904, Mar 2006.

[9] Rema Krishnaswamy, V. A. Raghunathan, and A. K. Sood. Reentrant phase transitions of dna-surfactant complexes. *Phys. Rev. E*, 69:031905, Mar 2004.

[10] Rema Krishnaswamy, Partha Mitra, Velayudhan Raghunathan, and A Sood. Tuning the structure of surfactant complexes with dna and other polyelectrolytes. *Europhysics Letters*, 62:357, 01 2007.

[11] Madhukar S. *Influence of some sterols and nucleotides on the structure of self-assembled amphiphilic systems*. PhD thesis, Raman Research Institute, Jawaharlal Nehru University, New Delhi, 2017.

[12] Joachim O. Rädler, Ilya Koltover, Tim Salditt, and Cyrus R. Safinya. Structure of dna-cationic liposome complexes: Dna intercalation in multilamellar membranes in distinct interhelical packing regimes. *Science*, 275(5301):810–814, 1997.

[13] Cyrus R Safinya. Structures of lipid-dna complexes: supramolecular assembly and gene delivery. *Current Opinion in Structural Biology*, 11 (4):440 – 448, 2001.

[14] Danilo D. Lasic, Helmut Strey, Mark C. A. Stuart, Rudolf Podgornik, and Peter M. Frederik. The structure of dna liposome complexes. *Journal of the American Chemical Society*, 119(4):832–833, 1997.

[15] H E Hofland, L Shephard, and S M Sullivan. Formation of stable cationic lipid/dna complexes for gene transfer. *Proceedings of the National Academy of Sciences*, 93(14):7305–7309, 1996.

[16] S.J Eastman, C Siegel, J Tousignant, A.E Smith, S.H Cheng, and R.K Scheule. Biophysical characterization of cationic lipid:dna complexes. *Biochimica et Biophysica Acta (BBA) - Biomembranes*, 1325(1):41 – 62, 1997.

[17] D. Harries, S. May, W. Gelbart and A. Ben-Shaul, Structure, stability, and thermodynamics of lamellar dna-lipid complexes. *Biophysical Journal*, 75(1):159–173, 1998.

[18] Alexandra Zidovska, Heather M. Evans, Kai K. Ewert, Joel Quispe, Bridget Carragher, Clinton S. Potter, and Cyrus R. Safinya. Liquid crystalline phases of dendritic lipid-dna self-assemblies: Lamellar, hexagonal, and dna bundles. *The Journal of Physical Chemistry B*, 113(12):3694–3703, 2009.

[19] S.A. Safran, P.A. Pincus, M. E. Cates, and F.C. Mackintosh. Growth of charged micelles. *Journal de Physique*, 51(6):503–510, 1990.

[20] F. C. MacKintosh, S. A. Safran, and P. A. Pincus. Self-assembly of linear aggregates: the effect of electrostatics on growth. *EPL (Europhysics Letters)*, 12(8):697, 1990.

[21] P. A. Hassan and J. V. Yakhmi. Growth of cationic micelles in the presence of organic additives. *Langmuir*, 16(18):7187–7191, 2000.

[22] S. A. Buckingham, C. J. Garvey and G. G. Warr, *The Journal of Physical Chemistry*, 1993, **97**, 10236–10244

[23] Jacob N. Israelachvili. *Intermolecular and surface forces*. Elsevier, Amsterdam, 3 edition, 2011.

[24] M. Levitt, *Proceedings of the National Academy of Sciences*, 1978, **75**, 640–644

[25] G. M. Grason and R. F. Bruinsma, *Phys. Rev. Lett.*, 2007, **99**, 098101

Chapter 5

Electron Density Map of MTAB-DNA Complexes

5.1 Introduction

As discussed in Chapter 4 , MTAB-DNA complexes form a two-dimensional (2D) hexagonal phase. In this chapter we generate the electron density map of the above hexagonal lattice from the scattering data and by intelligent guessing of phases of the diffraction peaks. An idea about the relative positions of micelles and DNA can be obtained from the generated map. On this basis, we further model the lattice to obtain several system parameters.

5.2 Construction of electron density maps

In this section we discuss how we generate the electron density map[1,2] for the MTAB-DNA complex, from the data obtained from SAXS. The MTAB-DNA complexes in water at [MTAB]=50 mM, self assemble into a 2 D hexagonal phase. SAXS data contain three peaks corresponding to this phase as shown in Fig.5.1. A 2D real space hexagonal lattice is shown in Fig. 5.2. We

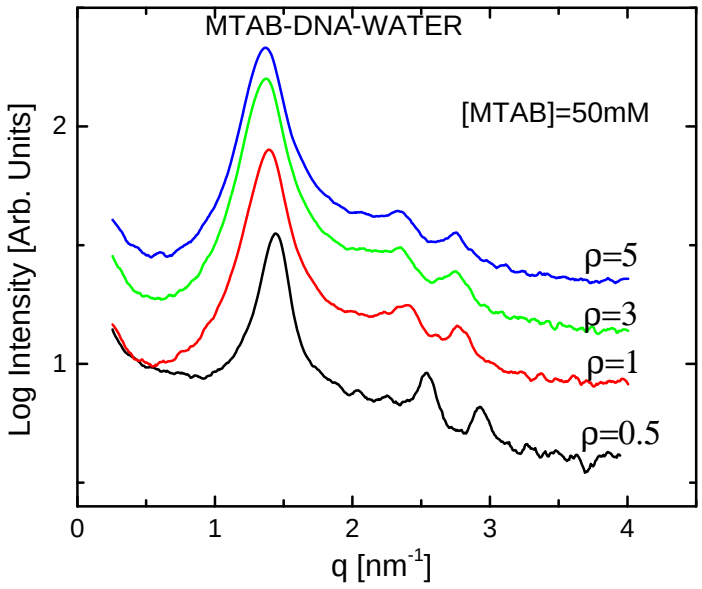

FIGURE 5.1: SAXS data of MTAB-DNA complexes in water at different values of ρ.

consider a centred rectangular unit cell with translational vectors $\vec{a}$ and $\vec{b}$, with $b = \sqrt{3}a$. Then any point in this lattice can be written as

$$\vec{r}_{uv} = u\vec{a} + v\vec{b} \tag{5.1}$$

The reciprocal lattice vectors, $\vec{q_{hk}}$ for this centred rectangular lattice are given by

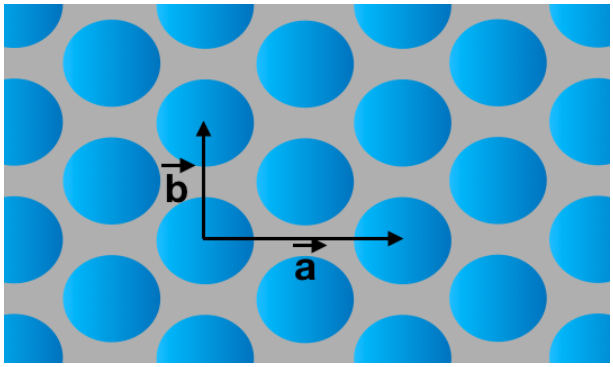

FIGURE 5.2: Translational lattice vectors $\vec{a}$ and $\vec{b}$ of a centred rectangular unit cell.

$$\vec{q}_{hk} = h\vec{a^*} + k\vec{b^*} \tag{5.2}$$

where, a^* and b^* form the translational vectors of the reciprocal lattice, which can be written as

$$\begin{aligned} a^* &= \frac{-\sqrt{3}\pi}{a}\hat{x} + \frac{\pi}{a}\hat{y} \\ b^* &= \frac{2\pi}{a}\hat{y} \end{aligned} \tag{5.3}$$

In the case of a hexagonal phase the peak positions in terms of scattering vector q, follow the ratio $1 : \sqrt{3} : 2$, corresponding to the (hk) planes (10), (11) and (20). By integrating area under each peak, corresponding intensities are obtained. Since the detector used for data collection in our case is 1 dimensional, each peak area is multiplied by q^2, to take care of the geometry of the unoriented sample[1–4]. Since we are interested in the relative intensities, the obtained intensity values were normalised, the square root of which give the amplitude of reflection, $A(\vec{q}_{hk})$. Thus we obtain the corrected intensity and the corrected amplitude[1–4]. Then the electron density can be written as

$$\rho_{hk}(\vec{r}) = \sum p_{hk} A(\vec{q}_{hk}) Cos(\vec{q}_{hk} \cdot \vec{r}) \tag{5.4}$$

In the above equation, p_{hk} defines the phase of the reflection. Since the structure is centro-symmetric, and taking the origin at the centre of symmetry, p_{hk} can take values $+1$ or -1. In our case the SAXS data has 3 prominent peaks. Keeping one of the phases fixed, all $2^2 = 4$ combinations are calculated (the remaining being just the inverse) and the corresponding electron

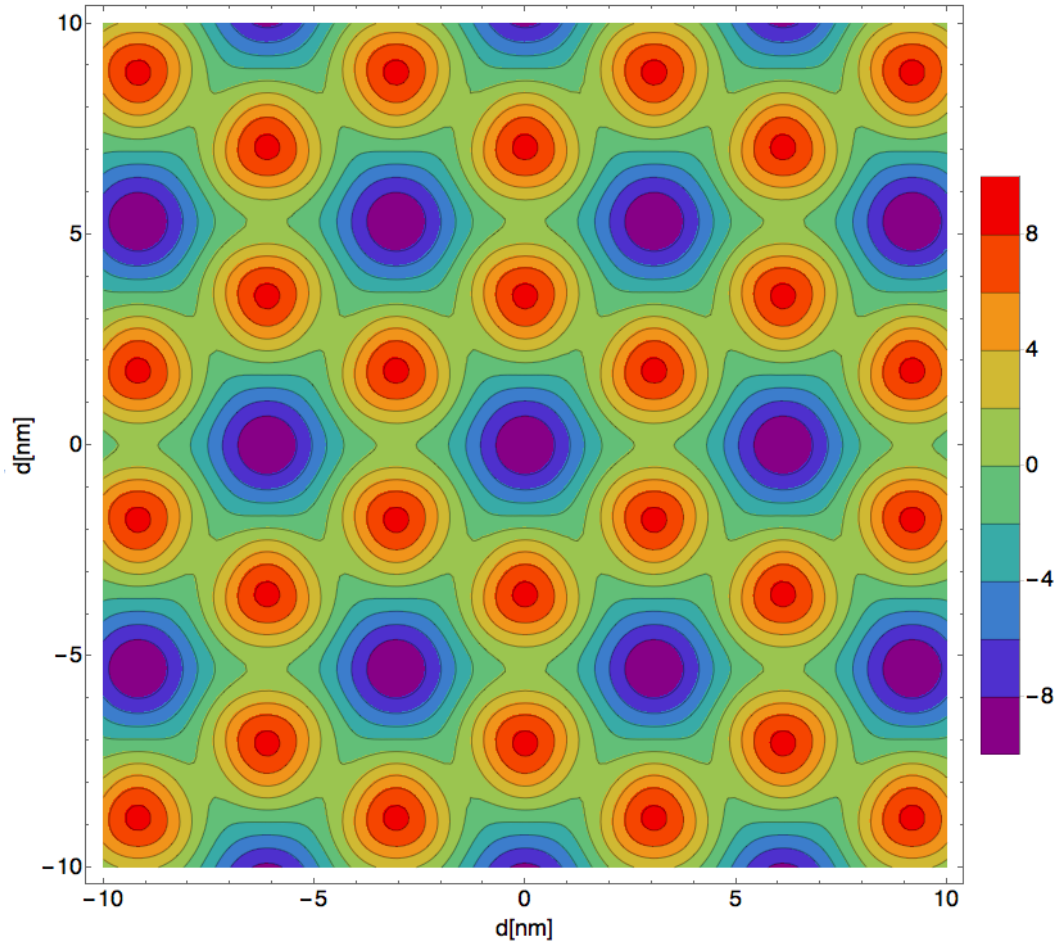

FIGURE 5.3: The relative electron density map of intercalated hexagonal phase obtained for MTAB-DNA complex.

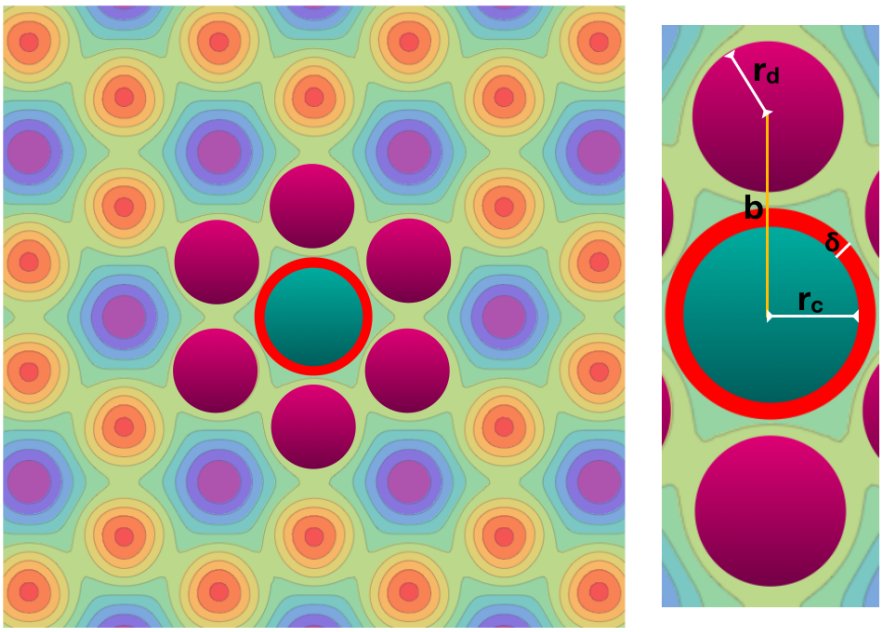

FIGURE 5.4: The relative positions of micelles (green core with red annular region) and DNA (pink disc) (*left*) and the repeating unit (*right*) of the intercalated hexagonal phase formed by MTAB-DNA complex.

densities are plotted. Fig. 5.3, gives the relative electron density map of the MTAB-DNA complex at [MTAB]=50 mM and ρ=5, which clearly shows the intercalated hexagonal phase of MTAB-DNA complex (Fig. 5.4). Now a model is constructed based on this map to obtain the relative intensity of the peaks and therefore understand its physical validity.

5.2.1 Modelling of the hexagonal phase

From the electron density map, we have a model of the arrangement of micelles and DNA in the hexagonal lattice. Fig. 5.4, shows the relative positions of the MTAB micelles whose hydrocarbon chain regions are denoted by the green inner core (of radius r_c) with the surface head group region denoted by the red outer shell(of thickness δ) and DNA solid discs in pink

(radius r_d). The repeating unit of the lattice is given in Fig. 5.4. For modelling of the structure, we follow the procedure described in references, 1–4, which is discussed below. To model the 2 dimensional structure, DNA are considered to be discs of radius r_d and electron density ρ_d. The micelles are modelled as discs with the hydrocarbon core of radius r_c and electron density ρ_c, surrounded by an annular region of width δ and electron density ρ_h[2]. $r_d = 1.25nm$ and $\rho_d = 400e/nm^2$[3]. Values of ρ_c and the electron density of water ρ_w were taken from the literature to be 280 e/nm^2 and 330 e/nm^2, respectively[3].

The electron density of the 2 dimensional lattice formed by DNA and micelles, $\rho_c(\vec{r})$ can be written as convolution of a lattice function $\rho_l(\vec{r})$ with a basis function $\rho(\vec{r})$. The lattice function is a set of delta functions which describes the lattice and basis function is the repeating unit, which when repeated generate the crystal (Fig. 5.4).

$$\rho_c(\vec{r}) = \rho_l(\vec{r}) \circledast \rho(\vec{r}) \tag{5.5}$$

the Fourier transform of which is given by,

$$f_c(\vec{q}) = f_l(\vec{q}) \times f(\vec{q}) \tag{5.6}$$

In case of the 2 dimensional intercalated hexagonal lattice (H_I^c) formed by the MTAB micelle and DNA, each repeating unit contains two DNA and one MTAB micelle. For our case then the electron density can be written as,

$$\rho(\vec{r}) = \rho_{dna}(\vec{r}) \circledast [\delta(r-b)\delta(\theta-\pi/2) + \delta(r-b)\delta(\theta+\pi/2)] + \rho_m(\vec{r}) \tag{5.7}$$

where b is the separation between the centres of micelle and DNA (Fig. 5.4). Since the structure is assumed to be close-packed, $b = r_c + \delta + r_d$. By doing Fourier transform of Eqn. 5.7, we obtain the form factor of the repeating unit which is given by,

$$f^{H_I^c}(q,\phi) = 2Cos(qbSin(\phi))f_d(q) + f_m(q) \tag{5.8}$$

where f_d and f_m are the form factors of the DNA and micelle respectively, given by

$$\begin{aligned} f_d(q) &= \frac{2\pi}{q}[(\rho_d - \rho_w)r_d J_1(qr_d)] \\ f_m(q) &= \frac{2\pi}{q}[(\rho_h - \rho_w)r_m J_1(qr_m) - (\rho_h - \rho_c)J_1(qr_c)] \end{aligned} \tag{5.9}$$

$J1$ is the Bessel function of first kind of order 1 defined as

$$J_1(x) = (1/\pi)\int_0^\pi Cos\theta\ Sin(xCos\theta)\mathrm{d}\theta$$

The data was fitted to the model with ρ_h and δ as adjustable parameters. The fits were obtained by constraining the value of ρ_h and δ between 280 to 400 e/nm^3 and 0.5 to 1.2 nm respectively.

The best fit parameters to the model are given in the Tab. 5.1. The calculated (I^c_{hk}) and observed (I^o_{hk}) values of intensities is given in Tab. 5.2. A parameter R is defined as $\sum|(I^c_{hk} - I^o_{hk})|/\sum I^o_{hk}$, to evaluate the goodness of the fit. The quality of fit is very good as indicated by the low value of R. This confirms the validity of the proposed model for the structure of these complexes.

$\rho_h(e/nm^3)$	$\delta(nm)$	$b(nm)$	$r_c(nm)$	$r_m(nm)$	R
330.49	0.66	3.01	1.09	1.76	0.06

TABLE 5.1: The best fit parameters obtained for the MTAB-DNA complexes at ρ=3 and [MTAB]=50mM

h,k	1,0	1,1	2,0	2,1
I^c_{hk}	100	6.09	7.71	0.41
I^o_{hk}	100	6.02	7.65	0
p_{hk}	-1	+1	-1	-1

TABLE 5.2: The relative peak intensities obtained from the best fit parameters (I^c_{hk}) and from SAXS (I^o_{hk}) for MTAB-DNA complex at ρ=3 and [MTAB]=50 mM. p_{hk} is the phase of reflection

5.3 Conclusions

In this chapter we have constructed electron density map of the 2 dimensional lattice formed by MTAB-DNA complexes. We also modelled it to an intercalated hexagonal phase and obtained the best fit parameters. We also checked the goodness of the fit by comparing the relative intensity values from experiment and model.

Bibliography

[1] A. V. Radhakrishnan. PhD thesis, Raman Research Institute, Jawaharlal Nehru University, New Delhi, 2012.

[2] A. V. Radhakrishnan, S. K. Ghosh, G. Pabst, V. A. Raghunathan, and A. K. Sood. Tuning dna - amphiphile condensate architecture with strongly binding counterions. *Proceedings of the National Academy of Sciences*, 109(17):6394–6398, 2012.

[3] Rema Krishnaswamy, Georg Pabst, Michael Rappolt, V. A. Raghunathan, and A. K. Sood. Structure of dna-ctab-hexanol complexes. *Phys. Rev. E*, 73:031904, 2006.

[4] Madhukar S. *Influence of some sterols and nucleotides on the structure of self-assembled amphiphilic systems*. PhD thesis, Raman Research Institute, Jawaharlal Nehru University, New Delhi, 2017.

Chapter 6

MTAB - DTAB - DNA Complexes

6.1 Introduction

In Chapter 4, we have seen the polymorphic behaviour of MTAB-DNA complexes with different counterions. From earlier studies, we also know the structural polymorphism of Dodecyltrimethylammonium bromide (DTAB)-DNA complexes[1,2]. The only difference between the two surfactant molecules is the number of carbons in the hydrophobic chain, with MTAB having 14 carbons and DTAB having 12 carbons. In this chapter we try to understand the vast difference in the phase behaviour of these two systems, by studying complexes of binary mixtures of MTAB-DTAB with DNA.

6.2 Earlier Studies

In Chapter 4 section 4.2, we have discussed in detail the structural polymorphism of complexes formed by CTAB, CTAT, MTAB and DTAB with DNA, based on several previous studies[1–6]. From our studies we know that MTAB-DNA complexes exhibit hexagonal phase in water, irrespective of the surfactant concentration, MTAB to DNA base molar ratio, etc. which is

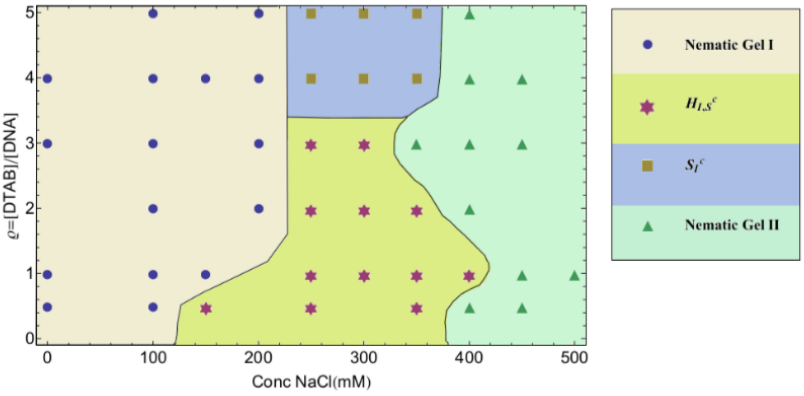

FIGURE 6.1: The figure shows partial phase diagram of DTAB-DNA complexes in NaCl solutions[2].

discussed in Chapter 4. In NaCl solutions, the complex swells and at very high salt forms an isotropic phase. In the presence of a strongly binding counterion like NaT, it forms a square phase.

Fig. 6.1, shows the partial phase diagram of DTAB-DNA complexes in the presence of NaCl[2]. At low $\rho = 0.5$ ($\rho = n_s/n_b$, as defined in Chapter 4), and at low NaCl concentrations, SAXS data show broad peaks. This phase is referred to as the nematic gel I, which has long range orientational order and short range translational order[2]. At [NaCl]=150mM, sample exhibits a super hexagonal phase, whose (10) peak is absent[2]. At still higher concentrations of NaCl, the sample undergoes transition to nematic gel II. At $\rho = 4$, they again observed a nematic gel I, in the absence of salt. As the salt concentration is gradually increased, system undergoes transition to a square S_I^c phase At yet higher concentrations of salt, sample transforms to nematic gel II. A detailed phase diagram of the above is given in Fig. 6.1[2].

In order to understand the formation of different structures in MTAB-DNA and DTAB-DNA complexes, surfactant solutions were prepared with binary

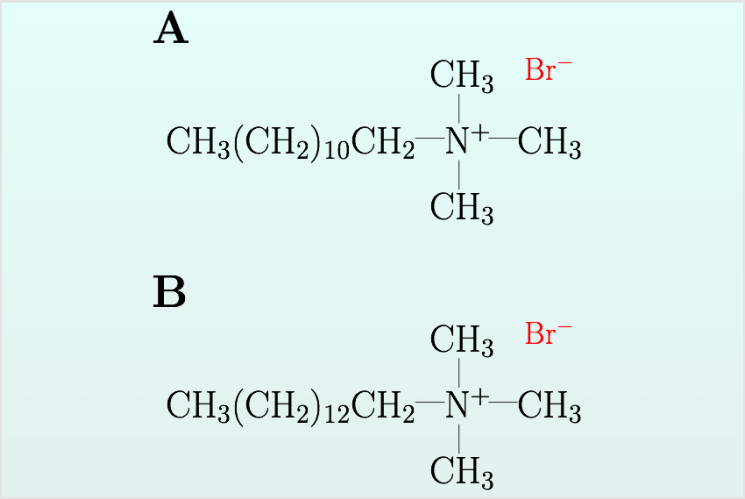

FIGURE 6.2: Chemical structure of (A) dodecyltrimethylammonium bromide (DTAB), (B) myristyltrimethylammonium bromide (MTAB).

mixtures of DTAB and MTAB. In each case the DTAB concentration was increased from around 10% to 98%, fixing the total [MTAB+DTAB] concentration. Studies were performed in water and also by varying several factors like, surfactant to DNA base ratio, external salt concentration etc.

6.3 Materials and Methods

Myristyltrimethylammonium bromide (MTAB), dodecyltrimethylammonium bromide (DTAB), sodium chloride (NaCl) and deoxyribonucleic acid sodium salt from calf thymus (DNA) were purchased from Sigma and used without any further purification. The chemical structures of these are depicted in Fig. 6.2. The surfactant samples of desired concentration in water or salt solution are prepared. The molar ratio of surfactants (MTAB and DTAB), to that of DNA base, n_s/n_b is defined as ρ.

For sample preparation, DNA strands were added to the surfactant solutions prepared at desired concentrations in water and salt solutions. For our

studies, the concentration of [MTAB+DTAB] is fixed at 50mM. These samples are then left for equilibration (T= 40°C) for around 5 days. Small angle x-ray scattering (SAXS), Cryogenic scanning electron microscopy (cryo-SEM) were used to study the structure and phase behaviour of the complexes. Different phases were identified from their SAXS patterns. For a square (S_I^c) phase q values of the peaks follow the ratio $1:\sqrt{2}:\sqrt{4}:\sqrt{5}$ and for a hexagonal (H_I^c) phase, q values of the peaks follow the ratio $1:\sqrt{3}:\sqrt{4}$.

6.4 Results

6.4.1 MTAB-DTAB-DNA complexes in water

At low molar ratio ρ=1

Samples were prepared as discussed in section 6.3. The complex, made up of surfactant and DNA form a white precipitate. The complexes from the equilibrated samples were used for the SAXS study. Depending on the value of ρ, excess aqueous solution contains excess surfactant or excess DNA. For SAXS the complexes were filled in glass capillaries along with the excess aqueous solution and flame sealed.

The samples were prepared with DTAB concentration in the surfactant mixture W_{DTAB}, increasing from 33% to 98% and [MTAB+DTAB]=50mM. At W_{DTAB}=33%, the SAXS data show 2 peaks, the second peak being much broader than the first. As the DTAB concentration is increased gradually, the peaks (both first and second) become broader. These peaks are very broad and cannot be fitted to a hexagonal or a square lattice. The SAXS data of the same is given in Fig. 6.3. The position of q is seen to shift as W_{DTAB} is

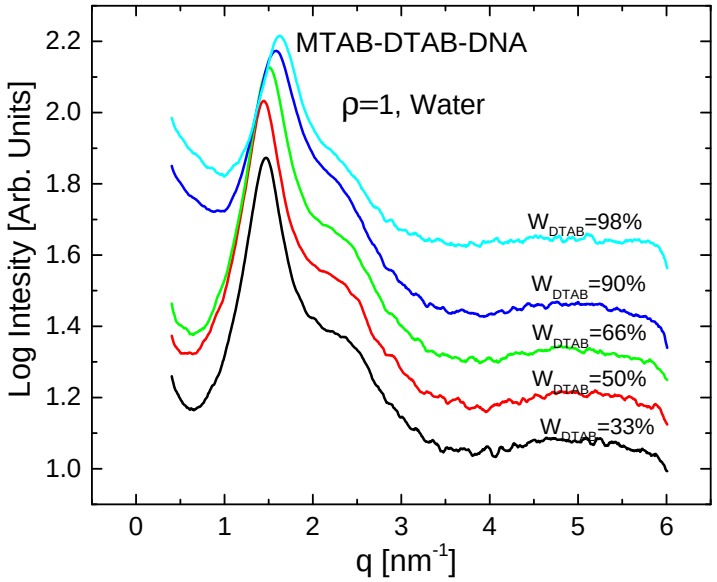

FIGURE 6.3: MTAB-DTAB-DNA complexes at ρ=1 in water with increasing [DTAB] concentrations. [MTAB+DTAB] = 50mM and T=30°C.

increased from 33% to 98%. The corresponding variation in d-spacings are given in Tab. 6.1

[DTAB]%	d=2π/q [nm]
33	4.28
50	4.35
66	4.26
90	3.97
98	3.87

TABLE 6.1: The lattice spacings obtained from SAXS data of the MTAB-DTAB-DNA complexes in water at [MTAB+DTAB] = 50mM and ρ=1.

At high molar ratio ρ=5

In this case the samples were made at a molar ratio of ρ=5. SAXS data with increasing DTAB concentration is shown in Fig. 6.4. At W_{DTAB}=10% and 30%, the complex show diffraction data corresponding to hexagonal phase

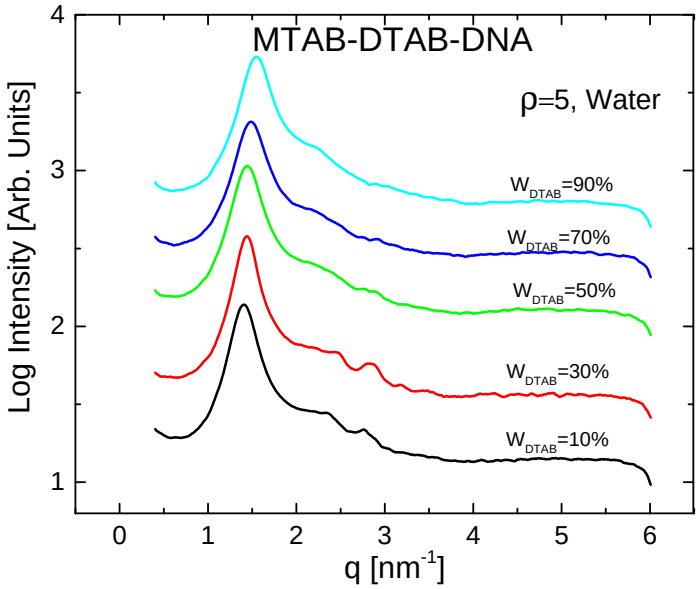

FIGURE 6.4: MTAB-DTAB-DNA complexes at ρ=5 in water with increasing [DTAB] concentrations. [MTAB+DTAB]=50mM and T =30°C.

(H_I^c), with lattice parameters 5.18 nm and 5.03 nm respectively. However, as W_{DTAB} was further increased, peaks became broader and shifted towards higher q values. Broad higher orders are also visible. However they do not fit to a hexagonal phase.

6.4.2 MTAB-DTAB-DNA complexes in salt solution

At low molar ratio of ρ=1

To study the influence of salt in these complexes, the samples were prepared in [NaCl]=300mM. At W_{DTAB} = 33% and 66%, the complex exists in a H_I^c phase, as shown in Fig. 6.5. The corresponding lattice parameters are around 5.4 nm. As the concentration of DTAB is increased to 75%, a set of peaks which can be fitted to a hexagonal phase, with a missing 1st order is

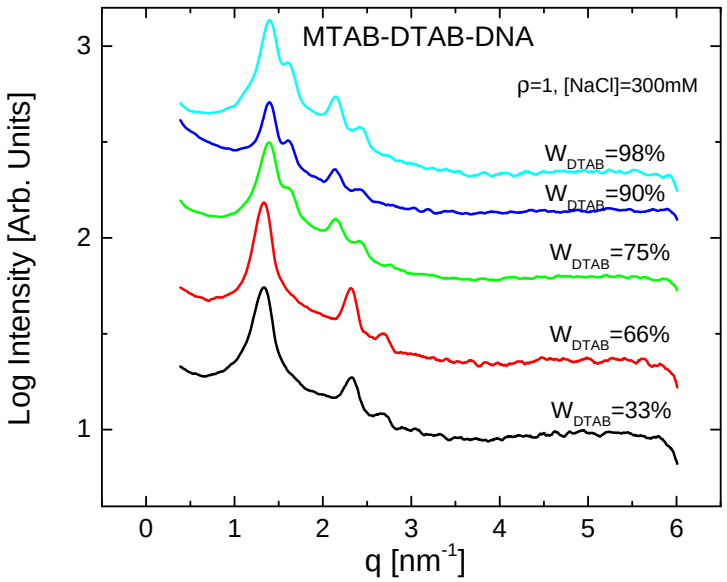

FIGURE 6.5: MTAB-DTAB-DNA complexes at ρ=1 in the presence of salt ([NaCl]=300mM) with increasing [DTAB] concentrations. T=30°C.

observed. The (10) peak of this phase, which we refer to as the super hexagonal (H_s^c) phase is absent in the SAXS data. Higher orders are visible in the scattering data. The lattice parameters are given in Table 6.2. From Figs. 6.5 and 6.3 we can observe the following : (i) at low DTAB concentrations, on addition of NaCl the broad peaks develop into a hexagonal H_I^c phase and (ii) at high DTAB concentrations, the complex undergo transition to a super hexagonal ($H_{I,s}^c$) phase.

TABLE 6.2: The lattice parameters obtained from SAXS at ρ=1 and [NaCl]=300mM. [MTAB+DTAB]=50mM and T =30°C.

W_{DTAB}%	Lattice parameter [nm]	Phase
33	5.43	H_I^c
66	5.43	H_I^c
75	9.02	H_s^c
90	9.02	H_s^c
98	8.91	H_s^c

At high molar ratio of ρ=5

To study the influence of salt, samples were made in [NaCl]= 200mM and 300mM. In the case of [NaCl]=300mM and low DTAB concentrations, W_{DTAB}=10%, 30% and 40%, the complex exist in a hexagonal (H_I^c) phase as shown in Fig. 6.6a.

At high W_{DTAB}=60% and above the sample shows a S_I^c phase. At an intermediate DTAB concentration of 50%, there is a coexistence of H_I^c and S_I^c. The lattice parameters in this case are given in Table 6.3. The SAXS data at [NaCl]= 200mM, also shows a similar behaviour, which is shown in Fig. 6.6b. In this case the H_I^c phase is seen at W_{DTAB}=10%, 30% and 40% with lattice parameters 5.27 nm, 5.14 nm and 5.43 nm respectively. There is a wide coexistence region ranging from 50 to 70%. At W_{DTAB}=90% a S_I^c phase is observed with a lattice parameter of 4.16 nm.

ρ=5 [NaCl]=300mM		
W_{DTAB}%	Lattice parameter (nm)	Phase
10	5.27	H_I^c
30	5.21	H_I^c
40	5.30	H_s^c
50	-	H_I^c+S_I^c
60	4.62	S_I^c
70	4.40	S_I^c
90	4.26	S_I^c

TABLE 6.3: The lattice parameters of MTAB-DTAB-DNA complexes obtained from SAXS data, with ρ=5 and [NaCl]=300mM. [MTAB+DTAB] = 50mM. T =30°C.

6.4.3 Cryo-SEM studies of the super hexagonal phase

Fig. 6.7, shows cryo-SEM images of the super hexagonal structure formed by MTAB-DTAB-DNA complexes. Samples are prepared in the same way as

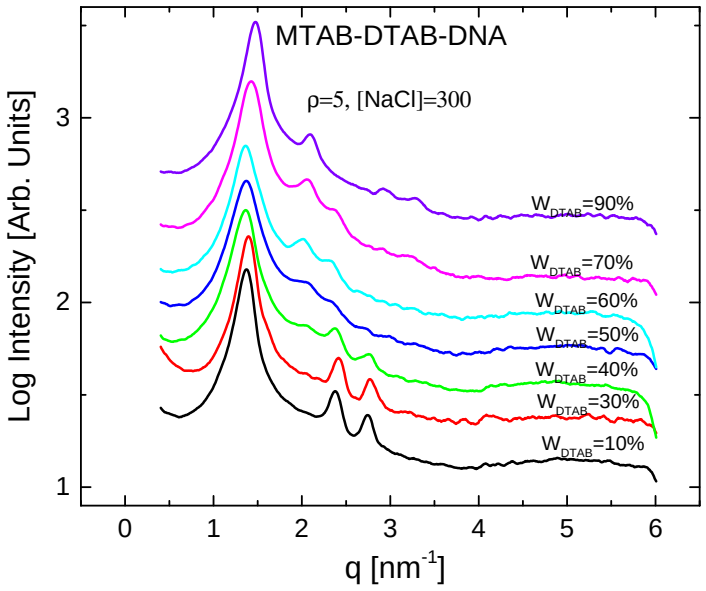

(a)

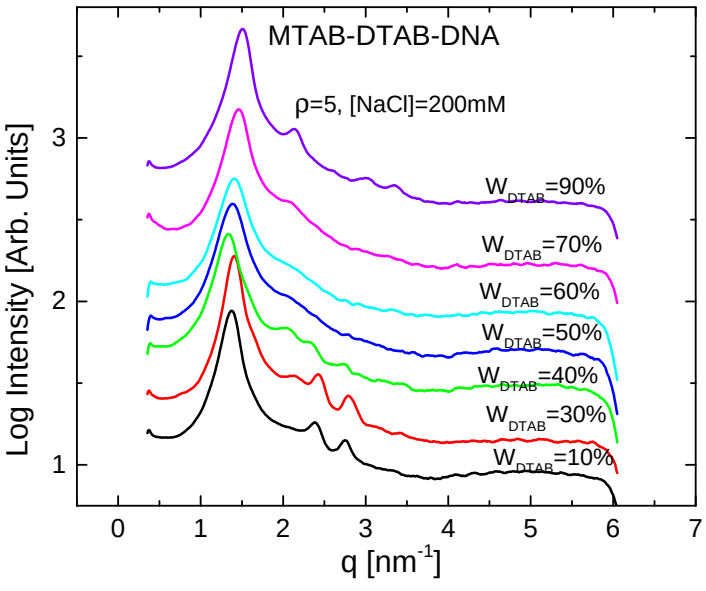

(b)

FIGURE 6.6: The SAXS data of MTAB-DTAB-DNA complexes at [MTAB+DTAB]=50mM and [NaCl]=200mM for (a) ρ=5 and (b) ρ=1. T=30°C.

for SAXS. For the study the complex formed at high DNA content (ρ=1) and [MTAB-DTAB]=50mM, W_{DTAB}=75% and [NaCl] = 300mM was used (Fig. 6.7). They show bundle like morphology similar to MTAB-DNA complexes.

6.5 Discussion

In this study we have used the surfactant mixture of MTAB and DTAB, with the [MTAB+DTAB] concentration fixed at 50mM, which implies a gradual reduction in MTAB concentration on gradual increase of the DTAB concentration. Studies show that in water and at very low concentrations of DTAB, it forms ellipsoidal micelles[7]. Addition of salt leads to growth of the micelle. In case of DTAB, on addition of NaBr, micelles grow in length[7]. In the previous chapter we have already discussed the structural polymorphism of complexes of cylindrical MTAB micelles with DNA.

In water and at low ρ (ρ=1), Fig. 6.3 shows the scattering profile with increasing concentration of DTAB. It was seen in the previous chapter that, under the same conditions when the system is made up of MTAB, there are sharp peaks corresponding to a hexagonal phase. On addition of DTAB, SAXS show broad peaks. This arises from the short range order resulting from the presence of short ellipsoidal DTAB micelles[7].

However in the presence of NaCl and ρ=1 (low ρ), the complexes behave differently. As DTAB concentration is increased from 33% to 66%, the scattering profiles have sharp peaks, corresponding to hexagonal lattice (H_I^c) as shown in Fig. 6.5. It is known from the literature that, on addition of salt, the counterion screen the charges on the head group reducing their mutual repulsion[8]. Therefore the micelles grow[7,8]. Such long cylindrical micelles

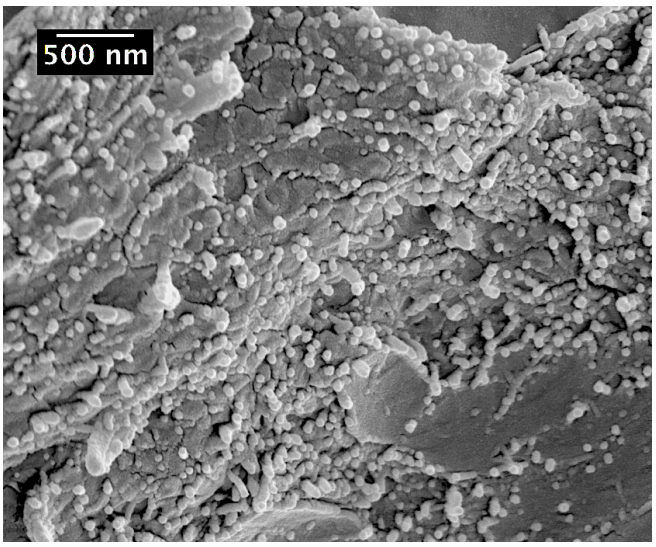

(a)

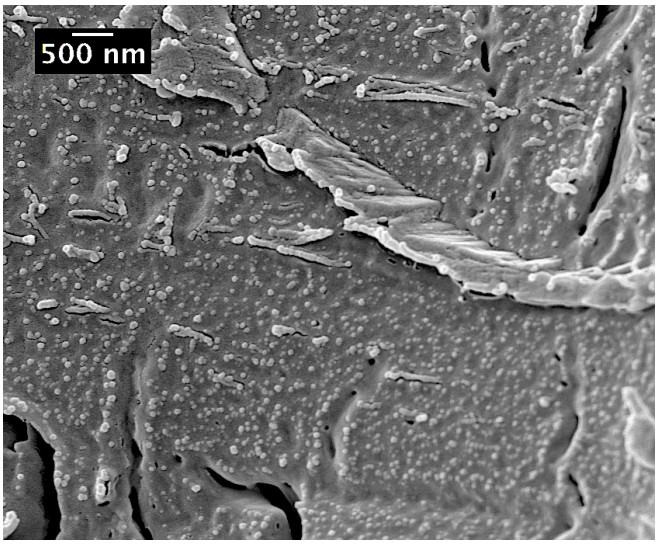

(b)

FIGURE 6.7: Cryo-SEM images obtained for the MTAB-DTAB-DNA complexes in the presence of [NaCl]=300mM at W_{DTAB}=75% and ρ=1.

can pack well with DNA thereby increasing translational order in the system. At low DTAB concentration the system arrange in a H_I^c phase and at high DTAB concentration in a $H_{I,s}^c$ phase which corresponds to a $\sqrt{3} \times \sqrt{3}$ super lattice of H_I^c[1,2]. In the presence of salt the complex swells, which results in the loss of their hexagonal close packing. As a result they arrange themselves in a $\sqrt{3} \times \sqrt{3}$ super lattice of H_I^c in order to retain some of the oppositely charged species in proximity.

For ρ =5 in water, we obtained the scattering profile as shown in Fig. 6.4. As evident from the figure, at low DTAB concentrations the complex exists in a hexagonal phase. As the DTAB concentration is increased, peaks become broader and cannot be fitted on to any lattice. In the presence of salt, and at low DTAB concentrations, the complex has a hexagonal phase. For example, at [NaCl]=300mM, the complex exists in a hexagonal phase at DTAB concentrations from 10% to 40%, with much sharper peaks (Fig. 6.6), indicating long range order in the system. We already mentioned the growth of micelle in the presence of salt[8], which leads to better packing of micelle with DNA. At higher DTAB concentrations, this H_I^c is seen to transform into S_I^c. In H_I^c, each micelle is surrounded by 6 DNA strands and in S_I^c, each micelle is surrounded by 4 DNA strands. Hence for the same micellar size, DNA-DNA repulsion can be expected to be much higher in the H_I^c compared to the S_I^c.

It is observed in our case that, as the DTAB concentration is increased, the complex undergo a transition from H_I^c to S_I^c. When the DTAB concentration in the sample is gradually increased, it implies an increase in the DTAB concentration in the micelle. Or in other words the number of C14 chains are replaced gradually by C12 chains which ultimately result in a smaller micellar size. This consequent reduction in the size of the micelle force the DNA cylinders to be closer, which is energetically unfavourable. As a result

this favours a $H_I^c \rightarrow S_I^c$ transition.

6.6 Conclusions

Due to the presence of ellipsoidal micelles of DTAB, the MTAB-DTAB-DNA complexes in water has short range translational order. At very low DTAB concentrations in the presence of salt, a hexagonal phase (H_I^c) is seen. On addition of salt and at high DTAB concentrations the complex shows a super hexagonal phase ($H_{I,s}^c$) at low ρ and a square phase (S_I^c) at high ρ. The H_I^c to $H_{I,s}^c$ transition at low ρ can be attributed to the effect of salt that swells the complex, whereas the H_I^c to S_I^c transition at high ρ can be understood in terms of increasing DNA-DNA repulsion due to the gradual decrease in the micellar diameter on increasing DTAB concentration.

Bibliography

[1] A. V. Radhakrishnan. PhD thesis, Raman Research Institute, Jawaharlal Nehru University, New Delhi, 2012.

[2] Madhukar S. *Influence of some sterols and nucleotides on the structure of self-assembled amphiphilic systems*. PhD thesis, Raman Research Institute, Jawaharlal Nehru University, New Delhi, 2017.

[3] Rema Krishnaswamy, Georg Pabst, Michael Rappolt, V. A. Raghunathan, and A. K. Sood. Structure of dna-ctab-hexanol complexes. *Phys. Rev. E*, 73:031904, Mar 2006.

[4] Rema Krishnaswamy, V. A. Raghunathan, and A. K. Sood. Reentrant phase transitions of dna-surfactant complexes. *Phys. Rev. E*, 69:031905, Mar 2004.

[5] Rema Krishnaswamy, Partha Mitra, Velayudhan Raghunathan, and A Sood. Tuning the structure of surfactant complexes with dna and other polyelectrolytes. 62:357, 01 2007.

[6] A. V. Radhakrishnan, S. K. Ghosh, G. Pabst, V. A. Raghunathan, and A. K. Sood. Tuning dna-amphiphile condensate architecture with strongly binding counterions. *Proceedings of the National Academy of Sciences*, 109(17):6394–6398, 2012.

[7] Magnus Bergström and Jan Pedersen. Structure of pure sds and dtab micelles in brine determined by small-angle neutron scattering (sans).

1:4437–4446, 09 1999.

[8] S.A. Safran, P.A. Pincus, M. E. Cates, and F.C. Mackintosh. Growth of charged micelles. *Journal de Physique*, 51(6):503–510, 1990.

Chapter 7

Conclusions

This thesis describes studies on the structure and interactions in surfactant - polyelectrolyte complexes. In the first part of the thesis we have presented detailed experiments on the interaction of a linear anionic polyelectrolyte with the lamellar phase of a cationic surfactant. In the second part, we describe the interaction of a cationic surfactant with DNA.

We have investigated the interaction of the fluid lamellar L_α phase formed by a cationic surfactant, DDAC with the anionic polyelectrolyte, PAANa. The salt-induced structural changes of the DDAC-PAANa complexes for polyelectrolyte molecular weight, M_w = 2100, 5100 and 8000 were studied. In the case of molecular weights 2100 and 5100 we observed the following. At low ionic strengths a collapsed lamellar phase L_α^{c1} is observed. At intermediate salt concentration, above a threshold concentration, an abrupt swelling leading to the formation of a swollen lamellar phase L_α^s is seen. At very high ionic strengths a second collapsed lamellar phase L_α^{c2} is observed. The formation of L_α^{c1} can be attributed to attractive patch charge attraction or bridging interaction of polymer adsorbed bilayers. The abrupt swelling leading to the formation of L_α^s arises from undulation repulsion between the bilayers, which are decorated by a homogeneous adsorption layer. A gradual reduction in the d-spacing is observed with further increase in the

salt concentration which is due to the gradual desorption of polymers from the bilayer surface. The L_α^{c2} phase is stabilised by Van der Waals attraction. At very high molecular weight of 8000, this swelling transition is absent, suggesting that the cohesive energy of the L_α^{c1} phase increases with increase in molecular weight. Therefore the formation of the collapsed phase in the PAANa8000 case can be attributed to increased attractive bridging interaction or patch charge attraction with increasing molecular weight of the polyelectrolyte. We also saw that this swelling behaviour is absent in the case of a charged lipid such as, DOTAP, whose bending rigidity is much higher than that of DDAC.

Further studies are required to understand the underlying interaction leading to the formation of the collapsed lamellar phase, L_α^{c1}. Both patch charge attraction and polymer bridging are possible mechanisms. Only the measurement of the dependence of the interaction on the separation between the bilayers will be able to resolve this issue. Another topic for further study is the role of undulation repulsion in stabilising the L_α^{s} phase. Although this interaction is consistent with many of our observations, a direct measurement of the effect of polyelectrolyte adsorption on the membrane rigidity is required to unambiguously confirm the proposed mechanism.

In the second half of the thesis we have studied the interaction of cationic surfactants with DNA. The cylindrical micelles of the surfactants in the presence of DNA arrange in 2D lattices resembling ionic crystals. They exhibit structural polymorphism depending on micellar size. In this part of the thesis we try to understand the polymorphic behaviour exhibited by these complexes. From the previous studies we know that CTAB-DNA complexes form hexagonal lattice in water. CTAT-DNA complexes show three different phases such as hexagonal phase, super hexagonal phase and square phase depending on the value of ρ. DTAB-DNA complexes show two kinds of

nematic gel phases at low and high NaCl concentrations, irrespective of the value of ρ. At intermediate NaCl concentrations, a super hexagonal phase is observed at low ρ and a square phase is observed at high ρ.

We studied the phase behaviour of MTAB-DNA complexes and MTAB-DTAB-DNA complexes. In the case of MTAB-DNA complexes in water SAXS, POM and cryo-SEM studies show that they form 2D hexagonal phase. On addition of salt the micelles grow, leading to long range translational correlations. However, at very high salt, the interactions are completely screened out leading to the destabilisation of the complex, resulting in an isotropic phase. In the presence of strongly binding counterion like NaT, a hexagonal to square lattice transition is observed at low ρ and high ρ. A square lattice contains one DNA corresponding to one micelle, whereas in a hexagonal lattice there are two DNA corresponding to one micelle. The tosylate counterions compete with DNA, because of its strong binding property. Therefore a square lattice is preferred. CHN studies of the MTAB-DNA complexes in water and salt also confirm the formation of a hexagonal lattice.

In the case of MTAB-DTAB-DNA complexes in water, SAXS data shows broad peaks. Hexagonal phase is observed at very high MTAB concentration. At [NaCl]=300 mM, as DTAB concentration is gradually increased at low ρ, a hexagonal (H_I^c) to super hexagonal ($H_{I,s}^c$) transition is observed. At high ρ, a hexagonal to square transition (S_I^c) is found. DTAB micelles are known to have an ellipsoidal structure. The presence of these ellipsoids, disrupt the long range translational order in the lattice, resulting in poor correlation and hence the presence of broad peaks. In the presence of salt, micelles grow leading to the formation of more ordered structures. The H_I^c to $H_{I,s}^c$ transition at low ρ can be attributed to the effect of salt that swells the complex, whereas the H_I^c to S_I^c transition at high ρ can be understood in

terms of increasing DNA-DNA repulsion due to the gradual decrease in the micellar diameter on increasing DTAB concentration. The super hexagonal phase is the $\sqrt{3} \times \sqrt{3}$ super lattice of the hexagonal phase.

From the above studies, we now have a qualitative understanding of the polymorphism of cationic surfactant-DNA complexes. Detailed theoretical studies and simulations are required for a complete understanding of these systems.